FP7-ICT Future Networks
SPECIFIC TARGETTED RESEARCH PROJECT
Project Deliverable

PHYDYAS Doc. Number	18
Project Number	**ICT - 211887**
Project Acronym+Title	PHYDYAS – PHYsical layer for DYnamic AccesS and cognitive radio
Deliverable Nature	Report
Deliverable Number	D4.2
Contractual Delivery Date	January 1st, 2010
Actual Delivery Date	09/02/2010
Title of Deliverable	MIMO Techniques and Beamforming
Contributing Workpackage	WP4. MIMO TRANSMIT AND RECEIVE PROCESSING
Project starting date; Duration	01/01/2008 ; 30 months
Dissemination Level	RE
Author(s)	Montse Nájar, Miquel Payaró, Eleftherios Kofidis, Mario Tanda, Jérôme Louveaux, Markku Renfors, Tobias Hidalgo, Didier Le Ruyet, C. Lélé, R. Zacaria, Maurice Bellanger

Abstract:
The techniques proposed in the previous deliverable D4.1 [8] for synchronization, channel estimation and equalization in FBMC, are now completed and some additional results presented.
The MIMO techniques for multiantenna radiocommunication systems have been analyzed and adapted to the FBMC context and new space diversity and multiplexing algorithms have been developed to exploit the particularities of FBMC. The performance of OFDM systems is taken as the reference to assess the performance of the FBMC schemes proposed.
The main achievements are summarized at the end of the document.

TABLE OF CONTENTS

1 Introduction

The implementation of the MIMO concepts in transmission systems implies two different phases, namely channel matrix estimation and signal processing algorithms for the extraction of the data.
The estimation of the channel matrix and the tracking was the subject of the previous document D4.1.
The theme of the present document is MIMO processing, with two main objectives

- see how the techniques developed for OFDM can be applied to the filter bank multicarrier (FBMC) context and how they can be adapted,
- whenever appropriate, develop specific techniques for FBMC.

In all cases, the performance of the OFDM systems, in theory and simulation, is taken as the reference to assess the performance of the FBMC schemes which are elaborated.
During the second year of the work, it appeared that some complements to the document D4.1 [8] on channel matrix estimation were desirable and useful. They are reported in the next section.

2 Synchronization, channel estimation and equalization in MIMO-FBMC

The techniques developed for the single antenna case have been used as a starting point for the multiantenna case studied in document D4.1 [8]. Here, improvements to the previous schemes are proposed, new approaches are investigated and more simulation results are provided.

2.1 Preamble-based CFO estimation

In this section is considered a closed-form carrier-frequency offset (CFO) estimation algorithm for MIMO FBMC systems based on a training sequence made up of two identical parts. In [1] it is stated that in a single-input single-output (SISO) FBMC context, a training symbol with two identical parts is obtained by applying K identical preamble multi-carrier symbols, with pseudo-noise data only on even subcarriers, at the input of the IFFT in the transmitter. Let us now consider a MIMO FBMC system with N_T transmit antennas and N_R receive antennas. In this case at each receive antenna the training sequence is equal to the sum of the N_T training transmitted signals. In particular, we can obtain at each receive antenna a training sequence with two identical parts by exploiting the frequency-division multiplexed (FDM) training sequences suggested in [2]. In this scheme the pilot symbols are placed over equally spaced subcarriers, and in particular, to obtain a periodic preamble with period $P = M/2$, the n-th entry $c_i(n)$, $i = 1,...,N_T$, of each of the K identical M-dimensional preamble symbols at the i-th transmit antenna is given by

$$c_i(n) = \begin{cases} d_i(n') & n = n'N + (i-1)2, \qquad 0 \le n' \le M/N - 1 \\ 0 & otherwise \end{cases} \tag{2.1}$$

where $N = 2Q$ with Q a power of two not smaller than N_T and, moreover, $|d_i(n')| = \sqrt{N/N_T}$ in order to normalize the energy used for the training [3]. Thus, by using the considered FDM scheme, the obtained training sequence at each receive antenna satisfies the condition

$$s_{TR}[k] = s_{TR}\left[k + \frac{M}{2}\right] \tag{2.2}$$

after a transient of $K-1$ multicarrier symbols, and, then, the CFO recovery can be accomplished by measuring the phase rotations between repetitive parts. Specifically, an estimate of the normalized CFO $\varepsilon = \Delta f T$, assumed to be the same for all the transmit-receive antenna pairs, can be obtained by

$$\hat{\varepsilon} = \frac{1}{\pi} \angle R_{MIMO} \tag{2.3}$$

where

$$R_{MIMO} = \sum_{i=1}^{N_R} \sum_{k=(K-1)M}^{(K-1)M+\frac{M}{2}-1} r_i^*[k] r_i[k+\frac{M}{2}] \tag{2.4}$$

with $r_i[k]$ the signal at the i-th receive antenna. The acquisition range of the considered CFO estimator is $|\varepsilon| < 1$. The performance of the considered CFO estimator has been assessed via computer simulations and compared with that obtained with the estimation algorithm proposed in [3] for OFDM systems exploiting a symbol with two identical parts. Specifically, a number of 10000 Monte Carlo trials has been performed. The number of subcarriers for both systems is M = 1024, and, moreover, in the OFDM case the length of the cyclic prefix has been assumed to be equal to CP=M/8. In the FBMC case the prototype filter of length L=4M=4096 with a roll-off factor of one proposed by CNAM [4] has been used. The performance in multipath fading ITU-Vehicular A and ITU-Vehicular B channels have been obtained, taking into account, in the OFDM case, the energy loss due to the cyclic prefix insertion. The normalized CFO has been randomly generated at each simulation with a uniform distribution in the range $[-0.5, 0.5)$, the channels between the different transmit-receive antenna pairs are statistically independent from one another. Moreover, all channels are fixed in each run but they are mutually independent from one run to another.

Figures 2.1-2.2 report the RMSE of the considered CFO estimators as a function of the SNR at each receive antenna in multipath channel A for a 2X2 MIMO system (Figure 2.1) and for a 4X4 system (Figure 2.2). The results show that both estimators assure nearly the same performance almost in the whole range of considered SNR values. The slight performance degradation of the CFO estimator for FBMC systems with respect to that for OFDM systems in high SNR conditions is due to the fact that in the first case and in multipath channel the exploited training symbol is not exactly periodic due to the absence of the cyclic prefix. The last observation, due to the adopted CP length, is true also for the OFDM system when the more dispersive multipath channel B in considered. Thus, in multipath channel B (see Figures 2.3 and 2.4) the performance of both CFO estimators present a floor at an RMSE value nearly equal to 10^{-3}. In regard to the performance behavior as a function of the number of receive and transmit antennas, as one would expect, a performance gain is observed as the number of receive antenna increases.

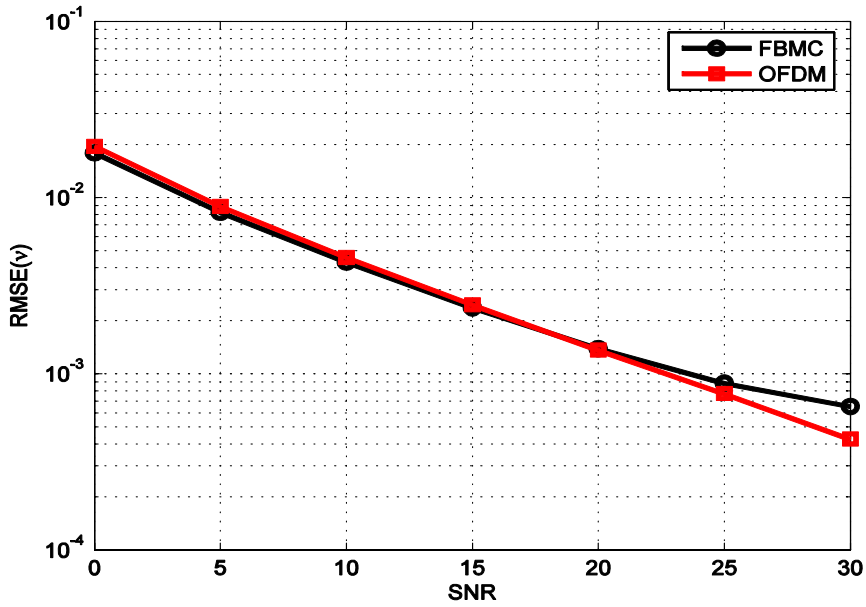

Figure 2.1 RMSE of the proposed CFO estimator as a function of the SNR in ITU-Veh. A channel, $M = 1024$, $N_T = N_R = 2$.

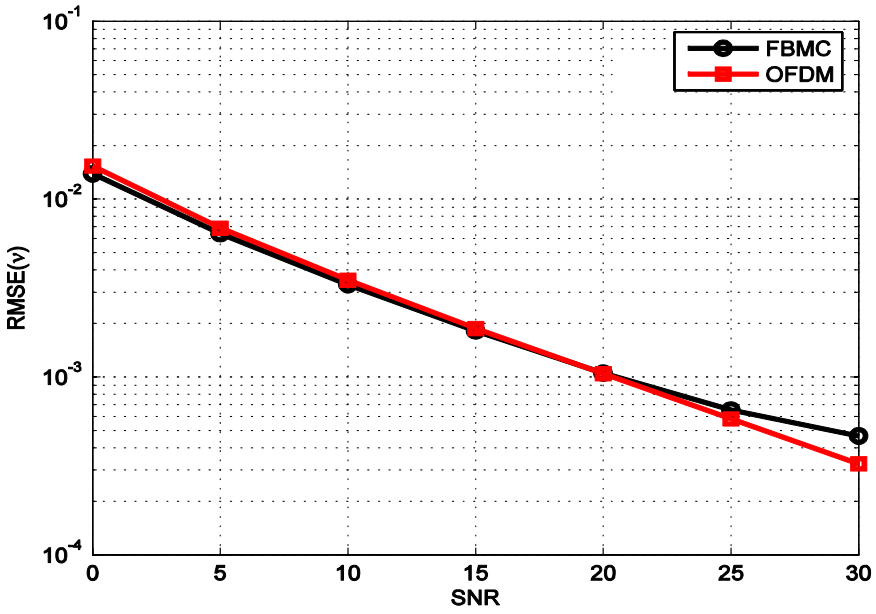

Figure 2.2 RMSE of the proposed CFO estimator as a function of the SNR in ITU-Veh. A channel, $M = 1024$, $N_T = N_R = 4$.

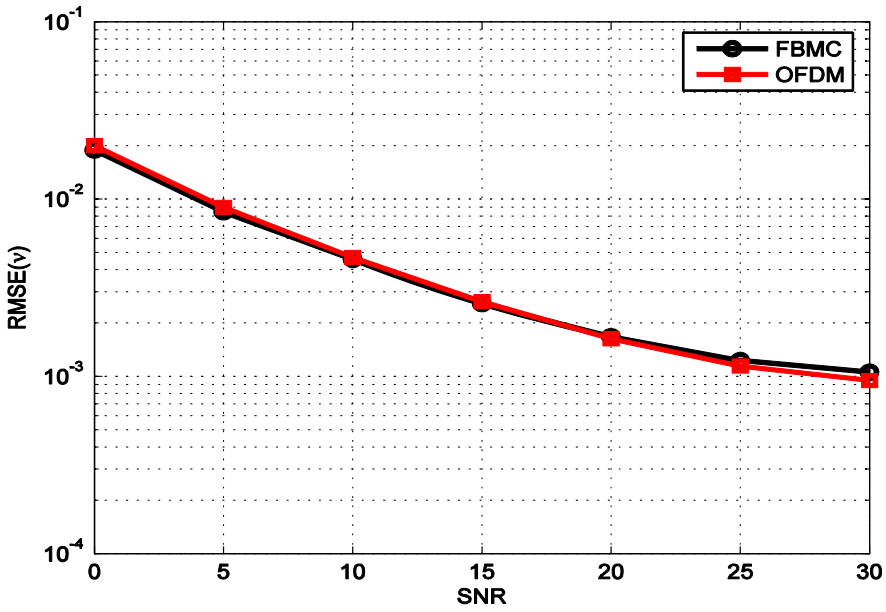

Figure 2.3 RMSE of the proposed CFO estimator as a function of the SNR in ITU-Veh. B channel, $M = 1024,\ N_T = N_R = 2.$

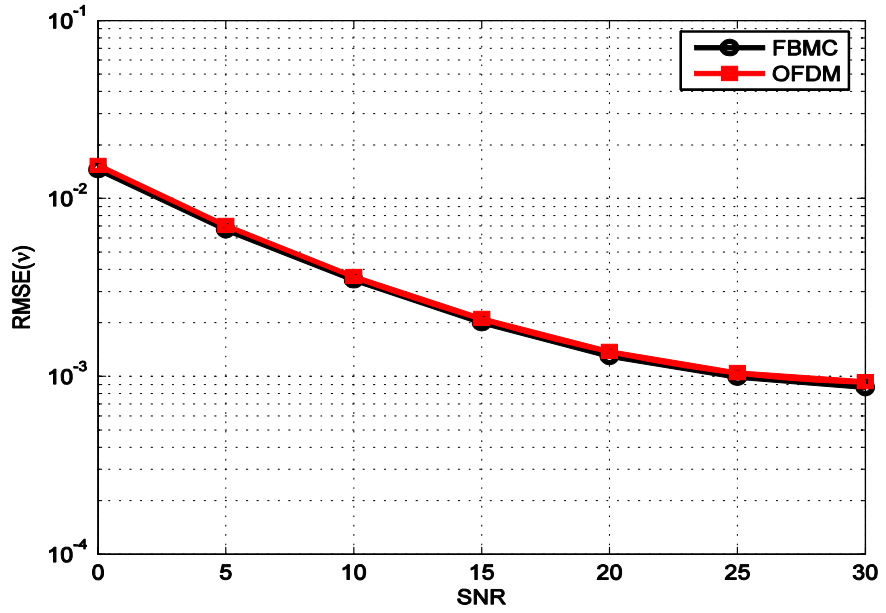

Figure 2.4 RMSE of the proposed CFO estimator as a function of the SNR in ITU-Veh. B channel, $M = 1024,\ N_T = N_R = 4.$

2.2 Auxiliary pilot based synchronization and channel estimation

When transmitting with multiple antennas in a realistic FBMC scenario that includes pilots, special care has to be taken to separate the pilots of one antenna from the pilots sent by the other. This can be done by silencing one antenna while the other is transmitting a pilot, i.e., at a certain frequency-time location *k,n* one tx. antenna transmits the pilot while all the others transmit a 0. In the auxiliary pilot based approach this includes not only sending the 0 at the given locations if the given antenna is to remain silent, but also using the auxiliary pilot that accompanies the 0 to ensure that the silent antenna does not generate interference at the receiver.

2.2.1 Iterative interference cancellation for joint channel and FTD estimation

The approach presented in Section 2.2.2 of deliverable D3.2 [5] performs joint fractional time delay (FTD) and channel estimation based on iterative interference cancellation (IIC) using the 3-tap equalizer in the single antenna case. This technique can further be generalized to the multiple antenna case with the help of matrix notation. The following derivation is presented for the 2x2 MIMO case (2 transmit (tx.) antennas and 2 receive (rx.) antennas), but can be generalized for any spatial multiplexing case, i.e., the number of rx. antennas Q is equal or larger than the number of tx. antennas P.

In the SISO case, the output of the 3-tap equalizer with correct center frequency equalization coefficient $w_{k,n}$ at subcarrier k and time index n, can be written as

$$\tilde{d}_{k,n} = w_{k,n}\tilde{y}_{k,n} + \psi w_{k,n}\widetilde{\Delta y}_{k,n}, \tag{2.5}$$

where $\tilde{y}_{k,n} = \theta^*_{k,n} y_{k,n}$, $y_{k,n}$ is the received signal at that time-frequency bin, $\theta_{k,n}$ (= j^{k+n}) performs the FBMC/OQAM mapping. ψ represents the equalizer phase difference correction between the subchannel center frequency and the edge and depends on the fractional time delay τ_{FTD} as

$$\psi = -\pi\tau_{FTD}\,. \tag{2.6}$$

Additionally, we define

$$\widetilde{\Delta y}_{k,n} = \theta^*_{k,n}\left(y_{k,n-1} - y_{k,n+1}\right)/2. \tag{2.7}$$

Equation (2.5) can be generalized to the 2x2 MIMO case as follows: We first assume that at a certain time instant n_1, transmit antenna 1 sends a pilot while transmit antenna 2 remains silent. In the following we will remove as much as possible the subcarrier and time indices for clearer presentation. The generalized equation (2.5) now reads

$$\begin{aligned} \tilde{d} &\simeq w^{11}\tilde{y}^1(n_1) + \psi w^{11}\ \widetilde{\Delta y^1}(n_1) + w^{12}\tilde{y}^2(n_1) + \psi w^{12}\widetilde{\Delta y^2}(n_1) \\ 0 &\simeq w^{21}\tilde{y}^1(n_1) + \psi w^{21}\widetilde{\Delta y^1}(n_1) + w^{22}\tilde{y}^2(n_1) + \psi w^{22}\ \widetilde{\Delta y^2}(n_1), \end{aligned} \tag{2.8}$$

which can be written in matrix notation as

$$\begin{aligned} \begin{pmatrix} \tilde{d} \\ 0 \end{pmatrix} &= \begin{pmatrix} w^{11} & w^{12} \\ w^{21} & w^{22} \end{pmatrix}\left[\begin{pmatrix} \tilde{y}^1(n_1) \\ \tilde{y}^2(n_1) \end{pmatrix} + \psi\begin{pmatrix} \widetilde{\Delta y^1}(n_1) \\ \widetilde{\Delta y^2}(n_1) \end{pmatrix}\right], \\ \tilde{d}\mathbf{e}_1 &= \mathbf{W}\left(\tilde{\mathbf{y}}(n_1) + \psi\widetilde{\Delta\mathbf{y}}(n_1)\right). \end{aligned} \tag{2.9}$$

Similarly, if a pilot in the same subcarrier at a not too distant point in time (assuming same channel response, so that the equalization/demixing matrix $\mathbf{W}$ does not change) coming from the other antenna is received, while the first antenna transmits a 0, we can write

$$\tilde{d}\mathbf{e}_2 = \mathbf{W}\left(\tilde{\mathbf{y}}(n_2) + \psi\widetilde{\Delta\mathbf{y}}(n_2)\right). \tag{2.10}$$

This can be regrouped as

$$\tilde{d}\mathbf{I}_{2x2} = \mathbf{W}\left(\widetilde{\mathbf{Y}} + \psi\widetilde{\Delta\mathbf{Y}}\right), \tag{2.11}$$

where $\mathbf{I}_{2x2}$ is the 2x2 identity matrix, $\widetilde{\mathbf{Y}} = \left(\tilde{\mathbf{y}}(n_1) \quad \tilde{\mathbf{y}}(n_2)\right)$ and $\widetilde{\Delta\mathbf{Y}} = \left(\widetilde{\Delta\mathbf{y}}(n_1) \quad \widetilde{\Delta\mathbf{y}}(n_2)\right)$.

Stacking the columns of the matrices into a vector, the SISO optimization problem presented in [5] can be rewritten for MIMO as the minimization of the error between the vector given by the pilots and 0's sent by the transmit antennas in the same subchannel at different time instants:

$$\left\{\hat{\psi}, \widehat{\mathbf{W}}\right\} = \underset{\psi,\mathbf{W}}{\arg\min}\left\{\sum_{k,n\in\Omega_{JE}}\left|\vec{\mathbf{d}} - \mathbf{\mathfrak{V}}\left(\vec{\tilde{\mathbf{y}}} + \psi\overrightarrow{\widetilde{\Delta\mathbf{y}}}\right)\right|^2\right\}, \tag{2.12}$$

where $\vec{\mathbf{d}} = d\begin{pmatrix}\mathbf{e}_1\\ \mathbf{e}_2\end{pmatrix}$, the block matrix $\mathbf{\mathfrak{V}} = \begin{pmatrix}\mathbf{W} & \mathbf{0}\\ \mathbf{0} & \mathbf{W}\end{pmatrix}$, $\vec{\tilde{\mathbf{y}}} = \begin{pmatrix}\tilde{\mathbf{y}}(n_1)\\ \tilde{\mathbf{y}}(n_2)\end{pmatrix}$ and $\overrightarrow{\widetilde{\Delta\mathbf{y}}} = \begin{pmatrix}\widetilde{\Delta\mathbf{y}}(n_1)\\ \widetilde{\Delta\mathbf{y}}(n_2)\end{pmatrix}$.

Now a similar iterative approach as in SISO can be applied.

1) Assuming that the phase slope is known from the previous iteration (0 in the beginning), $\mathbf{W}^i$ are solved from the pilot matrix and the inverse of the observation matrix $\left(\widetilde{\mathbf{Y}} + \psi(i-1)\,\widetilde{\Delta\mathbf{Y}}\right)$. Note that here i is the iteration index.

2) Assuming that $\mathbf{W}^i$ are known, the observation is a linear function of ψ and the optimum $\hat{\psi}$ can be calculated with the derivative of the expression in brackets in Equation (2.12) with respect to ψ and setting the result to 0, yielding

$$\hat{\psi} = \frac{\sum_{k,n\in\Omega_{JE}} \mathrm{Re}\left[\vec{\mathbf{d}}^H\mathbf{\mathfrak{V}}\overrightarrow{\widetilde{\Delta\mathbf{y}}}\right] - \mathrm{Re}\left[\vec{\tilde{\mathbf{y}}}^H\mathbf{\mathfrak{V}}^H\mathbf{\mathfrak{V}}\overrightarrow{\widetilde{\Delta\mathbf{y}}}\right]}{\sum_{k,n\in\Omega_{JE}} \overrightarrow{\widetilde{\Delta\mathbf{y}}}^H\mathbf{\mathfrak{V}}^H\mathbf{\mathfrak{V}}\overrightarrow{\widetilde{\Delta\mathbf{y}}}}, \tag{2.13}$$

which, from Equation (2.6) yields $\hat{\tau}_{FTD} = -\hat{\psi}/\pi$. The number of iterations needed for convergence depends on the FTD and Ω_{JE}.

It is expected, that in MIMO communications with reduced pilot density per tx-rx antenna link, the IIC method's advantage in FTD estimation range presents a significant advantage for synchronization and channel estimation.

Preliminary results with 500 channel realizations are presented in the next section, along with the results of the classical, phase rotation based estimation methods. The obtained performance curves show that the acceptable BER performance and FTD estimates regions are greatly extended compared to the methods that rely on phase rotation. However, the estimated FTD suffers a gradual degradation with the actual FTD, as compared to the SISO case with the same size of transmitted frame [5]. Also the BER performance degrades gradually, as compared to the SISO case, in which it remains constant throughout the studied FTD range.

Additionally, the SISO approach of (2.5) was used on the signal of one of the receive antennas in the MIMO simulation setup. If $^{(i)}$ denotes the signal of receive (y) or transmit (x) antenna i, then (2.5) can be written

$$\begin{aligned}\tilde{d}_{k,n} &= w_{k,n}\tilde{y}^{(1)}_{k,n} + \psi w_{k,n}\widetilde{\Delta y}^{(1)}_{k,n} \\ &= w_{k,n}(h^{11}{}_{k,n}x^{(1)}{}_{k,n} + h^{12}{}_{k,n}x^{(2)}{}_{k,n}) + \psi w_{k,n}(h^{11}{}_{k,n}\Delta x^{(1)}{}_{k,n} + h^{12}{}_{k,n}\Delta x^{(2)}{}_{k,n}) \\ &= w_{k,n}h^{11}{}_{k,n}\tilde{d}_{k,n} + \psi w_{k,n}(h^{11}{}_{k,n}\Delta x^{(1)}{}_{k,n} + h^{12}{}_{k,n}\Delta x^{(2)}{}_{k,n}),\end{aligned} \tag{2.14}$$

where the noise has been omitted and we have considered the moment in which transmit antenna 1 emits a pilot and antenna 2 is silent ($x^{(2)} = 0$). We see that we obtain an equation that is formally the same as in the SISO case, but the coefficient $w_{k,n}$ is not exactly an equalization coefficient anymore. Preliminary results with 300 channel realizations are also presented in the next section, and named IIC FTD estimation in the MIMO case. Only the signal of one of the receive antennas has been used, although the other could be exploited in a similar way and the obtained estimates averaged. The FTD estimates are of better quality than the ones obtained with the joint FTD and MIMO channel estimator presented above, and behave similarly and almost as good as in the SISO case [5]. However, the BER performance is worse, since the channel estimates do not profit now from the interference cancellation.

2.2.2 Pilot based channel estimation and equalization

In multiantenna communications with N_t transmit and N_r receive antennas there are N_t x N_r transmission links. For each transmission link between a transmit and a receive antenna, the channel parameters have to be estimated for compensating its distortions. If a similar approach as in SISO communications with auxiliary pilots is to be used, then the pilots have to provide snapshots of the link under consideration. The simplest way to do this at a given time-frequency bin is by transmitting a pilot from one transmit antenna and keeping the others silent. It is clear, that if a similar density of pilots is desired as in the SISO case, the pilot overhead grows accordingly to the number of links, i.e., N_t x N_r because the silent antennas cannot transmit data in the bin, in which another antenna transmits a pilot. On the other hand, if the pilot overhead has to remain constant, then the pilot density per antenna link diminishes and the channel parameter estimation based on them suffers. Obviously, intermediate solutions are also possible, tuning the performance of the channel parameter interpolation between the pilots and the pilot overhead. In the OFDMA based 802.16e standard [6] the pilot allocations for a multiantenna transmitter in some transmission modes are defined, such as the optional AMC and FUSC modes. For example, in the two antenna transmission, the density of pilots per link is reduced to half, whereas in the 3 antenna case, the overhead is doubled, as can be seen in Figure 2.5.

The 2-antenna configuration in Figure 2.5a) can be adapted to the auxiliary pilot based FBMC/OQAM transmission scheme with little effort. If the pilots and 0's are distributed as in Figure 2.6, the pilot locations of the standard can be realized. Even more, the calculation of the auxiliary pilot can be performed independently for each pilot or each 0 because they fall in a position in the interference area around the pilots (0's) in which they do not affect the following/preceding 0 (pilot). This helps to maintain a complexity similar as in the SISO case.

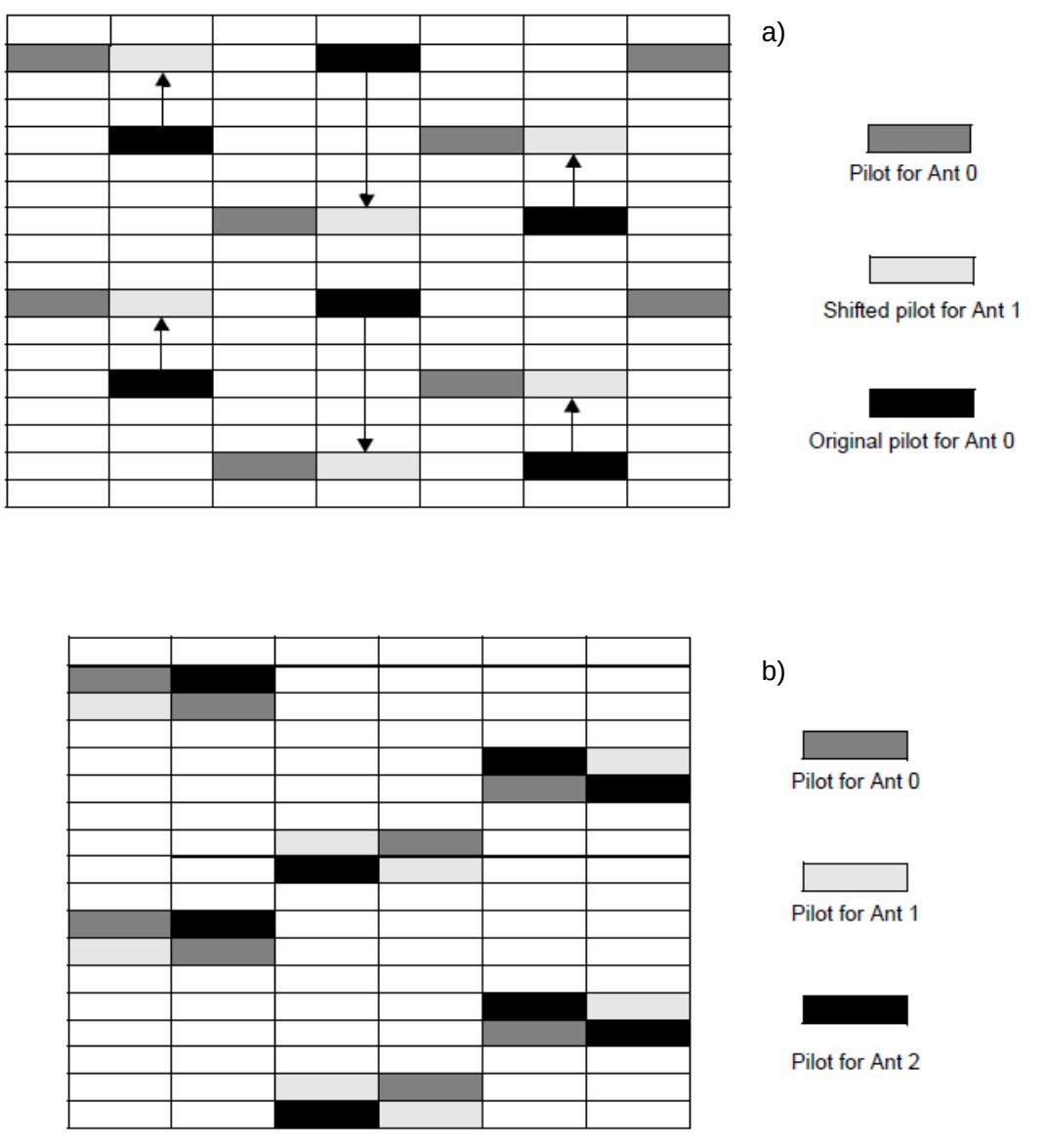

Figure 2.5 Pilot allocation for a) 2-antenna and b) 3-antenna base station for the optional FUSC and AMC zones

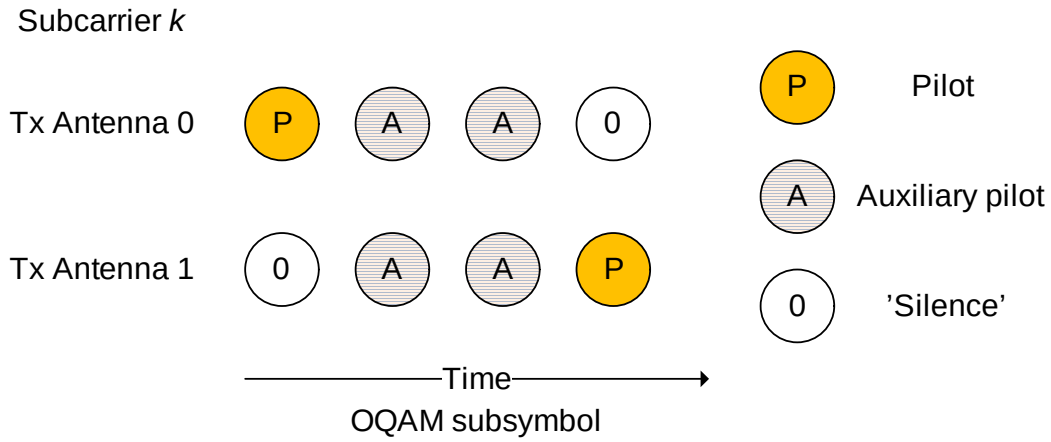

Figure 2.6. Convenient pilot and 0 allocation in the multiple transmit antenna FBMC/OQAM transmission.

SISO channel estimation performance with reduced pilot density

First simulations aimed at assessing the effect of reducing the pilot density. Figure 2.7 compares the performance of UL-AMC23 transmission in the SISO case with the original AMC pilot allocation and with the allocation corresponding to one antenna when having 2 transmit antennas. The modulation is 16-QAM and the ITU Vehicular-A channel model (Veh-A) is considered.

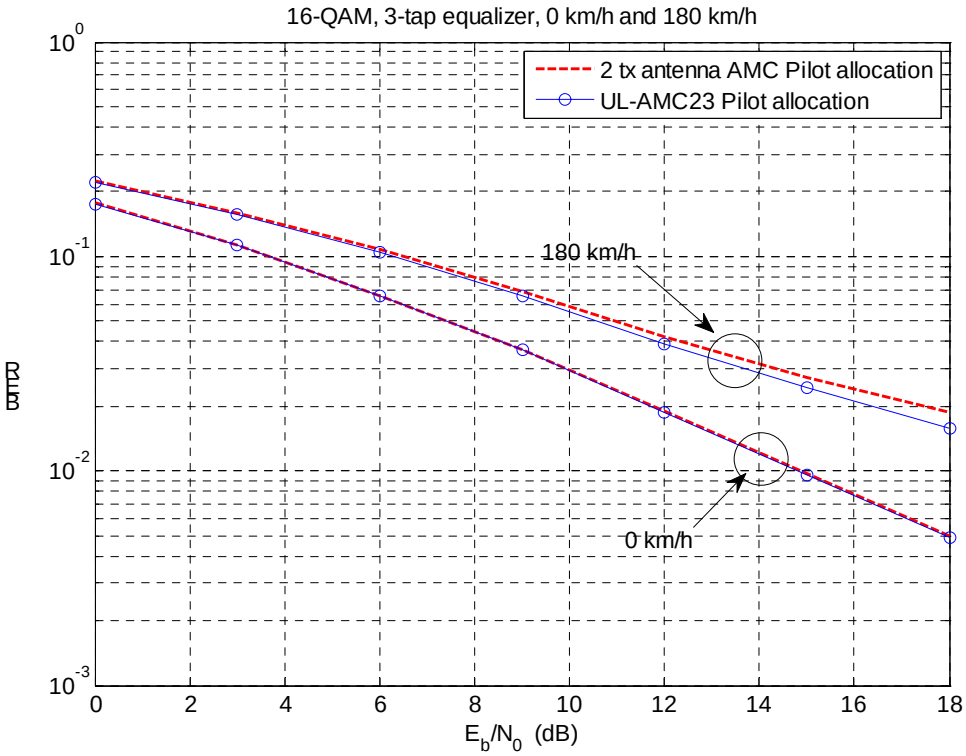

Figure 2.7 BER performance for the standard UL-AMC23 pilot configuration and the configuration for 2 transmit antennas with reduced density**.**

It can be seen, that the interpolation of the less dense pilot allocations yields similarly good channel estimates at other positions. In the quasi-stationary channel this is intuitive because the density of the pilots is reduced only in time direction, as shown in Figure 2.5. If the channel varies in time according to the mobile speed, it is necessary to 'accelerate' to high speeds in order to observe performance differences between the denser and less dense pilot grids. The figure shows the BER performance for a mobile at 180 km/h, and only at higher SNR the curves start to diverge.

MIMO channel estimation performance

Next, BER performance results for MIMO communications with channel estimation are presented. The transmission channels are modeled according to the quasi-stationary Veh-A channel model and each MIMO link is assumed to be independent from the other links. The subcarriers bear 16-QAM signals. We consider 2 transmit antennas and 2 or 3 receive antennas, and the multiantenna pilot allocation introduced above. Frequency and timing synchronization are assumed. Further, equalization is performed in a frequency-sampled way, as thoroughly described in Section 2.3.

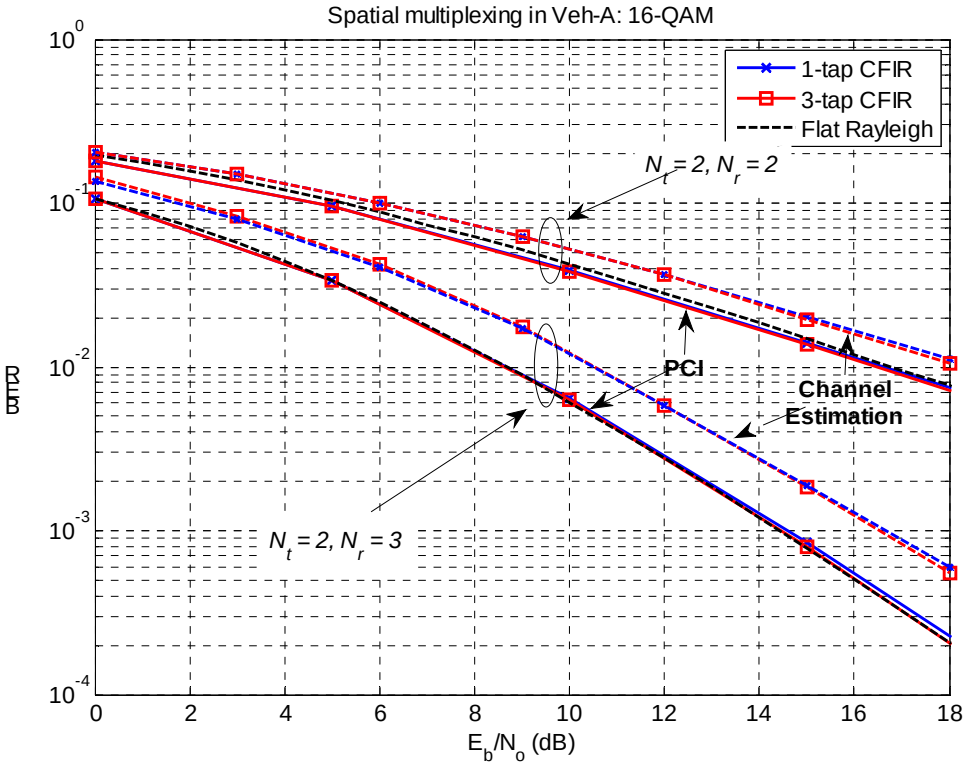

Figure 2.8 BER performance of the channel estimation in MIMO.

The results in Figure 2.8 show that the performance with channel estimation is approximately 2 dB worse than the PCI performance. This contrasts with the approximately 1 dB in SISO communications [7]. The reason for this is that now not only the channel gains are estimated with some error, which affects the equalization performance. The inaccurate channel estimates also affect the demixing matrix in the recovering of the spatially multiplexed signal. This, in turn, effects that the distortion on the desired signal is increased by the incorrect cancelation of the signal of the other antenna.

A superficial analysis for a certain subchannel shows that if $w = 1/h$ is the correct equalizer coefficient, being h the actual channel response, and instead of it the inaccurate $\hat{w} = w + \varepsilon_w$ is used, then the estimated signal is in the SISO case and neglecting noise

$$\begin{aligned} \hat{x} &= \hat{w}y = \hat{w}hx \\ &= x + \varepsilon_w hx. \end{aligned} \tag{2.15}$$

However, using the 2x2 MIMO with spatial multiplexing as an example, the estimated signal of the first transmit antenna can be written as

$$\begin{aligned} \hat{x}_1 &= \hat{w}_{11}y_1 + \hat{w}_{12}y_2 \\ &= \hat{w}_{11}\left(h_{11}x_1 + h_{12}x_2\right) + \hat{w}_{12}\left(h_{21}x_1 + h_{22}x_2\right) \\ &= x_1 + \varepsilon_{w_{11}}h_{11}x_1 + \varepsilon_{w_{11}}h_{12}x_2 + \varepsilon_{w_{12}}h_{21}x_1 + \varepsilon_{w_{12}}h_{22}x_2, \end{aligned} \tag{2.16}$$

yielding several more terms distorting the original signal due to the inaccurate equalizer coefficient. This quick analysis does not study if the error of the equalizer coefficients in SISO and MIMO is similar, but under that assumption, the relative degradation of the BER performance in the MIMO case can be understood.

MIMO FTD and CFO estimation (with classical methods)

In this section we present the performance when the whole synchronization/equalization stage is in use in a MIMO system with spatial multiplexing. The system parameters are set as follows: Bursts of 16 AMC23 slots in frequency direction and 8 slots in time direction are transmitted with 4-QAM data. Recall that one AMC23 slot comprises 18 subcarriers and 3 OQAM symbols. The data is being transmitted through a Veh-A channel at an E_b/N_0 = 14 dB, and the simple timing and frequency synchronization approaches thoroughly analyzed for the single antenna case in deliverable D2.2 [1] are applied. In these simulations the further synchronization iteration is omitted due to simulation time constraints, inducing slightly steeper performance degradation with increasing FTD. Figure 2.9 and Figure 2.11 present the BER performance results with increasing FTD and CFO for 2x2 and 2x3 MIMO respectively, while Figure 2.10 presents the 2x2 MIMO case with the iterative interference cancellation technique for joint FTD and channel estimation. The antennas are assumed synchronized, i.e., each MIMO link has the same CFO and FTD as the others.

The main difference with the SISO case is the reduction in CFO range. Because the two-antenna pilot allocation described above in Figure 2.5 is used, the pilot density in time direction is reduced by 2. With double the pilot spacing (one every 12 OQAM subsymbols), the estimation range is therefore also halved, to approximately 8% of the subcarrier bandwidth.

Regarding the estimation quality of the synchronization parameters, compared to the single channel in SISO, there are $N_t \times N_r$ MIMO links. Because the antennas are assumed synchronized among each others, each MIMO link has the same FTD and CFO, and this can be exploited for enhancing the synchronization parameter estimate. The performance gain is small, but best visible in CFO, as the CFO estimation RMS error graph in Figure 2.12 shows. The more links, the more accurately the frequency offset is estimated. Nevertheless, the estimation quality in the SISO case is already very good, so the extra accuracy might be not so crucial at these E_b/N_0 levels. The figure also reflects the shortening of the CFO estimation range mentioned above.

Similar results for the FTD are depicted in Figure 2.13 . As above, there is a marginal increase in estimation accuracy with higher number of links. We recall that in the FTD case, the error is limited by the estimation of the inherent FTD of the channel realization, as explained in [1].

With respect to the interaction between FTD and CFO, the same observations as in SISO results apply: the estimation accuracy of one of these parameters is quite independent from the other.

Finally, the CFO estimation behaviour with changing signal to noise ratio was studied in the SISO and 2x2 MIMO cases with similar simulation setup as above. Perfect timing synchronization is assumed. Simulation results are shown in the following figures. The BER performances behave as expected: similar performance in SISO and MIMO, showing a great degradation when the non-ambiguity region ends. As explained above, this occurs earlier in the MIMO case.

The CFO estimation performance in MIMO transmission is clearly better than in the SISO case because more pilots are used overall to obtain the CFO estimate and a better average is obtained, as can be seen in the following graph. Especially in the noisy case, the difference between SISO and MIMO increases. Nevertheless, the obtained CFO estimation accuracies are that good (error < 0.1%), that the effect on the BER performance is not very big. The small difference in performance between the MIMO and SISO cases is due to the outliers, i.e., the cases in which a bad channel returns a bad estimate and the number of errors increases. The MIMO diversity protects the transmission from these outliers.

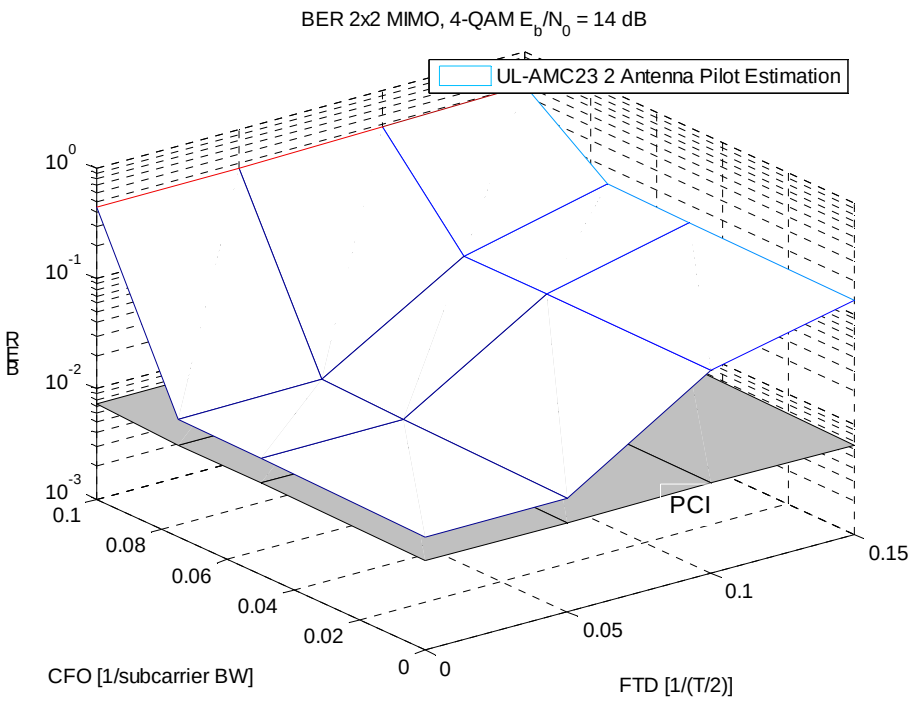

Figure 2.9 BER with respect to CFO and FTD with pilot based synchronization and channel estimation. 2x2 MIMO, Veh-A channels at E_b/N_0 = 14 dB.

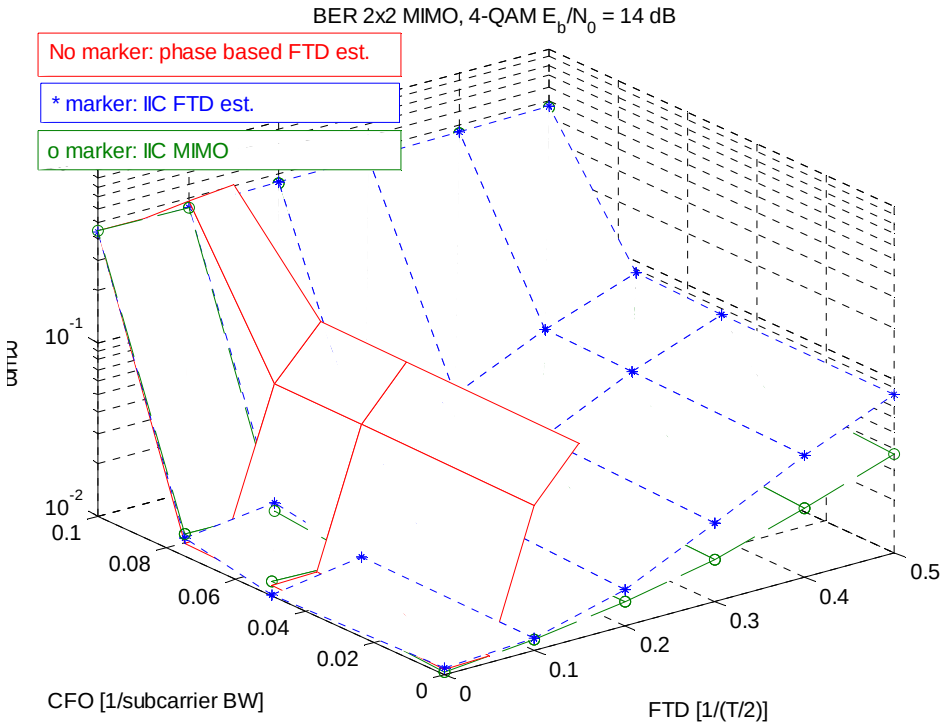

Figure 2.10 BER with respect to CFO and FTD with pilot based synchronization and channel estimation. 2x2 MIMO, Veh-A channels at E_b/N_0 = 14 dB. Comparison of phase rotation based and iterative interference cancellation approaches.

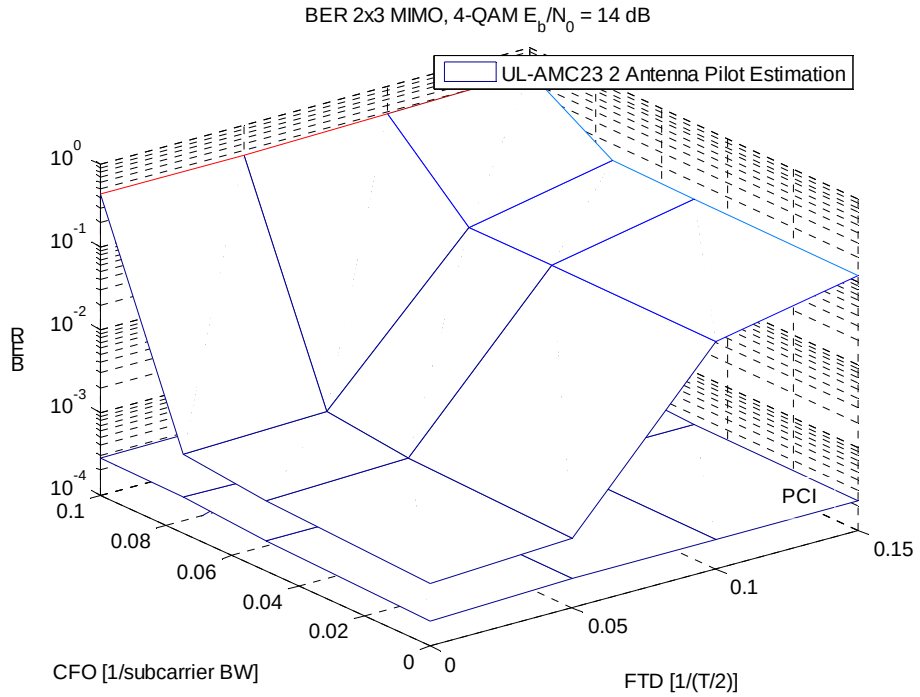

Figure 2.11 BER with respect to CFO and FTD with pilot based synchronization and channel estimation. 2x3 MIMO, Veh-A channels at E_b/N_0 = 14 dB.

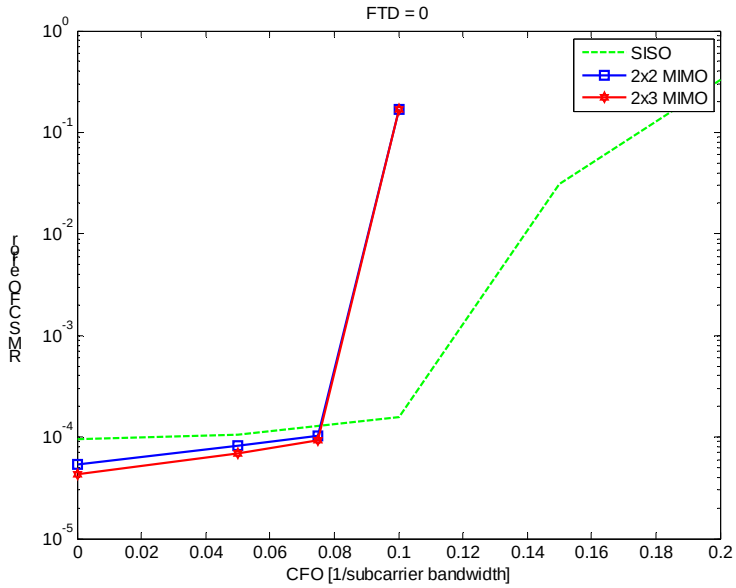

Figure 2.12 RMS CFO estimation error with respect to CFO and with fixed FTD = 0. Different antenna cases, Veh-A channels at E_b/N_0 = 14 dB.

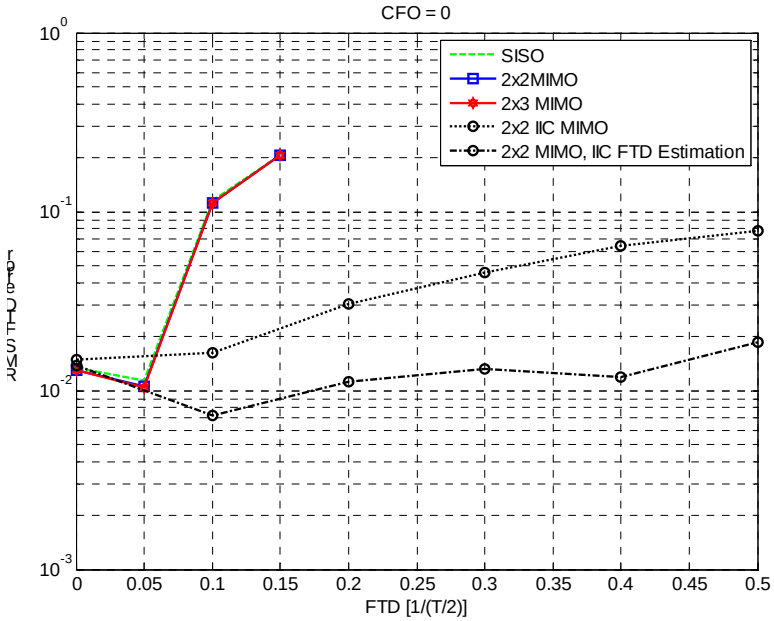

Figure 2.13 RMS FTD estimation error with respect to FTD and with fixed CFO = 0. Different antenna cases, classical FTD estimation and IIC approaches.Veh-A channels at E_b/N_0 = 14 dB.

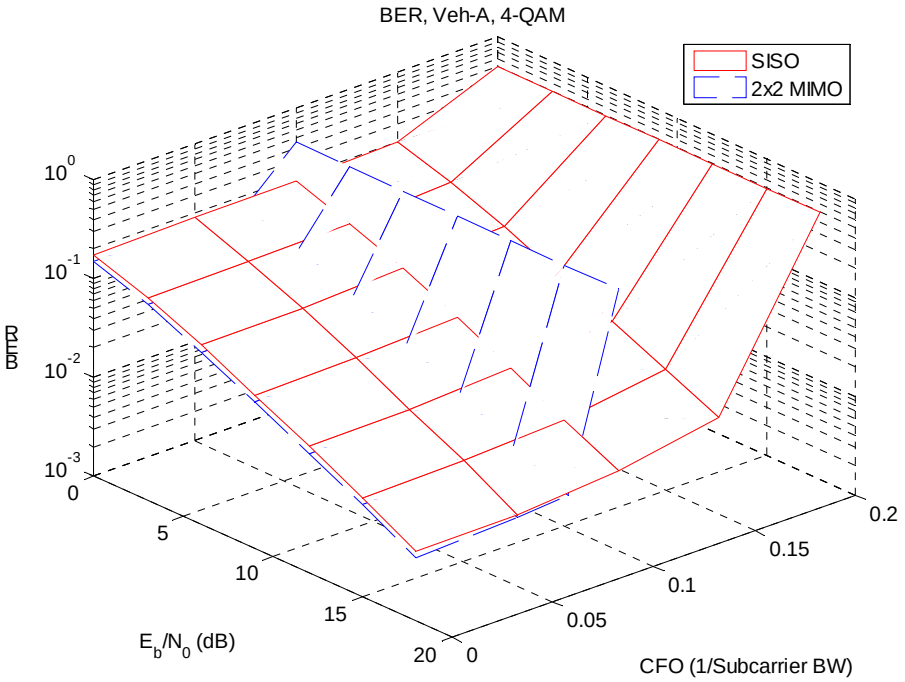

Figure 2.14 BER with respect to CFO and E_b/N_0 with pilot based synchronization and channel estimation. SISO and 2x2 MIMO, Veh-A channels.

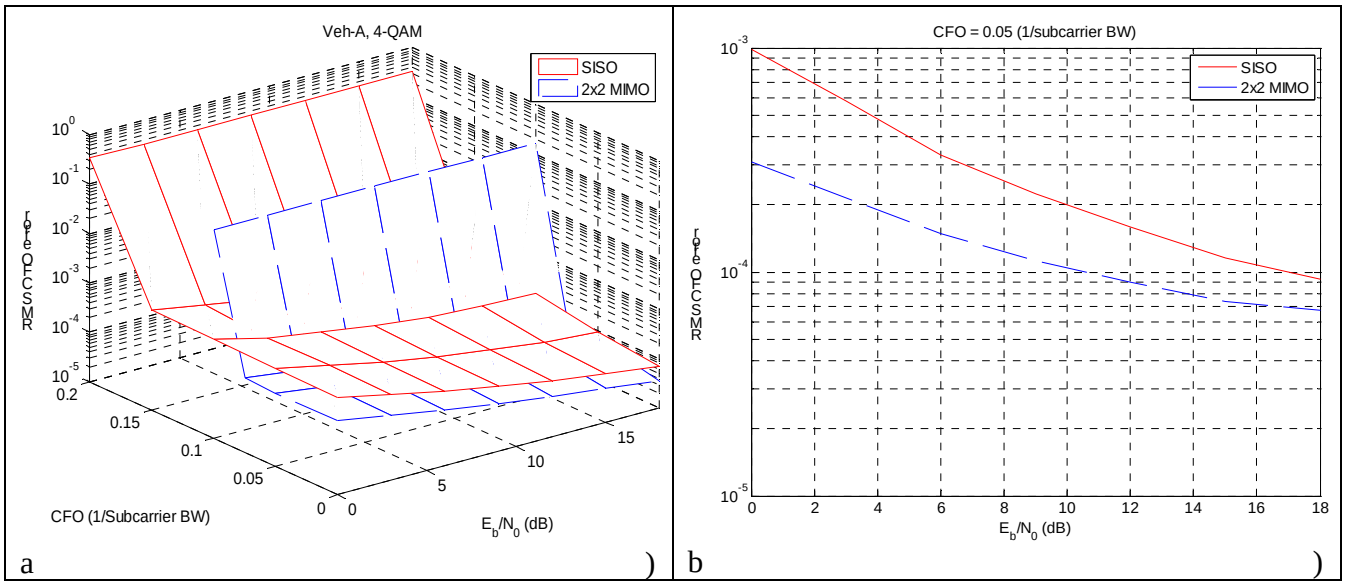

Figure 2.15 CFO estimation RMS error with respect to a) CFO and E_b/N_0 and b) E_b/N_0 with a fixed CFO = 5% of the subchannel bandwidth. Pilot based synchronization and channel estimation. SISO and 2x2 MIMO, Veh-A channels.

2.3 Frequency-sampling based equalization

The frequency-sampling (FS) based equalizer design methodology [9], considered earlier in the context of single-input single-output (SISO) and single-input multiple-output (SIMO) transmission [8], can further be extended to spatially multiplexed multiple-input multiple-output (MIMO) FBMC/OQAM system with frequency selective subchannels. Next, a FS based equalizer solution will be presented for efficient decoupling of different spatially multiplexed and MIMO channel -mixed data streams in an FBMC/OQAM receiver. We will restrict ourselves to linear receiver techniques, which are known to provide low-complexity suboptimal alternatives to the maximum likelihood (ML) detector. Specifically, we will consider the ZF and MSE detection schemes.

The principal idea is to solve the ZF- or MSE-optimized weight (MIMO decoupling) matrix for each of the frequency points considered in the FS design, and to use them as the corresponding target frequency response values. The coefficients of the subcarrier-wise MIMO equalizers can then be derived from a set of closed-form expressions similar to the ones in the SISO case.

Let us assume an $N_t \times N_r$ MIMO configuration with N_t transmit and N_r receive antennas. Further, let us restrict our analysis to antenna configurations satisfying $N_r \geq N_t$ and denote by $H_{k,(i)}^{qp}$ the effective complex-valued channel frequency response coefficient corresponding to the ith target frequency point in the k subchannel for the wireless link between the transmit antenna p and the receive antenna q. Moreover, let us assume that channel estimation can provide estimates of these coefficients for all radio links between different transmit-receive antenna pairs. Then, the MIMO channel induced mixing among different spatially multiplexed data streams $v_k^i[n]$, for $i = 1, \ldots, N_t$, can be modeled in the frequency domain, for each frequency point i and each subchannel k, by an $N_r \times N_t$ matrix given by

$$\mathbf{H}_{k,(i)} = \begin{bmatrix} H_{k,(i)}^{11} & \cdots & H_{k,(i)}^{1p} & \cdots & H_{k,(i)}^{1N_t} \\ \vdots & \vdots & \vdots & \ddots & \vdots \\ H_{k,(i)}^{q1} & \cdots & H_{k,(i)}^{qp} & \cdots & H_{k,(i)}^{qN_t} \\ \vdots & \vdots & \vdots & \ddots & \vdots \\ H_{k,(i)}^{N_r1} & \cdots & H_{k,(i)}^{N_rp} & \cdots & H_{k,(i)}^{N_rN_t} \end{bmatrix} \tag{2.17}$$

In case of the ZF scheme, the weight matrix is given by the Moore-Penrose pseudoinverse of the channel matrix $\mathbf{H}_{k,(i)}$ in (2.17) and can be expressed as

$$\mathbf{G}_{k,(i)}^{ZF} = (\mathbf{H}_{k,(i)}^H \mathbf{H}_{k,(i)})^{-1} \mathbf{H}_{k,(i)}^H \tag{2.18}$$

where superscripts $(.)^H$ and $(.)^{-1}$ represent the Hermitian transpose and an inverse of a square matrix, respectively. While this ZF solution fully decouples the MIMO matrix channel cancelling the interantenna interference (IAI), it ignores the AWGN and may therefore result in significant noise enhancement and performance degradation.

An MMSE receiver makes a tradeoff between IAI mitigation and noise enhancement. For the MSE scheme, the weight matrix writes

$$\mathbf{G}_{k,(i)}^{MMSE} = (\mathbf{H}_{k,(i)}^H \mathbf{H}_{k,(i)} + \rho \mathbf{I}_{N_t})^{-1} \mathbf{H}_{k,(i)}^H \tag{2.19}$$

where $\rho = \sigma_\eta^2/\sigma_v^2$ and $\mathbf{I}_{N_t}$ denote the noise-to-signal power ratio and the $N_t \times N_t$ identity matrix, respectively.
The MMSE solution introduces a bias slightly scaling the signal. This scaling can be compensated for by normalizing $\mathbf{G}_{k,(i)}^{MMSE}$ with the matrix $\mathbf{\Gamma} = \mathbf{D}_{\mathbf{GH}}^{-1}$, where $\mathbf{D}_{\mathbf{GH}}$ is a diagonal matrix. The values of the diagonal of this matrix are the values of the diagonal of the generally non-diagonal product $\mathbf{G}_{k,(i)}^{MMSE}\mathbf{H}_{k,(i)}$.

The FIR MIMO transfer function for a 3-tap equalizer in subchannel k can be expressed as

$$\boldsymbol{\mathcal{W}}_k(z) = \mathbf{W}_k[0]z + \mathbf{W}_k[1] + \mathbf{W}_k[2]z^{-1} \tag{2.20}$$

The frequency points corresponding to the frequency positions of $\mathbf{G}_{k,(i)}$, for $i = 0, 1, 2$, at the low rate are: $-\pi/2$, 0, and $\pi/2$, respectively. By evaluating the transfer function $\boldsymbol{\mathcal{W}}_k(z)$ in (2.20) at these frequency points of interest and setting the resulting expressions equal to $\mathbf{G}_{k,(i)}$, obtained from (2.18) or (2.19) for $i = 0, 1, 2$, the following set of matrix equations can be derived

$$\begin{aligned}
\boldsymbol{\mathcal{W}}_k(e^{-j\frac{\pi}{2}}) &= -j\mathbf{W}_k[0] + \mathbf{W}_k[1] + j\mathbf{W}_k[2] = \mathbf{G}_{k,(0)} \\
\boldsymbol{\mathcal{W}}_k(e^{j0}) &= \mathbf{W}_k[0] + \mathbf{W}_k[1] + \mathbf{W}_k[2] = \mathbf{G}_{k,(1)} \\
\boldsymbol{\mathcal{W}}_k(e^{j\frac{\pi}{2}}) &= j\mathbf{W}_k[0] + \mathbf{W}_k[1] - j\mathbf{W}_k[2] = \mathbf{G}_{k,(2)}
\end{aligned} \tag{2.21}$$

This set of three matrix equations with three unknown matrices $\mathbf{W}_k[0]$, $\mathbf{W}_k[1]$, and $\mathbf{W}_k[2]$, can be easily solved and yields

$$\begin{aligned}
\mathbf{W}_k[0] &= \tfrac{1}{4}((-1+j)\mathbf{G}_{k,(0)} + 2\mathbf{G}_{k,(1)} - (1+j)\mathbf{G}_{k,(2)}) \\
\mathbf{W}_k[1] &= \tfrac{1}{2}(\mathbf{G}_{k,(0)} + \mathbf{G}_{k,(2)}) \\
\mathbf{W}_k[2] &= \tfrac{1}{4}((-1-j)\mathbf{G}_{k,(0)} + 2\mathbf{G}_{k,(1)} - (1-j)\mathbf{G}_{k,(2)})
\end{aligned} \tag{2.22}$$

Now, in order to recover the spatially multiplexed data streams, it is sufficient to apply the solved subcarrier-wise MIMO equalizer $\boldsymbol{\mathcal{W}}_k(z)$ in (2.22) to the received signals in the following way. By writing

$$\mathbf{y}_k[n] = [y_k^1[n], y_k^2[n], \ldots, y_k^{N_r}[n]]^T \tag{2.23}$$

the output of the equalizer for the kth subchannel can be expressed as

$$\tilde{\mathbf{v}}_k[n] = \sum_{i=0}^{2} \mathbf{W}_k[i]\mathbf{y}_k[n-i] \tag{2.24}$$

where $\tilde{\mathbf{v}}_k[n] = [\tilde{v}_k^1[n], \tilde{v}_k^2[n], \ldots, \tilde{v}_k^{N_t}[n]]^T$. Finally, the estimates of the transmitted symbols, denoted by $\hat{\mathbf{a}}_k[l]$, are derived from $\tilde{\mathbf{v}}_k[n]$ by carrying out OQAM demodulation on $\tilde{\mathbf{v}}_k[n]$ and executing hard decisions on $\tilde{\mathbf{a}}_k[l]$.
In this section, we will assess the performance of FBMC/OQAM using the frequency sampling approach for equalization. Both SIMO and MIMO antenna configurations are analyzed in terms of uncoded bit error rate (BER). In SIMO simulations, the obtained error rate performance is compared with the theoretic flat Rayleigh fading reference. We consider the following simulation parameters: A sampling rate of 11.2 MHz, a filter bank with $M = 1024$ subchannels, and a 10 MHz system bandwidth.

The SIMO performance evaluations were carried out using 64-QAM (the alphabet for $a_k[l]$), whereas 16-QAM was considered for the MIMO setup. As for the prototype filter $p[m]$, a frequency-sampling designed NPR lowpass filter with an overlapping factor of $K = 4$ (PHYDYAS reference design) was considered.
We have considered three different multipath channel profiles: the Vehicular A (Veh-A), Extended Vehicular A (Veh-AE), and Vehicular B (Veh-B). In the simulations, random quasi-static channel instances of the above models with AWGN were considered. Moreover, perfect channel information was assumed in the receiver.

SIMO case: Receive diversity mode

The MRC receive diversity equalization was tested in 1×2 ($N_r = 2$) and 1×4 ($N_r = 4$) antenna configurations. Also the performance curves for 1×1 SISO ($N_r = 1$, no diversity) case are shown for comparison. Simulations were carried out using ZF-optimized 1-tap and 3-tap complex FIR equalizers. The BER metrics were estimated over 3000 frames.
Figures 2.16(a) and 2.16(b) show the uncoded BER as a function of E_b/N_o for the Veh-AE and Veh-B channels, respectively. As a general observation we can say that the diversity reception provides considerable SNR gain, when compared to the single-antenna receiver structure. This is true regardless of the channel model considered. Moreover, while the 1-tap and 3-tap CFIR structures obtain approximately equal performance in the Veh-A channel (not shown here), the 3-tap structure shows increasing benefit over the 1-tap structure for the Veh-AE and Veh-B channels with increasing delay spread. This is due to the fact that for these models the channel frequency responses show significant selectivity over the subchannel bandwidth that the one-tap equalizer is unable to compensate. The 3-tap structure, on the other hand, is able to perform frequency selective channel equalization.

MIMO case: Spatial multiplexing mode

Also the FS based MIMO equalizer was put under a test. The uncoded BER performance of the spatially-multiplexed FBMC/OQAM was evaluated in 2×2 and 2×3 antenna configurations. Figures 2.17(a) and 2.17(b) show the error rate performance over the Veh-A and Veh-B channels, respectively, for the 16-QAM modulation. The error rate statistics were obtained by simulating 3000 random quasi-static instances of a specific multipath channel profile. While the MSE-designed 1-tap and 3-tap equalizer structures provide approximately equal performance for both antenna configurations in the Veh-A channel, the results in Figure 2.17(b) clearly speak for the 3-tap solution when transmission over more time dispersive channel profiles is considered.
The theoretic flat Rayleigh fading error rate curves with diversity order of one and two are shown as a reference for the 2×2 and 2×3 antenna configurations, respectively. In case of the Veh-B channel, the FBMC/OQAM performance shows an error floor with respect to the flat fading reference in the high-SNR region. This floor is due to residual ISI, ICI, and IAI post-equalizer components. Equalizer filters of increased order would be required to push down the error floor. Nevertheless, the performance of the 3-tap equalizer in the SNR region of interest, say from 0 to 15 dB where flat Rayleigh fading BER varies within a range of [0.02, 0.2] and [0.001, 0.1] for the 2×2 and 2×3 cases, respectively, is very close to the reference. Moreover, in practice, multicarrier data transmission is always combined with channel coding and interleaving, which would effectively suppress the error floor in the high-SNR region. Figure 2.17(b) also shows that in severely time dispersive channels the multi-tap equalizer structure greatly improves the ability to make use of the increased order of receive diversity present in 2×3 configuration.

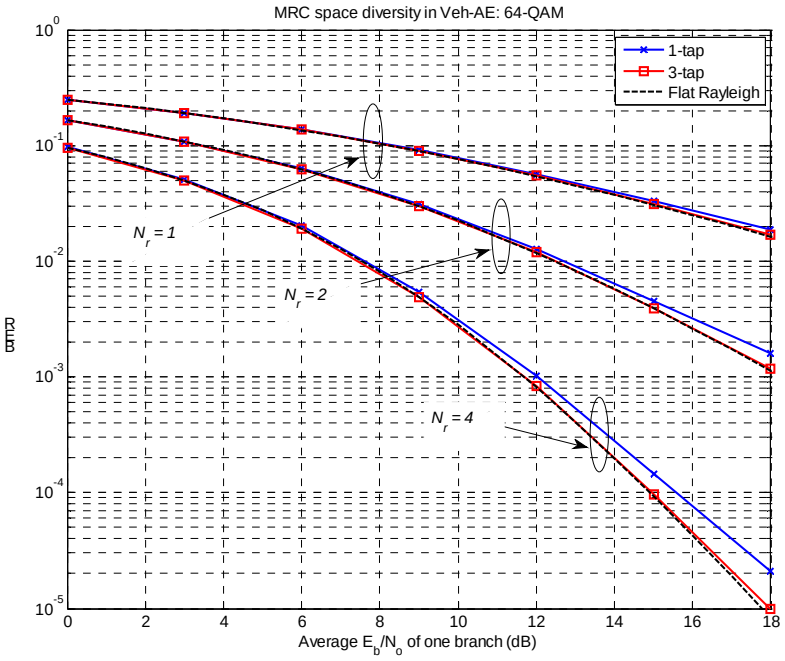

(a)

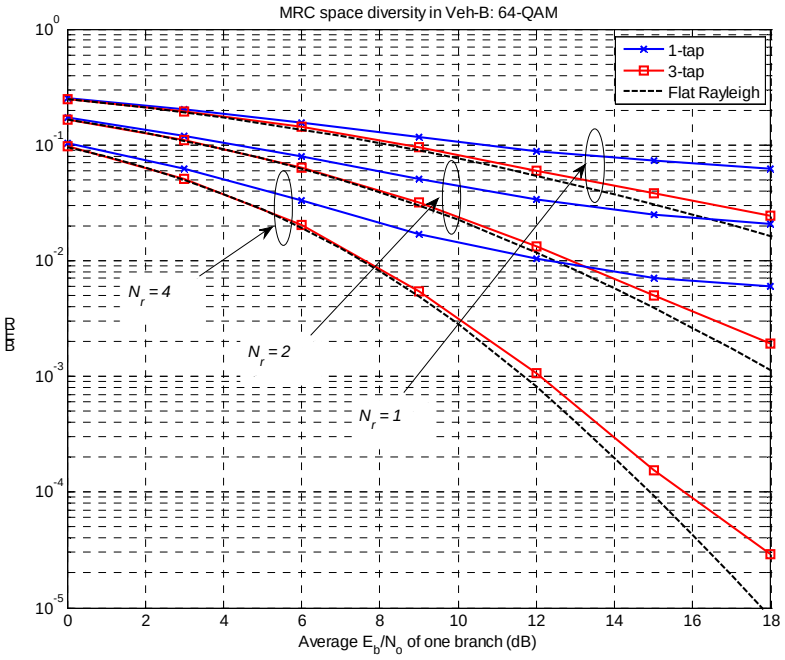

(b)

Figure 2.16 Uncoded bit error rate performance for an FBMC/OQAM system exploiting receive diversity of order N_r = {1,2,4} for transmission over (a) Veh-AE and (b) Veh-B multipath channels, respectively. Perfect channel information and timing synchronization is assumed in the receiver. 64-QAM modulation.

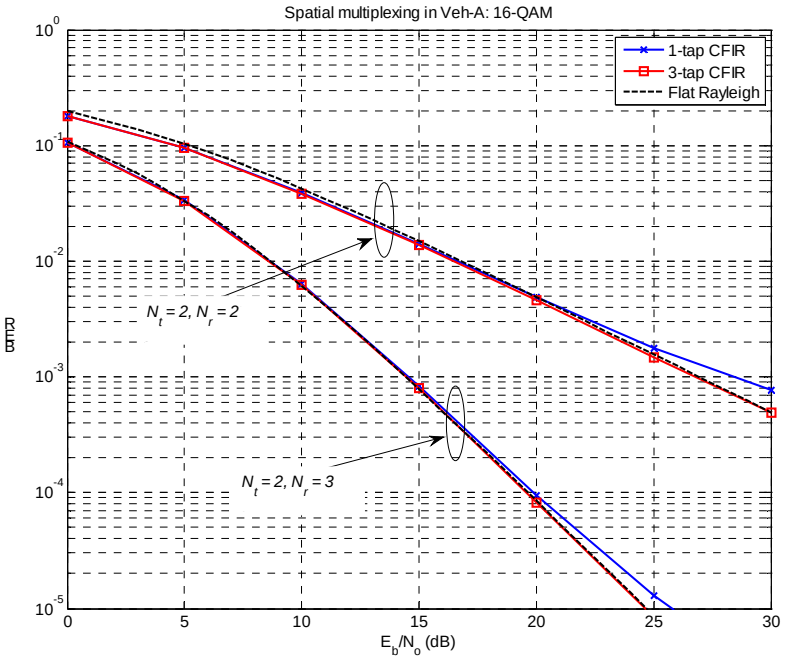

(a)

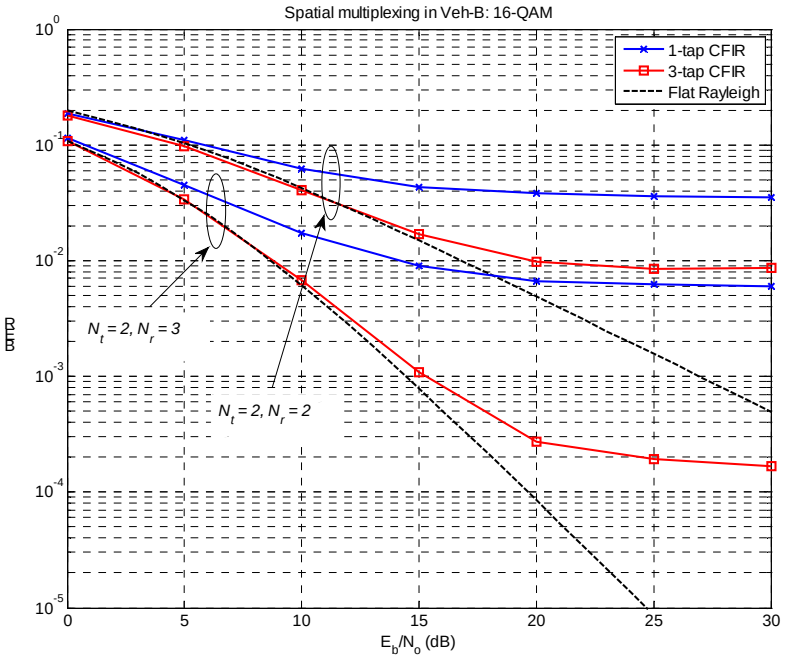

(b)

Figure 2.17. Uncoded bit error rate performance for spatially-multiplexed 2x2 and 2x3 MIMO FBMC/OQAM. The cases of (a) Veh-A and (b) Veh-B channels, respectively. Perfect channel information and timing synchronization is assumed in the receiver. 16-QAM modulation.

2.4 Blind equalization

In this section the problem of blind equalization for MIMO-FBMC is considered. In general, the channel between the transmitter and the receiver is supposed to be known. It can be estimated by sending a sequence from the transmitter, named training sequence, which is known at the receiver side. However, the training sequences do not carry any useful information and hence decrease the useful rate. Blind techniques allow eliminating training sequences and hence increasing the spectral efficiency of the system. They do not require the knowledge of the channel and the transmitted signal can be recovered using only the received signal. In what follows we will focus on the constant modulus (CM) criterion in order to achieve blind equalization. The constant modulus algorithm is probably the best known and most studied algorithm in blind equalization. It was initially designed for PSK signals. Besides its simplicity and robustness in practice, it can be applied even for non-constant modulus communication signals, e.g., QAM signals. The CMA was first implemented via stochastic gradient algorithm and later on many variants have been devised. The main principle of the CM consists in preventing the deviation of the squared modulus of the outputs from a constant named the dispersion constant. Here, we propose to use the CM criterion in order to compute the equalizer for MIMO-FBMC blindly. The proposed technique can be applied only in the case where the number of antennas at the receiver is greater or equal to the number of antennas at the transmitter, which usually corresponds to the uplink case.

We first recall the system model. The notations used below are the same as in Deliverable D4.1 [8]. Under the assumptions of good time-frequency localization for the prototype filter and relatively low frequency selectivity for the channel, the received signal at the output of the k-th analysis filter bank is given by

$$\mathbf{y}_k[n] = \mathbf{H}_k\, \mathbf{x}_k[n] + \boldsymbol{\eta}_k[n] \tag{2.25}$$

where $\mathbf{H}_k = [H_k^{p,q}]$, $p = 1, \dots, N_t$ and $q = 1, \dots, N_r$, with $H_k^{p,q}$ denotes the gain between the p-th transmit and the q-th receive antennas for subchannel k, and it is given by

$$H_k^{p,q} = \sum_{m=0}^{v} h_{pq}[m]\, e^{-j2\pi \frac{km}{M}} \tag{2.26}$$

where $\mathbf{y}_k[n] = [y_k^1[n], \dots, y_k^{N_r}[n]]^T$, $\mathbf{x}_k[n] = [x_k^1[n], \dots, x_k^{N_t}[n]]^T$, where $\theta_k^*[n]\, x_k^i[n] = d_k^i[n] + j u_k^i[n]$ is the complex symbol to be transmitted, and $\boldsymbol{\eta}_k[n] = [\eta_k^1[n], \dots, \eta_k^{N_r}[n]]^T$ is the additive noise vector.

Here, we assume that the channel matrices $\mathbf{H}_k$ are unknown at the receiver side and our aim is to recover the transmitted signals using only the received signals $\mathbf{y}_k[n]$. In the following, for each subchannel, we assume that: the channel matrix is full column rank (and hence $N_r \geq N_t$), the transmitted signals are *i.i.d.* and mutually independent, and the noise is additive and independent from the transmitted signal.

We assume a MIMO equalizer using 1-tap per subchannel and per antenna. Hence for subchannel k, in order to recover the signal part of $\mathbf{x}_k[n]$, the received signal $\mathbf{y}_k[n]$ is filtered using some equalization matrix $\mathbf{W}_k$. We have

$$\tilde{\mathbf{v}}_k[n] = \mathbf{W}_k^H \mathbf{y}_k[n] \tag{2.27}$$

Ideally, matrix $\mathbf{W}_k$ recovers the signal $\mathbf{x}_k[n]$, except for a possible permutation and up to a phase rotation (to remove these ambiguities a short training sequence is always required), i.e., in the noise free case, we have

$$\mathbf{W}_k^H \mathbf{y}_k[n] = \mathbf{P}_k \mathbf{D}_k \mathbf{x}_k[n] \tag{2.28}$$

where $\mathbf{P}_k$ is a permutation matrix and $\mathbf{D}_k$ is a nonsingular diagonal matrix.

In order to compute the equalization matrix $\mathbf{W}_k = [\mathbf{w}_{k,1}, \ldots, \mathbf{w}_{k,N_t}]$, we propose to minimize the classical CM criterion [10,11]. By taking the property of OQAM modulation, which is sending the real and imaginary part alternatively in both time and frequency axes, for even subchannels, the criterion is written as

$$J_k = \sum_{i=1}^{N_t} E\left[\Re\left(\tilde{v}_k^i[2n]\right)^2 + \Im\left(\tilde{v}_k^i[2n+1]\right)^2 - R\right]^2 \tag{2.29}$$

for even subchannel and as

$$J_k = \sum_{i=1}^{N_t} E\left[\Im\left(\tilde{v}_k^i[2n]\right)^2 + \Re\left(\tilde{v}_k^i[2n+1]\right)^2 - R\right]^2 \tag{2.30}$$

for odd subchannels, where $E[.]$ denotes the expectation, R is the dispersion factor given by

$$R = \frac{E[|a[i]|^4]}{E[|a[i]|^2]}, \tag{2.31}$$

where a represents the symbols to be transmitted, and $\Re\{.\}$ and $\Im\{.\}$ denote the real and imaginary parts, respectively.

Note that we can use the principle of the multimodulus algorithm (MMA) [12] where the real and imaginary parts can be constrained separately. In our case the MMA criterion can be written as

$$J_k = \sum_{i=1}^{N_t} E\left[\left(\Re\left(\tilde{v}_k^i[2n]\right)^2 - R_R\right)^2\right] + E\left[\left(\Im\left(\tilde{v}_k^i[2n+1]\right)^2 - R_I\right)^2\right] \tag{2.32}$$

where

$$R_R = R_I = \frac{E[\Re\{a[i]\}^4]}{E[\Re\{a[i]\}^2]} = \frac{E[\Im\{a[i]\}^4]}{E[\Im\{a[i]\}^2]}. \tag{2.33}$$

For odd subchannels we interchange the real and imaginary operations in (2.32). In the following, we only use the CM criterion and only consider the criterion for even subchannels, since the development is the same for odd subchannels. Note that the minimization of the CM criterion can be achieved in both batch and adaptive ways. Here, we are interested in the batch solution. For this purpose, let us suppose that K_s samples are available at the receiver side.

For the batch solution, we can write the problem as a least square problem [11]

$$\mathbf{W}_k = \arg\min_{\mathbf{W}_k} \frac{1}{L}\sum_{t=1}^{N_t}\sum_{n=0}^{L-1} E\left[\left(\Re\left(\tilde{v}_k^t[2n]\right)^2 + \Im\left(\tilde{v}_k^t[2n+1]\right)^2 - R\right)^2\right] \quad (2.34)$$

where $L = K_s/2$. Let

$$\bar{\mathbf{w}}_{k,t} = \begin{bmatrix}\Re\{\mathbf{w}_{k,t}\}\\ \Im\{\mathbf{w}_{k,t}\}\end{bmatrix},\ \bar{\mathbf{y}}_k[2n] = \begin{bmatrix}\Re\{\mathbf{y}_k[2n]\}\\ \Im\{\mathbf{y}_k[2n]\}\end{bmatrix} \text{ and } \bar{\mathbf{y}}_k[2n+1] = \begin{bmatrix}\Im\{\mathbf{y}_k[2n+1]\}\\ -\Re\{\mathbf{y}_k[2n+1]\}\end{bmatrix} \quad (2.35)$$

Then, we have

$$\Re\left\{\tilde{v}_k^t[2n]\right\} = \Re\left\{\mathbf{w}_{k,t}^H\mathbf{y}_k[2n]\right\} = \bar{\mathbf{w}}_{k,t}^T\bar{\mathbf{y}}_k[2n] \quad (2.36)$$

Similarly

$$\Im\left\{\tilde{v}_k^t[2n+1]\right\} = \Im\left\{\mathbf{w}_{k,t}^H\mathbf{y}_k[2n+1]\right\} = \bar{\mathbf{w}}_{k,t}^T\bar{\mathbf{y}}_k[2n+1] \quad (2.37)$$

By considering (2.36) and (2.37), (2.34) can be written as

$$\mathbf{W}_k = \arg\min_{\mathbf{W}_k} \frac{1}{L}\sum_{t=1}^{N_t}\sum_{n=0}^{L-1}\left[\left(\bar{\mathbf{w}}_{k,t}^T\bar{\mathbf{y}}_k[2n]\right)^2 + \left(\bar{\mathbf{w}}_{k,t}^T\bar{\mathbf{y}}_k[2n+1]\right)^2 - R\right]^2 \quad (2.38)$$

Moreover, we have

$$\begin{aligned}&\left(\bar{\mathbf{w}}_{k,t}^T\bar{\mathbf{y}}_k[2n]\right)^2 + \left(\bar{\mathbf{w}}_{k,t}^T\bar{\mathbf{y}}_k[2n+1]\right)^2\\ &= \bar{\mathbf{w}}_{k,t}^T\bar{\mathbf{y}}_k[2n]\bar{\mathbf{y}}_k[2n]^T\bar{\mathbf{w}}_{k,t} + \bar{\mathbf{w}}_{k,t}^T\bar{\mathbf{y}}_k[2n+1]\bar{\mathbf{y}}_k[2n+1]^T\bar{\mathbf{w}}_{k,t}\\ &= \left(\bar{\mathbf{y}}_k[2n]\otimes\bar{\mathbf{y}}_k[2n] + \bar{\mathbf{y}}_k[2n+1]\otimes\bar{\mathbf{y}}_k[2n+1]\right)^T\left(\bar{\mathbf{w}}_{k,t}\otimes\bar{\mathbf{w}}_{k,t}\right)\end{aligned} \quad (2.39)$$

Where $\otimes$ denotes the Kronecker product.

Let $\mathbf{\Gamma}_k = [(\bar{\mathbf{y}}_k[0]\otimes\bar{\mathbf{y}}_k[0] + \bar{\mathbf{y}}_k[1]\otimes\bar{\mathbf{y}}_k[1]),\dots,(\bar{\mathbf{y}}_k[K-2]\otimes\bar{\mathbf{y}}_k[K-2] + \bar{\mathbf{y}}_k[K-1]\otimes\bar{\mathbf{y}}_k[K-1])]^T$ be an $L\times 4N_r^2$ matrix and $\mathbf{z}_{k,t} = \bar{\mathbf{w}}_{k,t}\otimes\bar{\mathbf{w}}_{k,t}$ a $4N_r^2\times 1$ vector.

Therefore, the least square problem can be rewritten as [11]

$$J_k = \sum_{t=1}^{N_t}\left\|\mathbf{\Gamma}_k\mathbf{z}_{k,t} - \mathbf{1}\right\|^2 \quad (2.40)$$

where $\mathbf{1} = [1,\dots,1]^T$. Our aim is to minimize J_k under the constraint $\mathbf{z}_{k,t} = \overline{\mathbf{cw}}_{k,t}\otimes\bar{\mathbf{w}}_{k,t}$, $t = 1,\dots,N_t$, that is to say, find the vectors $\mathbf{z}_{k,t}$ of the particular form above that minimizes J_k. Our optimization problem is very similar to the optimization problem of the analytical CMA (ACMA) in [11], therefore in the following we will proceed exactly in the same way as in [11]. Here, we will give a rough description of the algorithm and for more details refer to [11]. Let $\mathbf{Q}$ be an $L\times L$ unitary matrix such that

$\mathbf{Q}\,\mathbf{1} = \sqrt{L}\begin{bmatrix}1\\0\end{bmatrix}$, which can be for example the Fourier matrix. By applying $\mathbf{Q}$ to $[\mathbf{1}\ \boldsymbol{\Gamma}_k]$ and partition the result as [11]

$$\mathbf{Q}\,[\mathbf{1}\ \boldsymbol{\Gamma}_k] = \sqrt{L}\begin{bmatrix}1 & \mathbf{p}_k^T\\ \mathbf{0} & \mathbf{G}_k\end{bmatrix} \tag{2.41}$$

Moreover

$$\boldsymbol{\Gamma}_k \mathbf{z}_{k,t} = \mathbf{1} \iff \mathbf{Q}\,[\mathbf{1}\ \boldsymbol{\Gamma}_k]\begin{bmatrix}-1\\ \mathbf{z}_{k,t}\end{bmatrix} = \mathbf{0} \iff \begin{cases}\mathbf{p}_k^T\mathbf{z}_{k,t} = 1\\ \mathbf{G}_k\,\mathbf{z}_{k,t} = \mathbf{0}\end{cases} \tag{2.42}$$

Using (2.42), (2.40) can be written as

$$J_k = \sum_{t=1}^{N_t}\left|\mathbf{p}_k^T\mathbf{z}_{k,t} - 1\right|^2 + \left\|\mathbf{G}_k\mathbf{z}_{k,t}\right\|^2 \tag{2.43}$$

The first term in (2.43) prevents the trivial solution $\mathbf{z}_{k,t} = \mathbf{0}$ and the second term requires that $\mathbf{z}_{k,t}$ should be in the nullspace of $\mathbf{G}_k$. In order to obtain explicit expressions for $\mathbf{p}_k$ and $\mathbf{G}_k$, we square (2.41), which results in

$$\mathbf{p}_k = \frac{1}{L}\boldsymbol{\Gamma}_k^T\mathbf{1} \qquad \text{and} \qquad \mathbf{C}_k = \mathbf{G}_k^T\mathbf{G}_k = \frac{1}{L}\boldsymbol{\Gamma}_k^T\boldsymbol{\Gamma}_k - \frac{1}{L}\boldsymbol{\Gamma}_k^T\mathbf{1}\,\mathbf{1}^T\boldsymbol{\Gamma}_k \tag{2.44}$$

Furthermore, we have

$$\mathbf{p}_k^T\mathbf{z}_{k,t} = \bar{\mathbf{w}}_{k,t}^T\bar{\mathbf{R}}_{\mathbf{y}}\bar{\mathbf{w}}_{k,t} \tag{2.45}$$

where $\bar{\mathbf{R}}_{\mathbf{y}} = \frac{1}{L}\left(\bar{\mathbf{y}}_k[2n]\bar{\mathbf{y}}_k[2n]^T + \bar{\mathbf{y}}_k[2n+1]\bar{\mathbf{y}}_k[2n+1]^T\right)$.

In order to simplify the following derivation, we first apply prewhitening to the received signal $\mathbf{y}_k[n]$. This procedure is described in detail in [11]. It first produces a covariance estimation based on the K_s received samples, and then computes the prewhitening matrix. After prewhitening, we now have $\bar{\mathbf{R}}_{\mathbf{y}} = \mathbf{I}$, and hence

$$\mathbf{p}_k^T\mathbf{z}_{k,t} = \bar{\mathbf{w}}_{k,t}^T\bar{\mathbf{R}}_{\mathbf{y}_k}\bar{\mathbf{w}}_{k,t} = \bar{\mathbf{w}}_{k,t}^T\bar{\mathbf{w}}_{k,t} = \left\|\bar{\mathbf{w}}_{k,t}\right\|^2 \tag{2.46}$$

Moreover, we have $\left\|\mathbf{z}_{k,t}\right\|^2 = \left\|\bar{\mathbf{w}}_{k,t}\right\|^4$. Then

$$\mathbf{p}_k^T\mathbf{z}_{k,t} = \left\|\bar{\mathbf{w}}_{k,t}\right\|^2 = \left\|\mathbf{z}_{k,t}\right\| \tag{2.47}$$

The optimization is difficult to carry out directly. So a simplified optimization is first performed by relaxing the constraint on $\mathbf{z}_{k,t}$. The problem is written as [11]

$$\mathbf{Z}_k = \arg\min_{\mathbf{Z}_k^T\mathbf{Z}_k = \mathbf{I}} \sum_{t=1}^{N_t}\sum_{n=0}^{L-1}\mathbf{z}_{k,t}^T\,\underline{\mathbf{C}}_k\,\mathbf{z}_{k,t} \tag{2.48}$$

where $\underline{\mathbf{C}}_k$ is $\mathbf{C}_k$ in (2.44) computed using the prewhitened received signal. In (2.48), $\mathbf{z}_{k,i}$ only needs to satisfy the unitary constraint but does no longer need to have the particular structure described above. Note that the prewhitening also reduces the size of the channel matrix from $N_r \times N_t$ to $N_t \times N_t$.

The solution of the optimization problem in (2.48) is known and corresponds to the N_t eigenvectors of $\mathbf{C}_k$ corresponding to the N_t least eigenvalues. Note that the solution $\mathbf{Z}_k$, represents an orthonormal basis for the nullspace of $\underline{\mathbf{C}}_k$. Once this first step is performed, $\bar{\mathbf{W}}_k$ can be found by looking for a set of N_t unit-norm vectors $\bar{\mathbf{w}}_{k,i} \otimes \bar{\mathbf{w}}_{k,i}$ that best spans the same subspace as $\mathbf{Z}_k$. As shown in [11], this final step can be shown to be equivalent to the following joint diagonalization problem,

$$\bar{\mathbf{W}}_k = \arg\min_{\bar{\mathbf{W}}_k, \mathbf{\Lambda}} \quad \sum_{i=1}^{N_t} \left\| \mathbf{Z}_{k,i} - \bar{\mathbf{W}}_k \mathbf{\Lambda}_i \bar{\mathbf{W}}_k^T \right\|_F^2 \tag{2.49}$$

where $\mathbf{\Lambda}_i$ is a diagonal matrix constructed from the i-th column of $\mathbf{\Lambda}$ which is in turn an $N_t \times N_t$ full column matrix, and $\mathbf{Z}_{k,i}$ is a matrix obtained by unstacking $\mathbf{z}_{k,i}$ into a $2N_t \times 2N_t$ matrix. A simple joint diagonalization algorithm is described in [11], where more details on a development similar to the above one can also be found. Note that the optimization here is performed jointly on $\bar{\mathbf{W}}_k$ and $\mathbf{\Lambda}$, but only the former matrix is of interest in our problem.

From (2.38), the equalization matrix $\mathbf{W}_k$ can easily be deduced from $\bar{\mathbf{W}}_k$. Now in order to recover the transmitted signal, we simply apply the equalization matrix, for each subchannel, to the prewhitened received signal, followed by the OQAM demodulation step.

We now assess the performance of the proposed blind algorithm and the classical MIMO frequency domain equalizer presented in [8], by comparing them in terms of uncoded bit error rate (BER). Note that in the frequency domain equalizer (also called one tap equalizer in [8]), the channel is assumed to be perfectly estimated by the receiver. We consider the following simulation parameters: $M = 64$ carriers, overlapping factor $K = 4$, 4-QAM and 16-QAM modulation, $N_t = 2$, $N_r = 3$. The MIMO FIR channels are chosen randomly. All simulation results are averaged over 100 independent realizations. For brevity, in the figures we refer to the proposed technique by the term “blind”, and the classical frequency domain equalizer by “one tap”. Note that the two techniques use one tap equalizer.
In Figure 2.18, we consider the 4-QAM constellation. We observe that the proposed algorithm (blind in the figure) provides good performance. The classical frequency domain equalizer (one tap in the figure), outperforms the proposed blind algorithm. For short channels, 2 taps, the gap is 2 dB for low SNRs and 1 dB for high SNRs. For longer channels, the gap is around 2 dB for almost all SNRs. It should be noted that with the proposed blind algorithm no training sequence is required, and hence the useful rate using this algorithm is higher than the one using the frequency domain equalizer [8].
Figure 2.19 shows the case of 16-QAM constellation. In this case, we observe that the two techniques have almost the same performance.

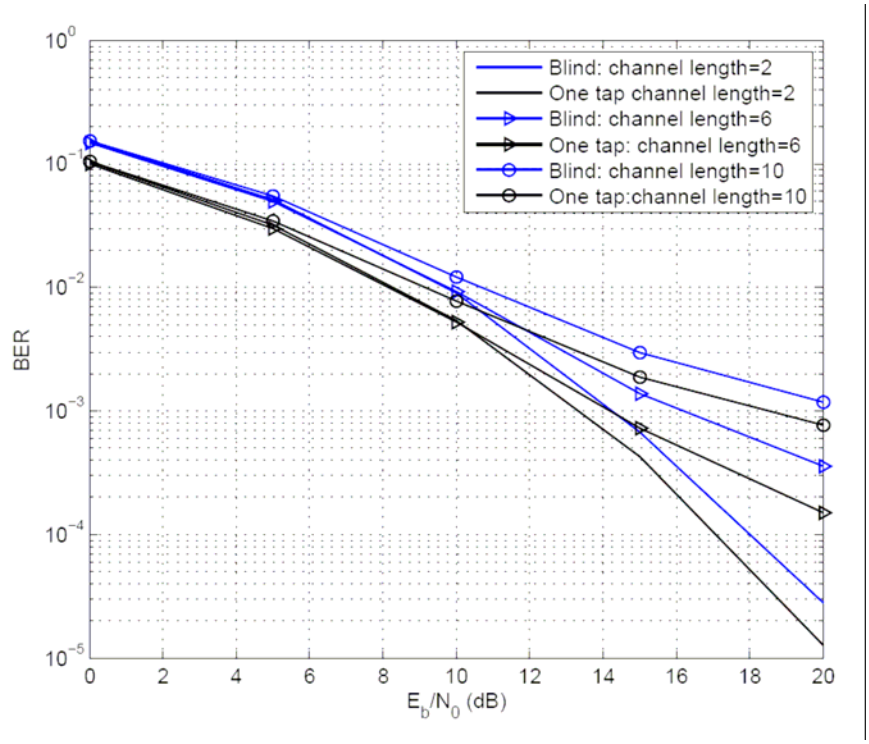

Figure 2.18 Comparison of the proposed blind technique with the classical frequency domain equalizer in terms of uncoded BER as a function of E_b/N_0 for different channel lengths. The case of 4-QAM constellation.

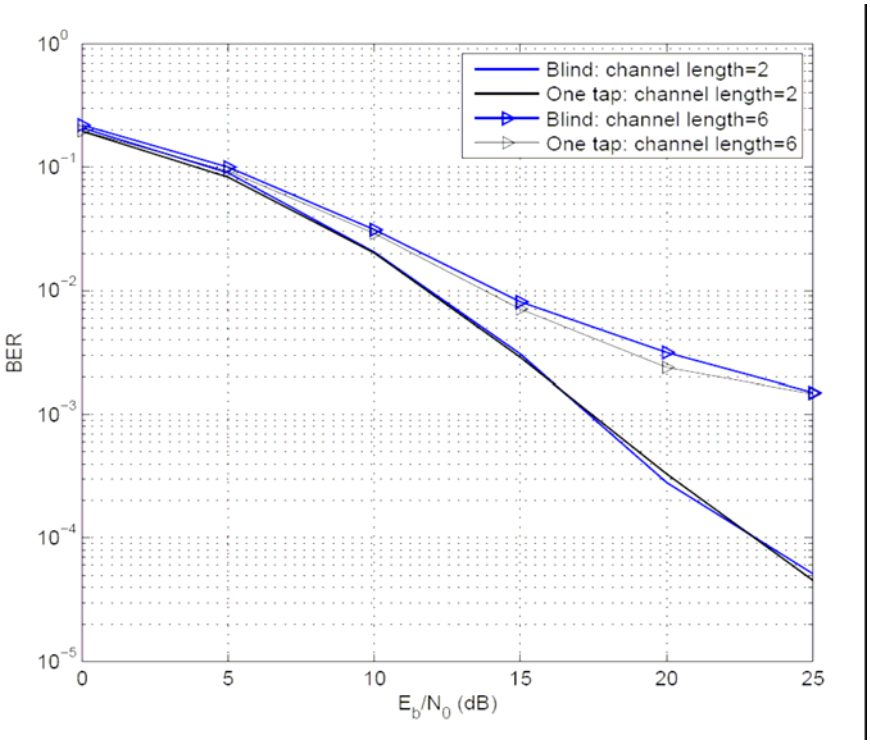

Figure 2.19 Comparison of the proposed blind technique with the classical frequency domain equalizer in terms of uncoded BER as a function of E_b/N_0 for different channel lengths. The case of 16-QAM constellation**.**

2.5 MIMO Channel Tracking

In a mobile environment, the channel may vary with time and hence its estimate acquired in the preamble needs to be kept up to date in the rest of the frame. In a previous deliverable (D4.1 [8]), a Kalman filter-based method for tracking the channel was presented for the case that a model for the channel time evolution is available. In this section, the problem of MIMO channel tracking in time-varying FBMC/OQAM systems is revisited, for the case that we don't have a model for the channel variation. Two scenarios are considered: (a) decision-directed (no pilots) and (b) pilot-aided tracking.

2.5.1 Decision-directed LMS Channel Tracking

Consider an $N_t \times N_r$ FBMC/OQAM system with well localized pulse shaping filters and recall that, in this case, the output of the AFB at the subcarrier k and symbol n, after de-rotation with $\theta_{k,n}^*$, can be well approximated by

$$\tilde{\mathbf{y}}_{k,n} = \mathbf{H}_{k,n}\tilde{\mathbf{x}}_{k,n} + \boldsymbol{\eta}_{k,n}, \tag{2.50}$$

where $\mathbf{H}_{k,n}$ is the $N_r \times N_t$ frequency response of the channel at the (k,n) point and $\tilde{\mathbf{x}}_{k,n} = \mathbf{d}_{k,n} + j\mathbf{u}_{k,n}$ the corresponding *virtual* (complex) input symbol, consisting of the *real* input symbol $\mathbf{d}_{k,n}$ and the associated *imaginary* (intrinsic) interference $j\mathbf{u}_{k,n}$. We will develop a scheme for tracking the channel using only a short preamble for obtaining an initial estimate. For the rest of the frame, the channel is tracked in a decision-directed manner. Let $k_0, k_1, \ldots, k_{P-1}$ be the set of P subcarriers where the decisions for the channel tracking are to be made. The AFB output at these subcarriers and for the qth receive antenna will be given by

$$\tilde{y}_{k_i,n}^q = H_{k_i,n}^{1,q}\tilde{x}_{k_i,n}^1 + H_{k_i,n}^{2,q}\tilde{x}_{k_i,n}^2 + \cdots + H_{k_i,n}^{N_t,q}\tilde{x}_{k_i,n}^{N_t} + \eta_{k_i,n}^q, \tag{2.51}$$

for $i = 0,1,\ldots,P-1$ and $q = 1,2,\ldots,N_r$. Collecting all the above samples in a $P\times 1$ vector $\tilde{\mathbf{y}}_n^q$ and expressing the frequency response in terms of the channel impulse response (of length L_h), we can write

$$\tilde{\mathbf{y}}_n^q = \mathbf{D}_n^1\mathbf{F}_{P\times L_h}\mathbf{h}_n^{1,q} + \mathbf{D}_n^2\mathbf{F}_{P\times L_h}\mathbf{h}_n^{2,q} + \cdots + \mathbf{D}_n^{N_t}\mathbf{F}_{P\times L_h}\mathbf{h}_n^{N_t,q} + \boldsymbol{\eta}_n^q, \tag{2.52}$$

where

$$\mathbf{D}_n^p = \mathrm{diag}\left(\tilde{x}_{k_0,n}^p, \tilde{x}_{k_1,n}^p, \ldots, \tilde{x}_{k_{P-1},n}^p\right), \qquad p = 1,2,\ldots,N_t, \tag{2.53}$$

$\mathbf{F}_{P\times L_h}$ is the $P\times L_h$ submatrix of the M th-order DFT matrix consisting of its first L_h columns and its rows corresponding to the *decision* subcarriers, and $\mathbf{h}_n^{p,q}$ is the impulse response of the channel from the transmit antenna p to the receive antenna q. The above can be written more compactly as

$$\tilde{\mathbf{y}}_n^q = \mathbf{T}_n\mathbf{h}_n^q + \boldsymbol{\eta}_n^q, \tag{2.54}$$

where

$$\mathbf{h}_n^q = \left[\left(\mathbf{h}_n^{1,q}\right)^T \quad \left(\mathbf{h}_n^{2,q}\right)^T \quad \cdots \quad \left(\mathbf{h}_n^{N_t,q}\right)^T\right]^T \tag{2.55}$$

is the collection of the channels from all transmit antennas to the qth receive antenna, and the $P\times N_t L_h$ matrix $\mathbf{T}_n$ is given by

$$\mathbf{T}_n = \left[\mathbf{D}_n^1\mathbf{F}_{P\times L_h} \quad \mathbf{D}_n^2\mathbf{F}_{P\times L_h} \quad \cdots \quad \mathbf{D}_n^{N_t}\mathbf{F}_{P\times L_h}\right] \tag{2.56}$$

The $P \geq N_t L_h$ subcarriers should be chosen so as to be *equispaced*, as in this case $\mathbf{F}_{P\times L_h}$ is in its best condition, with $\mathbf{F}_{P\times L_h}\mathbf{F}_{P\times L_h}^H = L_h\mathbf{I}_P$, and $E\left(\mathbf{T}_n\mathbf{T}_n^H\right) = \sigma_x^2 N_t L_h \mathbf{I}_P$ with $\sigma_x^2 = E\left(\left|\tilde{x}_{k,n}^p\right|^2\right)$.

Stacking the above equations for all receive antennas, we obtain

$$\tilde{\mathbf{y}}_n = \underbrace{\left(\mathbf{I}_{N_r} \otimes \mathbf{T}_n\right)}_{\mathbf{S}_n}\mathbf{h}_n + \boldsymbol{\eta}_n = \mathbf{S}_n\mathbf{h}_n + \boldsymbol{\eta}_n, \tag{2.57}$$

where

$$\tilde{\mathbf{y}}_n = \left[\left(\tilde{\mathbf{y}}_n^1\right)^T \quad \left(\tilde{\mathbf{y}}_n^2\right)^T \quad \cdots \quad \left(\tilde{\mathbf{y}}_n^{N_r}\right)^T\right]^T, \tag{2.58}$$

$$\mathbf{h}_n = \left[\left(\mathbf{h}_n^1\right)^T \quad \left(\mathbf{h}_n^2\right)^T \quad \cdots \quad \left(\mathbf{h}_n^{N_r}\right)^T\right]^T, \tag{2.59}$$

and

$$\mathbf{S}_n = \mathbf{I}_{N_r} \otimes \mathbf{T}_n \tag{2.60}$$

Based on the above formulation, we can develop a decision-directed tracking scheme as follows. Let the decisions at the selected subcarriers at time n be made on the basis of the channel estimate available at the previous time, $n-1$. For example, using a zero-forcing (ZF) frequency-domain equalizer[1], the decision making step can be expressed as:

$$\hat{\mathbf{x}}_{k_i,n} = \hat{\mathbf{H}}_{k_i,n-1}^{\dagger}\tilde{\mathbf{y}}_{k_i,n} \tag{2.61}$$

and

$$\hat{\tilde{\mathbf{x}}}_{k_i,n} = \hat{\mathbf{d}}_{k_i,n} + j\hat{\mathbf{u}}_{k_i,n} = \mathrm{dec}\left[\mathrm{Re}\left(\hat{\mathbf{x}}_{k_i,n}\right)\right] + j\,\mathrm{Im}\left(\hat{\mathbf{x}}_{k_i,n}\right), \tag{2.62}$$

where $\hat{\mathbf{H}}_{k_i,n-1}^{\dagger}$ is the pseudo-inverse of the estimated channel frequency response at subcarrier k_i and time $n-1$, and $\mathrm{dec}[\bullet]$ is the quantization function associated with the input OQAM constellation. These decisions are then used to build matrices $\hat{\mathbf{D}}_n^p$ and hence the matrix $\hat{\mathbf{S}}_n$ as above. The channel estimate can then be updated invoking the LMS recursion [13]:

$$\mathbf{e}_n = \tilde{\mathbf{y}}_n - \hat{\mathbf{S}}_n\hat{\mathbf{h}}_{n-1}, \tag{2.63}$$

$$\hat{\mathbf{h}}_n = \hat{\mathbf{h}}_{n-1} + \mu\hat{\mathbf{S}}_n^H\mathbf{e}_n, \tag{2.64}$$

with μ being the step size of the algorithm. Note that the initial estimate for the channel can come from a preamble-based channel estimation step (see [8]).

Observe that in the above decision making process, the intrinsic interference is simply taken as the imaginary part of the soft estimate of $\tilde{\mathbf{x}}$. This tracking scheme will be called "Tracking A" in the following. Nevertheless, a better estimate of the interference part can be computed, especially for low-order constellations, by quantizing the imaginary part of $\hat{\tilde{\mathbf{x}}}$ over the codebook of all possible interference values. This codebook can be *a-priori* computed based on the assumption that interference mainly comes from the first-order time-frequency neighbors and using our knowledge of the prototype filter used in our filter banks. The latter yields readily the weights of the contributions from the neighbors of any given point to the interference at that point. Thus, for example with OQPSK input, the eight first-order neighbors result in $2^8 = 256$ possible interference values, which, in fact, reduce to only

[1] One can also use other, more sophisticated equalizers, such as the MMSE one or a V-BLAST equalizer.

65, due to the underlying symmetries. One can then quantize the interference estimate above to the closest value out of these 65 levels. Although this increases the cost of the decision making step, it can significantly improve the performance of the above tracking scheme, as the following simulation results will exemplify. It should also be noted that the codebook of interference levels is to be computed *off-line*. Let us call this modified tracking scheme as "Tracking B."

Figure 2.20 shows some results from simulating the above tracking scheme in a 2×2 system. The normalized MSE (NMSE), $E\left(\left\|\mathbf{h}_n-\hat{\mathbf{h}}_n\right\|^2 \Big/ \left\|\mathbf{h}_n\right\|^2\right)$, is plotted versus the number of iterations. The channel is M -block fading, of the Veh-A type. OQPSK input is used, at an SNR of 15 dB. The transmultiplexer employs the PHYDYAS reference filter bank with $M=128$ and $K=4$. The initial channel estimate in each frame is provided by the preamble-based channel estimation technique presented in Section 3.1.3.4 of [8] (see also [14]). This is based on an MSE-optimal preamble of a single FBMC symbol (followed by a guard of two null FBMC symbols to protect it from interference from the data section). The minimum number of decision subcarriers, $P = N_t L_h$, is used in each transmit antenna.

Figures. 2.20(a)-(d) show the results of averaging 200 frames of 106 FBMC symbols each, for (a) a static channel, and for time-varying channels of mobility (b) 5 km/h, (c) 15 km/h, and (d) 30 km/h. The step size values used in each case are noted on the figures. For comparison purposes, the result of no tracking is also shown. Evidently, Tracking B is much better than its A version, which, except for very low speeds, seems not to be able to correctly track the channel variations. Note from Figure 2.20(a), that the above decision-directed tracking scheme can be useful even in static channels as it significantly improves the preamble-based channel estimate. We can thus also view it as a *semi-blind* channel estimation technique.

2.5.2 Channel Tracking via Pilot-aided Time Interpolation

The above tracking scheme is quite simple to implement, as well as data efficient as it only requires a minimal set of pilot symbols, placed in the preamble. However, as one can also see from the results in Figure 2.20, it is only effective for rather low to medium mobilities. Moreover, the step size μ has to carefully chosen. In order to be able to track faster varying channels, one has to resort to pilots scattered within the frame. In this subsection, we investigate a pilot-aided tracking scheme which can cope with very high speeds while being simple in its implementation.

Let us place the pilot tones of the preamble FBMC symbol (Section 3.1.3.4 [8]) in the data section of the frame, in a periodic fashion. To avoid the intrinsic interference phenomenon at the pilot positions (k,n), we also use auxiliary (help) pilots at the positions $(k,n+1)$, where the interference is stronger. This way, the pilot set used in the preamble can still be used for channel estimation within the frame in the same way and is still MSE-optimal. The period of pilot symbol placement depends on the variation rate of the channel and should be shorter (denser pilots) for faster varying channels. Once the estimates at the pilot symbols become available, the channel in the rest of the symbols can be simply estimated through *linear interpolation* [15][16]. This scheme will prove to be much more effective in tracking fast varying channels. Its limitation is that one has to experience a delay in providing the channel estimates, equal to at most the period of pilot placement.

Two examples of the use of this pilot-aided tracking scheme are shown in Figure 2.21. The PHYDYAS reference filter bank is used, with $M = 128$ and $K = 4$. The channels are 2×2 M-block fading and follow the Veh-A model. OQPSK input is used, at an SNR of 15 dB. $N_t L_h$ pilots (and an equal number of auxiliary pilots) are used at each pilot position. The results of averaging 200 frames of 106 FBMC symbols each are illustrated, for mobile speeds of (a) 60 km/h and (b) 120 km/h. The pilots are placed at every 10 and 5 FBMC symbols, respectively. The results of no tracking are again included, for comparison purposes. It can be seen that the method is able to track the channel, by not allowing the MSE to exceed its initial level. One can also observe that, as expected, the best channel estimates are obtained at the pilot symbols, whereas the MSE is maximized at half the distance between two pilot symbols. The application of this channel tracking scheme in adaptive equalization and the resulting detection performance will be studied in the next section.

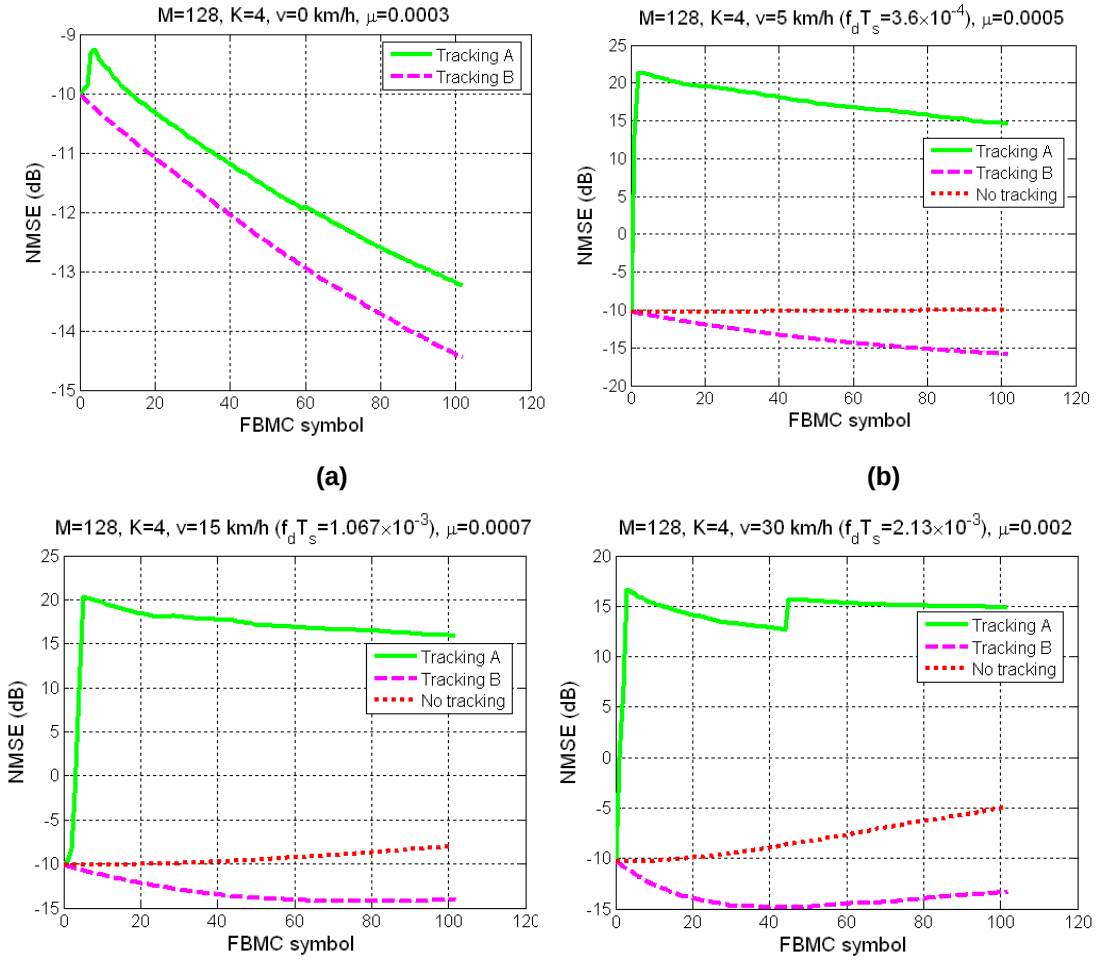

Figure 2.20 Tracking performance of the decision-directed LMS tracking scheme, variants A and B, for a FBMC/OQAM system with $M = 128, K = 4$ and Veh-A channels. Mobile speeds: (a) 0 km/h, (b) 5 km/h, (c) 15 km/h, and (d) 30 km/h.

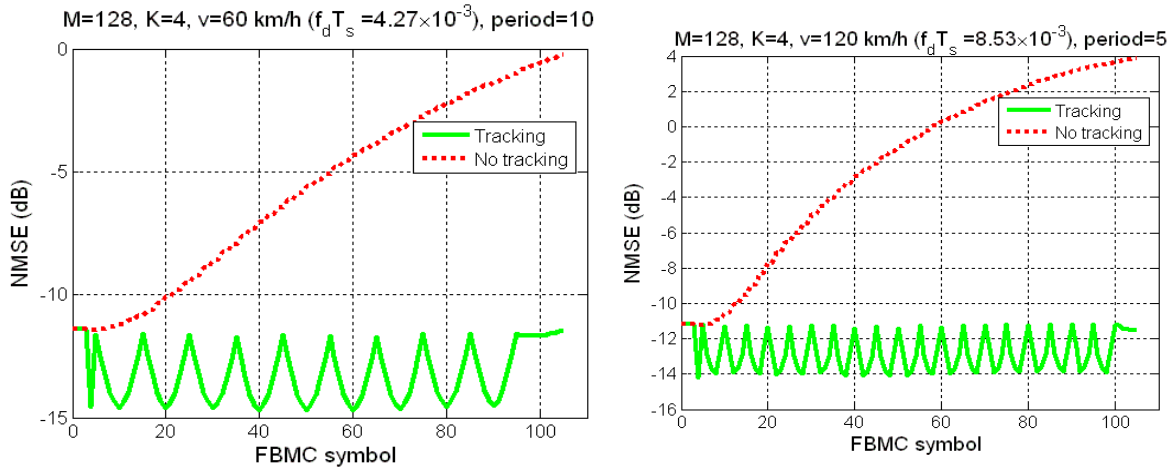

Figure 2.21 Tracking performance of the pilot-aided interpolation tracking scheme for an FBMC/OQAM system with $M = 128, K = 4$, Veh-A channel with OQPSK input at SNR=15 dB, and mobility of (a) 60 km/h and (b) 120 km/h.

3 MIMO techniques in FBMC

Space diversity and multiplexing schemes are considered in turn, starting with the most simple, widely known and practical MIMO technique, a space time block code for transmit diversity, often called Alamouti scheme.

3.1 Alamouti

Alamouti space-time coding is a famous transmit diversity scheme for two transmit antennas. We consider here mostly the basic scheme with single receiver antenna. Orthogonal sequences of two complex data symbols are transmitted from both transmit antennas as follows:

$$\begin{aligned} &\text{Antenna 1: } \left[d_1, -d_2^* \right] \\ &\text{Antenna 2: } \left[d_2, \quad d_1^* \right] \end{aligned} \tag{3.1}$$

The corresponding received samples are:

$$\begin{aligned} r_1 &= h_1 d_1 + h_2 d_2 + n_1 \\ r_2 &= -h_1 d_2^* + h_2 d_1^* + n_2 \end{aligned} \tag{3.2}$$

Assuming knowledge of the channel gains, the decision variables are obtained by combining the two observations as follows:

$$\begin{aligned} \tilde{d}_1 &= h_1^* r_1 + h_2 r_2^* = \left(|h_1|^2 + |h_2|^2 \right) d_1 + h_1^* n_1 + h_2 n_2^* \\ \tilde{d}_2 &= h_2^* r_1 - h_1 r_2^* = \left(|h_1|^2 + |h_2|^2 \right) d_2 + h_2^* n_1 + h_1 n_2^* \end{aligned} \tag{3.3}$$

Maximum likelihood detection is the optimum way to make the symbol decisions [17], but just using a slicer after scaling the decision variables for unity gain provides close to optimal performance in most cases (except for high-order QAM constellations in the high SNR region).

The Alamouti code was formulated here for the case of flat-fading channels, which is quite valid model when the coding is done for the subcarrier symbol sequences in a CP-OFDM system. However, due to the OQAM signal structure, it has turned out very difficult, if not impossible, to apply the Alamouti

scheme for symbol-wise coding in FBMC. Then, it becomes interesting to consider applying block-wise Alamouti schemes in FBMC. Such schemes have earlier been applied in single-carrier transmission in frequency-selective channels [18].

3.1.1 Block-wise Alamouti scheme

We start by stating the proposed block-wise transmission scheme. In the basic scheme, two symbol-block sequences are transmitted from the two antennas as follows:

$$\begin{aligned}\mathbf{D}_1 &= \left[\mathbf{0},\mathbf{d}_1,\mathbf{0},-\overleftarrow{\mathbf{d}}_2^*,\mathbf{0},\mathbf{d}_3,\mathbf{0},-\overleftarrow{\mathbf{d}}_4^*,\mathbf{0}\ldots\right] \\ \mathbf{D}_2 &= \left[\mathbf{0},\mathbf{d}_2,\mathbf{0},\ \overleftarrow{\mathbf{d}}_1^*,\mathbf{0},\mathbf{d}_4,\mathbf{0},\ \overleftarrow{\mathbf{d}}_3^*,\mathbf{0}\ldots\right]\end{aligned} \tag{3.4}$$

Here the elements are symbol blocks in the time-frequency domain, consisting of subcarrier samples following the complex OQAM signal model. The left arrow on top of a variable denotes time-reversal of the corresponding sequence. Figure 3.1 illustrates the block structure for single Alamouti code frame. For example, the elements $d_{1,n}$ and $d_{2,n}$ are Alamouti-coded together.

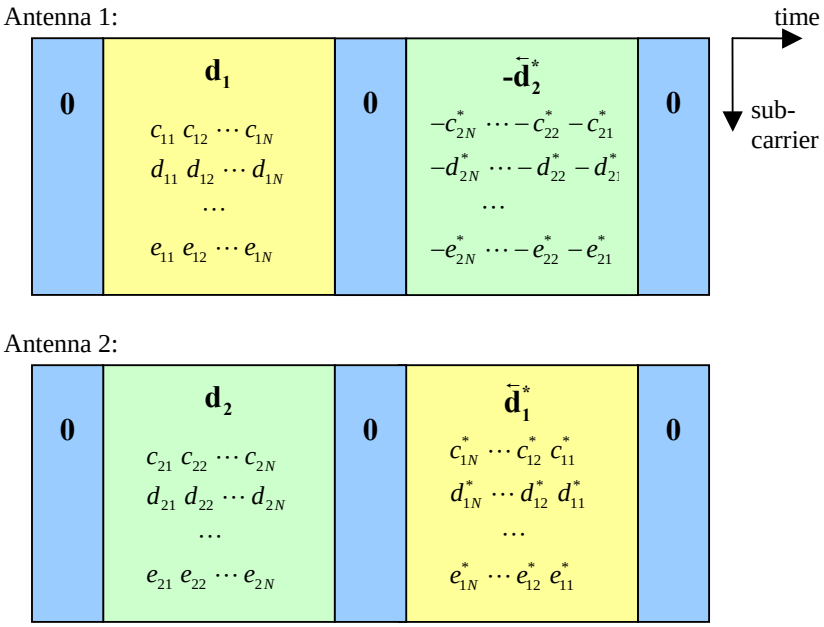

Figure. 3.1 Basic structure of the block Alamouti code frame.

This construction has the following essential characteristics:

1. Complex-conjugate time-reversal retains the "complex interference" structure of FBMC-OQAM signals.

   As discussed in PHYDYAS documents and OFDM-OQAM literature, when **d** is an input data block to an ideal transmultiplexer system (with ideal channel) the output is

   $$\mathbf{x} = \mathbf{d} + \mathbf{u} \tag{3.5}$$

   Here **u** is referred to as the secondary part, or complex interference. For each subcarrier symbol, $x_{k,m}$, within the data block, the corresponding element of **d**, $d_{k,m}$,is purely real or purely imaginary and the corresponding element of **u**, $u_{k,m}$, is purely imaginary or purely real,

respectively. Further, each element of **u** depends on the surrounding elements of **d** within a certain window.

The output **x** can be considered as a 2D convolution of **d** and the transmultiplexer response **T**, shown in Table 2-1 of [19] for the PHYDYAS reference filter bank. In general, **T** is conjugate symmetric along the time axis, which leads to the following properties:

$$\mathbf{X} = \mathbf{D} + \mathbf{U} = \mathbf{D} * \mathbf{T}$$

$$\Rightarrow \overleftarrow{\mathbf{X}}^* = \overleftarrow{\mathbf{D} * \mathbf{T}}^* = \overleftarrow{\mathbf{D}}^* * \overleftarrow{\mathbf{T}}^* = \overleftarrow{\mathbf{D}}^* * \mathbf{T} \tag{3.6}$$

This proves that the following two processing sequences produce exactly the same secondary parts (and consequently the same complex output sequences), when applied to isolated FBMC-OQAM symbol blocks:

- Transmitting **d** through a transmultiplexer system
- Transmitting $\overleftarrow{\mathbf{d}}^*$ through the transmultiplexer system and taking the conjugate time-reversed version of the output.

This is exactly what is needed in the block-wise Alamouti scheme. The remaining issue is that at the edges of the transmission blocks, the symmetry properties are not always satisfied, and this may introduce additional interference.

2. In FBMC systems with sufficient frequency localization (like the PHYDYAS reference filter bank), the transmission blocks can be well isolated from each other in the frequency direction by leaving an empty subcarrier as a guardband between the blocks.

3. Guard periods have to be included between transmission blocks to isolate them properly.

In the proposed scheme, zero-symbols are inserted between the two parts of the Alamouti coded frames. Considering the PHYDYAS filter bank with *K*=4, a gap of 4 subcarrier samples (2 OQAM symbols) is need to completely isolate the blocks. With 3 zero symbols, the interference between the blocks is still at a very low level. Also shorter distance may be considered, depending on the intended SNR operation range. On the other hand, it is not easy (and it may be impossible) to use the scheme with even number of 0 symbols in such gaps, so 1 or 3 zeros are the remaining choices. It can also be shown that inserting any pattern of non-zero symbols in the center gap introduces additional interference in the Alamouti scheme.

In the proposed scheme, pilot blocks are inserted between different block Alamouti code frames, in such a way that they are not distorting the required symmetry patterns:

$$\mathbf{D}_1 = \left[\mathbf{p}_1, \mathbf{d}_1, \mathbf{0}, -\overleftarrow{\mathbf{d}}_2^*, -\overleftarrow{\mathbf{p}}_2^*, \mathbf{d}_3, \mathbf{0}, -\overleftarrow{\mathbf{d}}_4^*, -\mathbf{p}_1 \ldots\right]$$

$$\mathbf{D}_2 = \left[\mathbf{p}_2, \mathbf{d}_2, \mathbf{0}, \overleftarrow{\mathbf{d}}_1^*, \overleftarrow{\mathbf{p}}_1^*, \mathbf{d}_4, \mathbf{0}, \overleftarrow{\mathbf{d}}_3^*, -\mathbf{p}_2 \ldots\right] \tag{3.7}$$

With this structure of pilot blocks, they don't introduce any more interference to the data symbols than zero symbols in these places. Naturally, there is some interference between different Alamouti code blocks (e.g., between $-\overleftarrow{\mathbf{d}}_2^*$ and $\mathbf{d}_3$), if the length of the pilot block is lower than 4 samples (with the PHYDYAS filter bank). The received secondary parts of the pilot symbols are not under control in this scheme, but this is not critical for the proposed channel estimation scheme. In the gaps between different block Alamouti code frames, also even values

of the pilot block length are feasible. In the continuation, we consider the length of 3 subcarrier samples, based on preliminary simulation studies.

The auxiliary pilot scheme has been extensively considered in PHYDYAS for channel estimation and fine synchronization purposes. In the proposed Alamouti scheme, such pilot pairs could be inserted only within the data blocks; in the pilot areas they cannot be introduced without distorting the symmetries. The needed gaps introduce significant overheads in data transmission capacity, which would be further affected by the introduction of auxiliary pilots. Therefore, we consider using only the pilot blocks between Alamouti code frames for channel estimation. In the following we assume that the subchannels are essentially flat-fading, and the block-wise Alamouti scheme can be utilized without any further equalization.

Our idea for channel estimation is based on (3.3). For each Alamouti-coded pair of pilots we can write (notice that in the complex OQAM sample domain, the equation may be for the imaginary part, instead of real part, depending on the pilot location):

$$\begin{aligned} \mathrm{Re}\left[\overline{h}_1^* r_{1,n} + \overline{h}_2 r_{2,n}^*\right] &= p_{1,n} \ (+\,noise) \\ \mathrm{Re}\left[\overline{h}_2^* r_{1,n} - \overline{h}_1 r_{2,n}^*\right] &= p_{2,n} \ (+\,noise) \end{aligned} \tag{3.8}$$

where

$$\begin{aligned} \overline{h}_1 &= \frac{h_1}{\left(|h_1|^2 + |h_2|^2\right)} \\ \overline{h}_2 &= \frac{h_2}{\left(|h_1|^2 + |h_2|^2\right)} \end{aligned} \tag{3.9}$$

Consequently, ignoring the noise term, we obtain two linear equations in terms of four unknowns $\mathrm{Re}\left[\overline{h}_1\right]$, $\mathrm{Im}\left[\overline{h}_1\right]$, $\mathrm{Re}\left[\overline{h}_2\right]$ and $\mathrm{Im}\left[\overline{h}_2\right]$, real and imaginary parts of the observations $r_{1,n}$ and $r_{2,n}$, and known purely real-valued or purely imaginary-valued pilots $p_{1,n}$ and $p_{2,n}$. Using multiple pilots, we can easily obtain a set of more than four linear equations in four unknowns, which can be solved in the MSE sense to find the channel coefficients. Such equations can be obtained also for the 0-pilots. However, preliminary experiments indicate that the 0-pilots form the center gap contribute only marginally to the performance, and are probably not worth the added complexity.

Performance evaluation

We have tested the proposed scheme using the ITU-R vehicular A channel model and WiMAX-like system parameters typically considered in the PHYDYAS simulation studies. Block-fading channel model is assumed, i.e., the channel remains constant over each Alamouti-coded block. Here we use just random QPSK data sequences as pilots.

After some preliminary evaluations, it seems that 3 is the right choice for the pilot sequence length. For the center gap length, both 1 and 3 are considered. In both cases, we use the two pilot samples which are closest to the Alamouti code block. We consider using pilots also from the immediately adjacent subchannels. More specifically, for an Alamouti code sequence on subcarrier k starting at time index n and ending at $n+n_0$, we use pilots n-2, n-1, $n+n_0$+1 and $n+n_0$ +2 at subcarriers k-1, k, and k+1 for estimating the channel gain.

To evaluate the pilot overhead, we use the WiMAX downlink PUSC mode as a reference. It uses 1 pilot per 6 QAM data symbols with pilot boost of 2.5 dB. To reach the same pilot overhead in spectral

efficiency, the data block length should be chosen as 18 subcarrier samples (9 OQAM symbols) when using the 3-sample center gap, or 12 subcarrier samples (6 OQAM symbols) when using the 1-sample center gap. The distance between consecutive pilot blocks is about 20 or 13 OQAM symbols, respectively. To reach the same pilot energy to data energy ratio as in WiMAX, pilot boost of 5.5 dB or 5 dB should be used with long or short center gap, respectively.

Figure 3.2 shows the average MSE and BER performance after combination as a function of Eb/No for both pilot schemes and QPSK data modulation. We can see that at in the low-to-medium Eb/No range, the performance with shorter center gap is quite acceptable. Figure 3.3 shows the average MSE and BER performance after combining as a function of mobile velocity (with 2.5. GHz carrier frequency) for both pilots schemes. We can see that the shorter gap is clearly more robust with significant mobility.

In conclusion, the performance of the proposed block-wise Alamouti was found to be quite good in case of stationary channel. With significant mobility, there is a trade-off between detection performance and code block length. With increasing mobility, the data block length has to be reduced, leading to increased overheads due to the pilots/guard periods. Considering system parametrization and pilot overheads similar to those of WiMAX downlink PUSC mode, acceptable performance is achieved with mobilities of some tens of km/h.

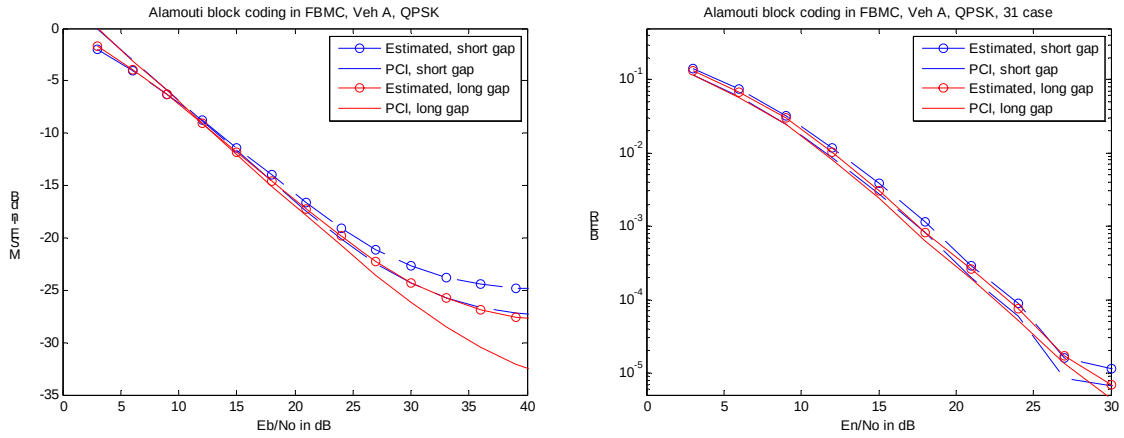

Figure. 3.2. MSE and BER performance for block-wise Alamouti scheme for FBMC. QPSK modulation, Vehicular A channel, pilot block length 3 samples, 0-block length 1 or 3 samples.

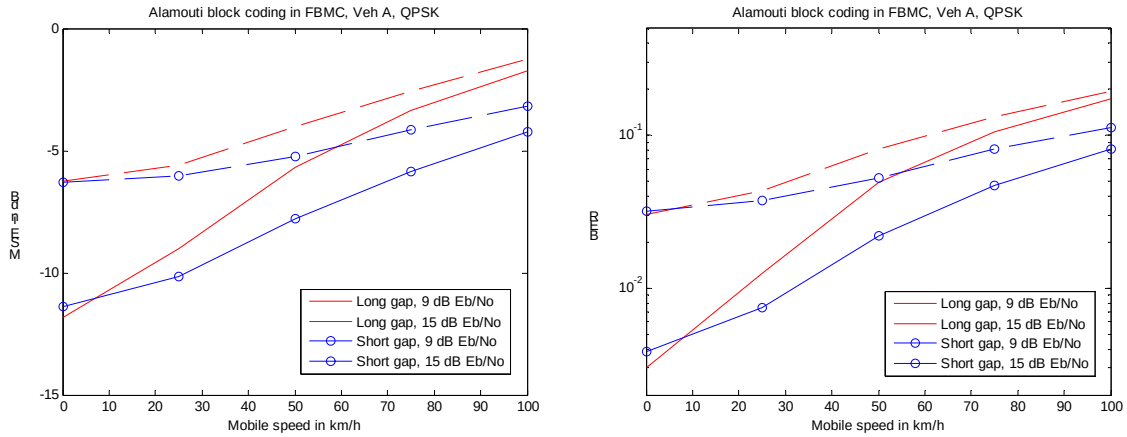

Figure 3.3. MSE and BER performance for block-wise Alamouti scheme for FBMC as a function of mobility. QPSK modulation, Eb/No of 9 or 15 dB, Vehicular A channel, pilot block length 3 samples, 0-block length 1 or 3 samples.

3.2 Spatial Multiplexing

The objective of spatial multiplexing is to establish a number of channels between the groups of transmit and receive antennas, in order to increase the data throughput.
The approach has been studied in depth for OFDM and two classes of algorithms have been worked out. The first and simplest class exploits the minimum mean square error (MMSE) criterion. A more involved approach, based on the maximum likelihood (ML) principle, may yield significant performance improvements, since it has the potential to reach the optimal signal-to-noise ratio [20].
Regarding MMSE techniques, they apply to FBMC and OFDM and there is nothing special with FBMC. Here, the focus is on ML techniques.

3.2.1 FBMC and maximum likelihood

If QAM modulation is used in the sub-channels of an FBMC, the techniques developed for OFDM can be employed. However, with OQAM modulation, due to the presence of the interference terms in the received signals, specific algorithms have to be developed. An illustration of the context is given for MIMO 2x2.
The system has two transmit antennas and two receive antennas. At a particular time, in a particular sub-channel, the following signals are received

$$\begin{aligned} x_1 &= h_{11}(d_1 + ju_1) + h_{12}(d_2 + ju_2) + b_1 \\ x_2 &= h_{21}(d_1 + ju_1) + h_{22}(d_2 + ju_2) + b_2 \end{aligned} \tag{3.10}$$

where d, u, b designate, respectively, the data symbols, the OQAM interference terms and the noise terms. The complex scalars h_{11}, h_{12}, h_{21} and h_{22} represent the MIMO transmission channel elements at the center frequency of the sub-channel under consideration, assuming perfect frequency and time synchronization after sub-channel equalization.
The maximum likelihood principle implies the calculation of the cost function

$$J = \left|x_1 - h_{11}d_1 - h_{12}d_2\right|^2 + \left|x_2 - h_{21}d_1 - h_{22}d_2\right|^2 \tag{3.11}$$

for all possible values of the data symbols. Assuming binary data, $d_1 = \pm 1$ and $d_2 = \pm 1$, 4 evaluations are needed. Then, the minimum cost function value is picked and the data set which is involved is the output of the ML detector. Next, considering the other cost function values, equivalent signal-to-noise ratios are computed, which gives, for erroneous d_1

$$SNR_{d1} = \frac{\left[\left|h_{11}\right|^2 + \left|h_{21}\right|^2 \pm u_2 \,\mathrm{Im}(h_{11}h_{12}^* + h_{21}h_{22}^*)\right]^2}{(\left|h_{11}\right|^2 + \left|h_{21}\right|^2)\sigma^2/2} \tag{3.12}$$

for erroneous d_2

$$SNR_{d2} = \frac{\left[\left|h_{22}\right|^2 + \left|h_{12}\right|^2 \pm u_1 \,\mathrm{Im}(h_{11}h_{12}^* + h_{21}h_{22}^*)\right]^2}{(\left|h_{22}\right|^2 + \left|h_{12}\right|^2)\sigma^2/2} \tag{3.13}$$

and for erroneous d_1 and d_2

$$SNR_{d1,d2} = \frac{\left[\left|h_{11} + h_{12}\right|^2 + \left|h_{21} + h_{22}\right|^2 \pm (u_1 \pm u_2)\,\mathrm{Im}(h_{11}h_{12}^* + h_{21}h_{22}^*)\right]^2}{(\left|h_{11} + h_{12}\right|^2 + \left|h_{21} + h_{22}\right|^2)\sigma^2/2} \tag{3.14}$$

The performance of the scheme, in terms of bit error rate, depends on the quantity $\mathrm{Im}(h_{11}h_{12}^{*}+h_{21}h_{22}^{*})$ which is known and the interference terms u_1 and u_2 which are unknown.

A systematic search over all the possible values is impractical, because these terms take their values in a large set. In fact, the interference terms are weighted sums of previous and past data in the sub-channel under consideration and the two neighbouring sub-channels. For example, if the system impulse response is limited to the immediate neighbours of the reference term, the vector of the weighting coefficients is W=[0.564, 0.564, 0.239, 0.239, 0.206, 0.206 0.206, 0.206] and *u* can take on 45 different values, in the interval ± 2.43.

A first approach consists of estimating the interference terms, using the MMSE technique for example, and introducing the estimated values $\tilde{u}_1$ and $\tilde{u}_2$ in the cost funtion, which becomes

$$J=\left|x_1-h_{11}(d_1+j\tilde{u}_1)-h_{12}(d_2+j\tilde{u}_2)\right|^2+\left|x_2-h_{21}(d_1+j\tilde{u}_1)-h_{22}(d_2+j\tilde{u}_2)\right|^2 \tag{3.15}$$

Then the performance depends on the accuracy of the estimation.

Two approaches are investigated below, in the general case. One relies on the known probability distribution of the interference terms, it is called local-ML, because the received signal is processed symbol by symbol, the other one performs an estimation of the interference terms using a reduced set of the coefficients of the system impulse response and exploits an iterative method.

3.2.2 Local ML decoder

The system model presented in deliverable D4.1 is considered [8]. Under the assumptions of good time-frequency localization for the prototype filter and relatively low frequency selectivity for the channel, the received signal at the output of the k-th analysis filter bank is given by

$$\mathbf{r}_{k,n}=\mathbf{H}_{k,n}(\mathbf{d}_{k,n}+j\mathbf{u}_{k,n})+\mathbf{n}_{k,n} \tag{3.16}$$

The maximum likelihood (ML) decoder is the optimum decoder. It searches for the vector $\mathbf{d}_{k,n}$ which maximizes the probability to receive a vector $\mathbf{r}_{k,n}$ assuming that $\mathbf{d}_{k,n}$ is transmitted [21], so we can write:

$$\hat{\mathbf{d}}_{k,n}=\underset{\mathbf{d}_{k,n}}{argmax}\{P(\mathbf{r}_{k,n}/\mathbf{d}_{k,n})\}. \tag{3.17}$$

Consequently, it is necessary to calculate the analytic expression of $P(\mathbf{r}_{k,n}/\mathbf{d}_{k,n})$. To simplify, we omit frequency and time indices in this section. So, we rewrite the equation (3.16) as follows:

$$\begin{aligned}\mathbf{r} &= \mathbf{Hd}+j\mathbf{Hu}+\mathbf{n}\\ &= \mathbf{Hd}+\mathbf{n}',\end{aligned} \tag{3.18}$$

where $\mathbf{n}'$ is the sum of the noise vector and the interference vector term. We have:

$$P(\mathbf{r}/\mathbf{d})=P_{\mathbf{N}'}(\mathbf{r}-\mathbf{Hd}). \tag{3.19}$$

Let us denote $\mathbf{v}=j\mathbf{Hu}$, so $\mathbf{n}'=\mathbf{v}+\mathbf{n}$. Since $\mathbf{u}$ is linearly dependent on transmitted data vectors and takes only certain vector values, then it is considered as a discrete random vector. So, we can write the marginal density function of $\mathbf{n}'$ as follows [22]:

$$P_{\mathbf{N}'}(\mathbf{n}')=\sum_{\mathbf{v}}P_{\mathbf{V}}(\mathbf{v})P_{\mathbf{N}}(\mathbf{n}'-\mathbf{v})$$

$$= \frac{1}{|det(\mathbf{H})|}\sum_{\mathbf{u}} P_{\mathrm{U}}(\mathbf{u}) P_{\mathrm{N}}(\mathbf{n}' - j\mathbf{H}\mathbf{u}). \quad (3.20)$$

Therefore, according to (3.20) and (3.19), we obtain:

$$P(\mathbf{r}/\mathbf{d}) = \frac{1}{|det(\mathbf{H})|}\sum_{\mathbf{u}} P_{\mathrm{U}}(\mathbf{u}) P_{\mathrm{N}}(\mathbf{r} - \mathbf{H}(\mathbf{d} + j\mathbf{u})). \quad (3.21)$$

$P_{\mathrm{N}}(\mathbf{n})$ is the probability density function of the multivariate Gaussian distributed $\mathbf{N} \sim N(0, \sigma^2 \mathbf{I}_2)$, described as:

$$P_{\mathrm{N}}(\mathbf{n}) = \frac{1}{2\pi\sigma^2}\exp(-\frac{\|\mathbf{n}\|^2}{2\sigma^2}). \quad (3.22)$$

According to (3.17), we have to maximize the equation (3.21). Taking account (3.22) and omitting the positive factor term $(2\pi\sigma|det(\mathbf{H})|)^{-1}$ we have:

$$\hat{\mathbf{d}} = \underset{\mathbf{d}}{argmax}\{f(\mathbf{d})\}$$

$$= \underset{\mathbf{d}}{argmax}\{\sum_{\mathbf{u}} Pr(\mathbf{U} = \mathbf{u})\exp(-\frac{\|\mathbf{r} - \mathbf{H}(\mathbf{d} + j\mathbf{u})\|^2}{2\sigma^2})\}. \quad (3.23)$$

So, the discrete probability distribution $Pr(\mathbf{U} = \mathbf{u})$ should be known. Since it depends only on transmit-receive impulse response coefficients, we have to evaluate it just once. We have:

$$\mathbf{u} = \sum_{(p,q)\neq(0,0)} \alpha_{p,q}\mathbf{d}_{p+k,q+n} \quad (3.24)$$

with $\alpha_{p,q} = \langle g_{k,n}, g_{k+p,n+q} \rangle$.

In continuation with the work presented in [23][30], the IOTA prototype filter described in [48] is used, assuming that similar results would be obtained with the Phydyas reference filter.

In order to limit the computation load, the filter impulse response is limited to the terms adjacent to the reference term. Accordingly, the interference term in the i^{th} antenna is written as a finite linear sum of independent uniformly distributed BPSK data:

$$u^{(i)} = \sum_{k=1}^{8} \alpha_k d_k^{(i)} \quad (3.25)$$

with $\alpha_k = 0.4411$ for $k = 1,...,4$ and $\alpha_k = 0.228$ for $k = 5,...,8$. Numerical calculations of the discrete probability distribution $P(u^{(i)})$ lead to the following table:

When considering a 2x2 MIMO system where $\mathbf{u}$ is a two-element vector and since the components of $\mathbf{u}$ are independent, we can write:

$$P(\mathbf{U} = \mathbf{u}) = P(U^{(1)} = u^{(1)}).P(U^{(2)} = u^{(2)}) \quad (3.26)$$

The simulation results lead to the curve shown in figure 3.7. The performance of the local-ML decoder is slightly better than MMSE, but far from the optimum.

An alternative approach, based on interference cancellation, is presented next.

$u^{(i)}$	$P(U^{(i)} = u^{(i)})(\times 10^{-1})$
0	1.4069
± 0.0298	0.1567
± 0.4262	0.6254
± 0.4560	0.9340
± 0.8524	0.0389
± 0.8822	0.9381
± 0.9120	0.2341
± 1.3084	0.1559
± 1.3382	0.6258
± 1.7644	0.2355
± 1.7942	0.1564
± 2.2204	0.1565
± 2.6764	0.0392

Table 3.1 Interference Discrete probability distribution

3.2.3 Iterative decoding using maximum-likelihood decoder

The local maximum-likelihood detector described in the previous section suffers from its high complexity since it requires to compute the marginal probability over all interference terms to detect each transmitted symbol. In this section, we present an iterative receiver based on interference cancellation.

Following the signal model defined in [8], the transmitted sequence at SFB output can be written as:

$$s[m] = \sum_{k=0}^{M-1} \sum_{n \in Z} d_{k,n} g_{k,n}[m] \tag{3.27}$$

where $g_{k,n}[m]$ are the shifted versions of the prototype filter impulse response $g[m]$ in time and frequency. In the absence of channel, the demodulated symbol over the k^{th} sub-carrier and the n^{th} instant is determined using the inner product of $s[m]$ and $g_{k,n}[m]$:

$$\begin{aligned} r_{k',n'} &= \langle s, g_{k',n'} \rangle = \sum_{m=-\infty}^{+\infty} s[m] g^*_{k',n'}[m] \\ &= \sum_{m=-\infty}^{+\infty} \sum_{k=0}^{M-1} \sum_{n \in Z} d_{k,n} g_{k,n}[m] g^*_{k',n'}[m]. \end{aligned} \tag{3.28}$$

After adding the noise contribution $n_{k',n'}$, equation (3.28) becomes:

$$r_{k',n'} = h_{k',n'} d_{k',n'} + I_{k',n'} + n_{k',n'}, \tag{3.29}$$

where $h_{k',n'}$ is the channel coefficient at subcarrier k' and time index n', $I_{k',n'}$ is defined as an intrinsic interference and is written:

$$I_{k',n'} = \sum_{(k,n) \neq (k',n')} h_{k,n} d_{k,n} \sum_{m=-\infty}^{m=\infty} g_{k,n}[m] g^*_{k',n'}[m], \tag{3.30}$$

Most part of the energy (98%) is localized in the first-order neighbors around the considered symbol and we can assume that the intrinsic interference term depends only on this restricted set Ω. Moreover, assuming that the channel is constant at least over this summation zone, we can write as in [23]:

$$r_{k',n'} \approx h_{k',n'}(d_{k',n'} + \underbrace{\sum_{(k,n)\in\Omega} d_{k,n} \sum_{m=-\infty}^{\infty} g_{k,n}[m] g^{*}_{k',n'}[m]}_{ju_{k',n'}}) + n_{k',n'} \tag{3.31}$$

At the first step, we use a MMSE equalizer to estimate the data. According to equation (3.16), the estimated intrinsic interference caused by FBMC modulation is:

$$\hat{I}_{k,n} = \sum_{(k',n')\in\Omega} \hat{d}_{k',n'} \sum_{m=-\infty}^{\infty} g_{k',n'}[m] g^{*}_{k,n}[m], \tag{3.32}$$

$\hat{d}_{k',n'}$ are the estimated data at the MMSE equalizer output. Thus, the interference terms are also estimated and their contribution is cancelled from the demodulated received symbols. So we have:

$$\begin{aligned} y_{k,n} &= r_{k,n} - h_{k,n}\hat{I}_{k,n} \\ &\approx h_{k,n}(d_{k,n} + \underbrace{\sum_{(k',n')\in\Omega} (d_{k',n'} - \hat{d}_{k',n'}) \sum_{m=-\infty}^{\infty} g_{k',n'}[m] g^{*}_{k,n}[m]}_{\hat{\varepsilon}_{k,n}}) + n_{k,n} \end{aligned} \tag{3.33}$$

Assuming almost perfect interference estimation, so $\hat{\varepsilon}_{k,n} \approx 0$, we consider that the vector $\mathbf{y}_{k,n}$ at the output of the interference canceller is free of interference, and thus we can apply a simple conventional ML detector to get the estimated symbols $\tilde{d}_{k,n}$. The interference estimation is done thanks to the estimated symbols which belong to the neighborhood set $\{\hat{d}_{k',n'} \setminus (k',n') \in \Omega_{k,n}\}$. We update continuously this set. Indeed, since some of these positions are already estimated using the ML detector $\{\tilde{d}_{k',n'} \setminus (k' < k) \quad or \quad (k' = k, n' < n)\}$, we can substitute $\hat{d}_{k,n}$ by $\tilde{d}_{k,n}$. We have called this receiver Recursive ML, and we note it Rec-ML.

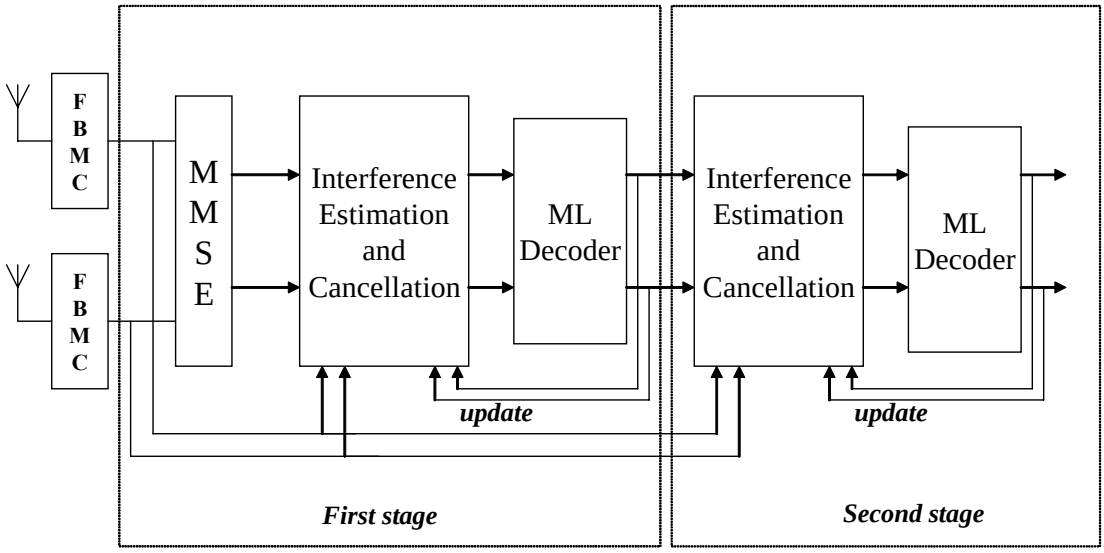

Figure 3.4 Complete block scheme of the iterative receiver

Unfortunately, $\hat{\varepsilon}_{k,n} \neq 0$, so an additional noise is added and then we cannot reach the optimal bit-error-rate performance. To improve the performance, we propose to add a second stage where we use the ML decoder outputs to perform a second interference estimation. After interference cancelation we apply

again a ML decoder. Another stage can be added but simulation results show that performance converge after the second stage. The complete scheme of this receiver is described in Figure 3.4. We called it TSRec-ML for "two stages recursive ML".

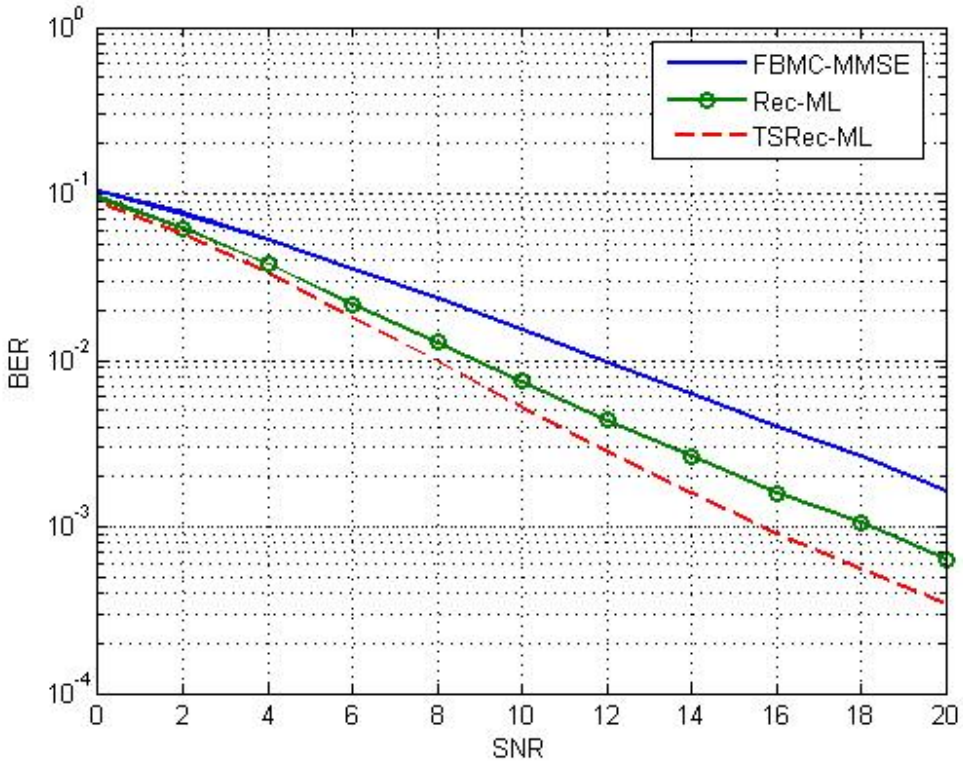

Figure 3.5 Performances of the iterative receiver

In Figure 3.5, we give the performance of the proposed receiver compared to the MMSE equalizer. We have considered a (2x2) MIMO system with flat fading channels. We note that we obtain significant gains with Rec-ML and TSRec-ML compared to MMSE. However, TSRec-ML cannot exploit the whole space diversity. Compared to local-ML, TSRec-ML is slightly better, but still far from optimum.
In fact, the superior performance of OFDM in ML receivers comes from the QAM modulation. Then, for the sake of completion, the filter banks were combined with QAM modulation.

3.2.4 QAM modulation and Viterbi decoding

In this section, we propose to use QAM modulation: instead of transmitting real-valued symbols, we transmit complex valued symbols but only at even time indices as described in Table 3.2. This leads to the same rate as OQAM/OFDM.

	$n-2$	$n-1$	n	$n+1$	$n+2$	$n+3$
k	$c_{k,n-2}$	0	$c_{k,n}$	0	$c_{k,n+2}$	0
$k+1$	$c_{k+1,n-2}$	0	$c_{k+1,n}$	0	$c_{k+1,n+2}$	0
$k+2$	$c_{k+2,n-2}$	0	$c_{k+2,n}$	0	$c_{k+2,n+2}$	0

Table 3.2 Mapping table

Again, in the continuation of the work in [23][30], the prototype filter IOTA is considered, and only the symbols located around a position contribute to the interference term. We can evaluate the power of these contributions as:

$$p = 1 - \sum_{l=-1}^{1}\sum_{k=-1}^{1} |\alpha_{l,k}|^2 \approx -18.6dB. \tag{3.34}$$

In fact, since we set null data at even time indices, we have less interference terms. To evaluate its power we refer to equation (3.28) and write:

$$\begin{aligned} p &= \sum_{(k,i)\in Z^2} |r_{k,n_0+2i}|^2 \\ &= \sum_{(k,i)\in Z^2} |\sum_m g[m]g[m-iM]e^{-j\frac{2\pi}{M}m\Delta k}|^2 \\ &\approx -22dB. \end{aligned} \tag{3.35}$$

We can now assume that each symbol vector $\mathbf{c}_{k,n}$ overlaps only with both neighbors $\mathbf{c}_{k\pm1,n}$. Consequently the demodulated symbol vector over the k^{th} sub-carrier and the n^{th} instant can be written as:

$$\mathbf{r}_{k,n} = \mathbf{H}\sum_{l=-1}^{1}\alpha_{l,0}\mathbf{c}_{k+l,n} + \mathbf{n}_{k,n} \tag{3.36}$$

According to this equation, the system is considered as a set of independent sequences -for each integer value of n, $\mathbf{r}_{k,n}$ is an independent sequence- and each sequence is filtered by a non causal digital filter which can be expressed as an equivalent tapped delay line with 3 taps as shown in Figure 3.6. Omitting the time index, let us denote respectively by $\mathbf{c}[k]$ and $\mathbf{r}[k]$ the transmitted and received vectors with length M equal to the number of sub-carriers and $\alpha = [\alpha_{-1,0} \quad \alpha_{0,0} \quad \alpha_{1,0}]$. The optimal detector searches for the transmitted sequence $\hat{\mathbf{c}}[k]$ among all the possible ones which satisfies the following criterion:

$$\hat{\mathbf{c}}[k] = \underset{\mathbf{c}}{argmin}\left(\sum_{k=0}^{M-1} \| \mathbf{r}[k] - \mathbf{H}\sum_{l=-1}^{1}\alpha[l]\mathbf{c}[k+l] \|^2\right). \tag{3.37}$$

To find the ML sequence, we will use the Viterbi algorithm. According to Figure 3.6, since we have two taps and taking into account that $\mathbf{c}[k]$ are two-element vectors with QPSK symbols, the total number of states is 256 denoted by $S_0,...,S_{255}$. At each stage k, each transition branch is labeled by its corresponding input vector $\mathbf{c}[k+1]$, thus, there are 16 transitions out of each state to 16 different states. The considered metric for a branch in the k^{th} stage and which transits from state $S_i = (\mathbf{c}[k-1], \mathbf{c}[k])$ to $S_j = (\mathbf{c}[k], \mathbf{c}[k+1])$ is:

$$\mathcal{M}_{ij}(k) = \| \mathbf{r}[k] - \mathbf{H}\sum_{l=-1}^{1}\alpha[l]\mathbf{c}[k+l] \|^2, \tag{3.38}$$

denoting $\mathbb{S}_i$ the set of all possible states from which we can lead to S_i, the accumulated metric $c_i(k)$ associated to each node (state) S_i in the m^{th} stage is defined as:

$$c_i(k) = \min\{c_j(k-1) + \mathcal{M}_{ij}(k) / S_j \in \mathbb{S}_i\}. \quad (3.39)$$

Each node memorizes its parent node, so at the sequence end ($k = M-1$), when choosing the node with the least accumulated metric, we can reconstitute the optimal path which fulfills equation (3.37).
Unfortunately, such a detector still suffers from high complexity since at each state we have to calculate the accumulated metric defined in (3.39) 256×16 times regardless of the other operations.
A reduced complexity version of Viterbi algorithm is the M-algorithm [24] but is suboptimal. It retains only a limited number $J \leq 256$ of nodes per step having the smallest accumulated metric (this number is also called the number of survivors). Since a limited number of states are considered, the correct path may be lost [25]. The error probability in M-algorithm depends on the number of survivors. To keep the probability of an error event as low as possible, the number of survivors J should be sufficiently high. However, increasing J leads to higher complexity.

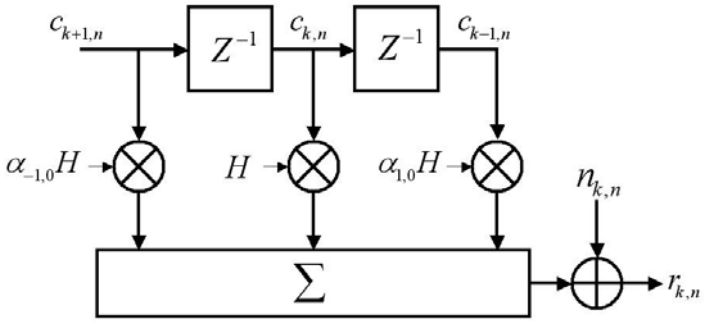

Figure 3.6 Equivalent tapped delay line with 3 taps

Simulation results

In this section, we shall compare FBMC/IOTA in both schemes studied above to CP-OFDM in 2×2 SDM MIMO configuration. For simulations, we have considered flat fading Rayleigh channels.
First, we present FBMC/IOTA and CP-OFDM performance with MMSE and local-ML detector. The results presented have been obtained with the following parameters

- No coding scheme
- BPSK modulation.
- Flat fading Rayleigh channels.
- Number of subcarriers $M = 512$.

In figure 3.7, we notice that, in the case of the MMSE equalizer, we obtain the same performance for both FBMC and OFDM systems. Using the local-ML decoder with FBMC, we obtain a slight gain compared to the MMSE equalizer (2 *dB* at $BER = 10^{-2}$), but with much higher complexity.
Simulation results for the system scheme described in this section are presented in figures 3.8 and 3.9. FBMC/Viterbi is compared to OFDM with ML decoder for QPSK modulation. In Figure 3.8, we observe that for low signal-to-noise ratio (SNR), FBMC/Viterbi reaches OFDM performance, but it suffers from degradation in case of high SNR. In fact, this degradation is due to the neglected interference terms. This degradation will not be important if we add an outer code like a convolutional code. Simulation results for the M-algorithm are presented in Figure 3.9 for different numbers of survivors $J = 16, 8$ and 4. With $J = 16$, we obtain practically the same performance as FBMC/Viterbi, whereas it has less complexity (16 branches kept instead of 256). For $J = 8$, we remark a slight

degradation for SNR less than $14dB$ (about $1dB$ at $BER = 10^{-2}$). However, when $J = 4$, it is clear that the performance is much worse. We should note that even if J is small, the curves tend to reach FBMC/Viterbi performance at high SNR, and all of them converge to the same bit-error value.

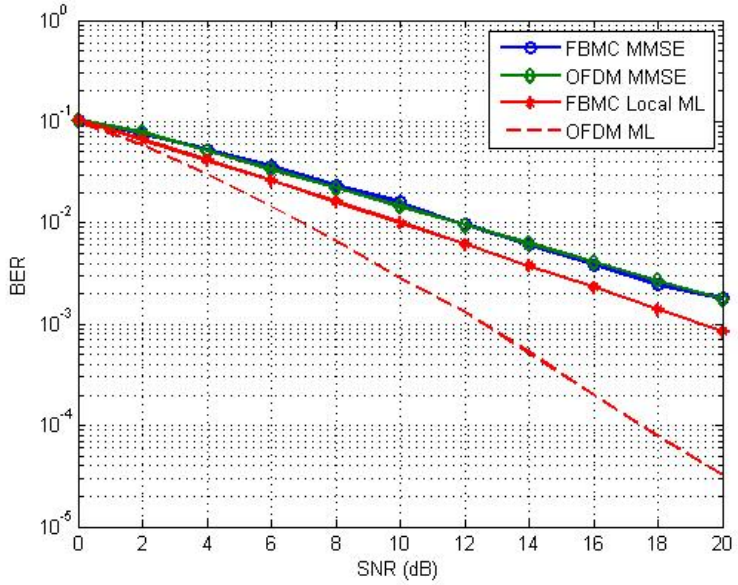

Figure 3.7 Performance of the Local ML receiver

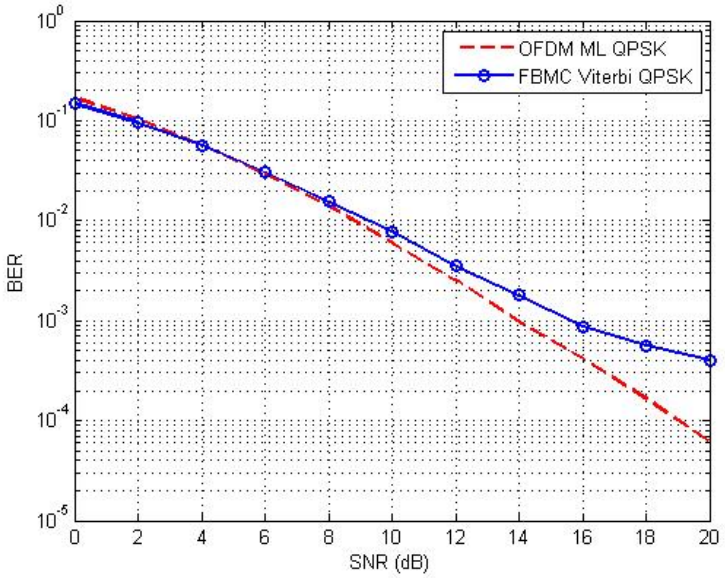

Figure 3.8 Performance comparaison between ML-OFDM and Viterbi-FBMC equalizer

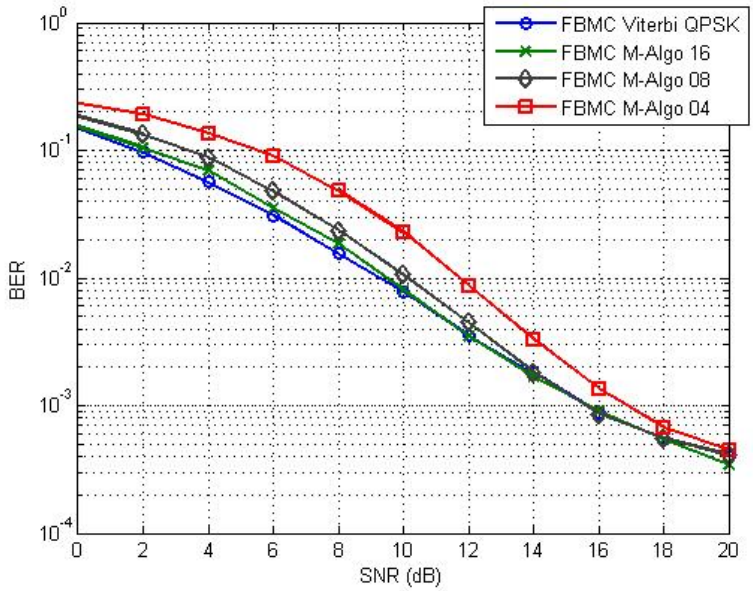

Figure 3.9 Performance comparaison between different value of J

3.2.5 Frequency-domain Adaptive V-BLAST Per Subcarrier Equalizer

The channel tracking methods presented in Section 2.5 can be combined with a per-subcarrier equalizer to yield an adaptive equalization scheme. To this end, we can resort to the relation (2.50), valid for each subcarrier, for inverting the channel and estimating its complex input. The V-BLAST detection algorithm [26] is known to result in the maximum post-detection SNR. It can also be adapted to a multicarrier system, as suggested, for example, in [27], for MIMO-OFDM. The V-BLAST iteration for the MIMO FBMC/OQAM system described in (2.50) and with the MMSE criterion can be described as follows:

At time n and for each subcarrier k :[2]

- $o_0 = 0$, $\tilde{\mathbf{y}}_{k,n}^{(o_0)} \equiv \tilde{\mathbf{y}}_{k,n}$, $\hat{\mathbf{H}}_{k,n}^{(o_0)} \equiv \hat{\mathbf{H}}_{k,n}$

- Compute the MMSE equalizer:

$$\mathbf{W}_{k,n}^{(o_0)} = \hat{\mathbf{H}}_{k,n}^{(o_0)} \underbrace{\left(\left(\hat{\mathbf{H}}_{k,n}^{(o_0)} \right)^H \hat{\mathbf{H}}_{k,n}^{(o_0)} + \frac{\sigma_\eta^2}{\sigma_x^2} \mathbf{I}_{N_t} \right)^{-1}}_{\mathbf{Q}_{k,n}^{(o_0)}} = \hat{\mathbf{H}}_{k,n}^{(o_0)} \mathbf{Q}_{k,n}^{(o_0)} ,$$

where σ_x^2 is the power of $\tilde{x}_{k,n}$ and σ_η^2 the noise power per receive antenna.[3]

- $O = \{1, 2, \ldots, N_t\}$

[2] We are using the Matlab notation $\mathbf{A}(:, i)$ to denote the i th column of a matrix $\mathbf{A}$.

[3] Note that the noise is assumed spatially white. Moreover, due to the filter bank orthogonality, the noise power at the AFB output is the same with that at its input.

- For p = 1 to N_t

  - $o_p = \underset{l \in O \setminus \{o_1, o_2, \ldots, o_{p-1}\}}{\arg\min} \left\{ \left[\mathbf{Q}_{k,n}^{(o_{p-1})} \right]_{ll} \right\}$

  - $\mathbf{w}_p = \mathbf{W}_{k,n}^{(o_{p-1})} \left(:, o_p \right)$

  - $\hat{x}_{k,n}^{o_p} = \mathbf{w}_p^H \tilde{\mathbf{y}}_{k,n}^{(o_{p-1})}$

  - Detect $d_{k,n}^{o_p}$ and $u_{k,n}^{o_p}$ to form $\hat{\tilde{x}}_{k,n}^{o_p} = \hat{d}_{k,n}^{o_p} + j\hat{u}_{k,n}^{o_p}$

  - Subtract the contribution of the o_p-th stream from the received signal:
    $\tilde{\mathbf{y}}_{k,n}^{(o_p)} = \tilde{\mathbf{y}}_{k,n}^{(o_{p-1})} - \hat{\mathbf{H}}_{k,n} \left(:, o_p \right) \hat{\tilde{x}}_{k,n}^{o_p}$

  - Update the MMSE equalizer:

$$\mathbf{W}_{k,n}^{(o_p)} = \hat{\mathbf{H}}_{k,n}^{(o_p)} \underbrace{\left(\left(\hat{\mathbf{H}}_{k,n}^{(o_p)} \right)^H \hat{\mathbf{H}}_{k,n}^{(o_p)} + \frac{\sigma_\eta^2}{\sigma_x^2} \mathbf{I}_{N_t} \right)^{-1}}_{\mathbf{Q}_{k,n}^{(o_p)}} = \hat{\mathbf{H}}_{k,n}^{(o_p)} \mathbf{Q}_{k,n}^{(o_p)},$$

    where $\hat{\mathbf{H}}_{k,n}^{(o_p)}$ results from $\hat{\mathbf{H}}_{k,n}^{(o_{p-1})}$ by zeroing its o_p-th column.

end

The iteration outlined above can be also used along with a *fast* V-BLAST algorithm (e.g., [28]) to lower the computational requirements in systems with a large number of transmit antennas. The computational cost from the iterations may also be reduced by computing the optimal ordering not in every symbol but once in every block of symbols. The equalizer weights in between may, for example, be computed via linear interpolation, as suggested in [15].

The detection step for the OQAM input is clearly realized as $\hat{d}_{k,n}^{o_p} = \mathrm{dec}\left[\mathrm{Re}\left(\hat{x}_{k,n}^{o_p} \right) \right]$. To estimate the interference part, we may again employ the rule adopted in the decision-directed tracking scheme of Section 2.5.1, namely to quantize $\hat{x}_{k,n}^{o_p}$ to the nearest level among all the possible levels of interference from the first-order neighbors. In the present context, we can further reduce the cost of this operation, by making use of the decisions already made for the previous FBMC symbol. Then only 5 out of the 8 first-order neighbors are unknown and this leads, for example with OQPSK input, to $2^5 = 32$ possibilities. Again, exploiting symmetries, this number is further reduced to 20 different interference levels.[4]

We have applied the above equalization scheme, with the channel estimates obtained with the aid of the tracking method of Section 2.5.2, to the examples of Figure 2.21. The results are depicted in Fig. 3.10.

[4] Note that this interference detection rule can also be used in the LMS-based tracking scheme of Section 2.5.1.

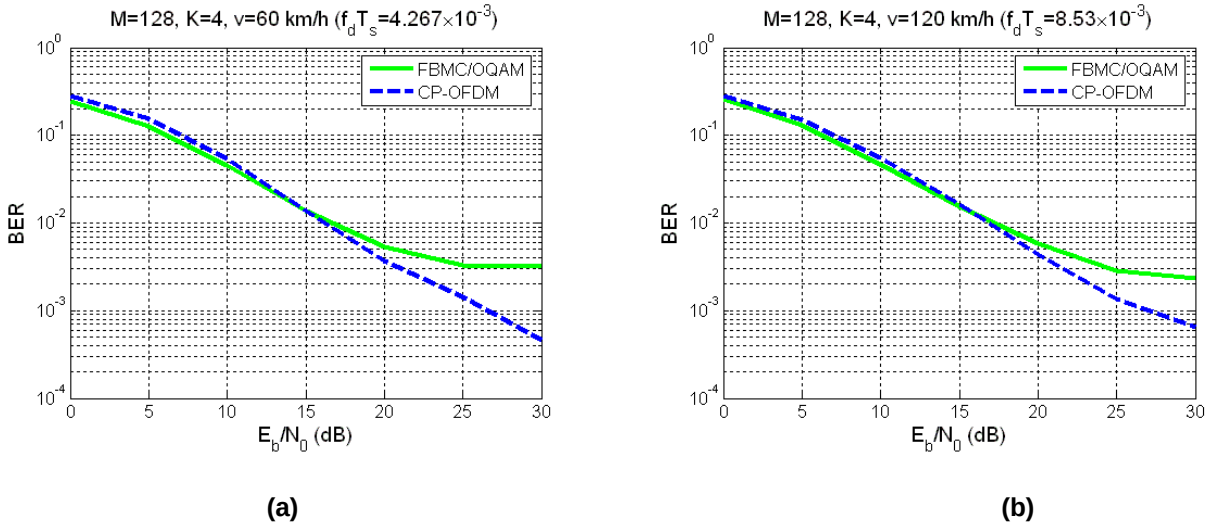

Figure 3.10. BER performance of the adaptive frequency-domain MMSE V-BLAST algorithm, for FBMC/OQAM and CP-OFDM. $M = 128, K = 4$. Veh-A channel, with OQPSK input, and mobility of (a) 60 km/h, and (b) 120 km/h.

The bit error rates (BER) for a CP-OFDM system are also included. The CP length was chosen to be the minimum allowable, i.e. equal to the channel order. Moreover, the power wasted in the CP was taken into account when calculating the SNR for CP-OFDM. One can see that, in both cases tested, FBMC is (slightly) better than CP-OFDM for low and moderate SNRs. With weaker noise, the intrinsic interference prevails and results in the well-known error floor for FBMC.

Better results for FBMC could be obtained by also using present and future decisions to estimate and cancel interference. However, this would require iterative passes on the data (in the vein of, e.g., [29][30]), thus further complicating the equalization task.

3.2.6 Adaptive Square-Root Decision-Feedback Equalizer

In this subsection, we present and evaluate an adaptive decision-directed decision-feedback equalization (DFE) scheme implementing the V-BLAST idea. This is based on the well-known equivalence of V-BLAST with the generalized DFE (GDFE) [31] and involves a MIMO DFE per subcarrier. Such a DFE was initially proposed, for flat fading channels, in [32], and its block structure is shown in Figure 3.11.

The equalizer consists of N_t serially connected stages, each one equalizing one of the N_t symbol streams according to BLAST ordering, which is adaptively updated. Both the DFE coefficients and the stream ordering are updated via an RLS-based algorithm. It must be emphasized that the equalizer does not rely on a channel estimate being available as above. This DFE scheme can be directly applied in each subcarrier of a MIMO-OFDM system, where the subchannels are known to be flat. As demonstrated in [33], the algorithm in [32] may diverge after a number of iterations due to numerical instability. A numerically stable version was developed in [33], based on the square-root factorization of the DFE input autocorrelation matrix.

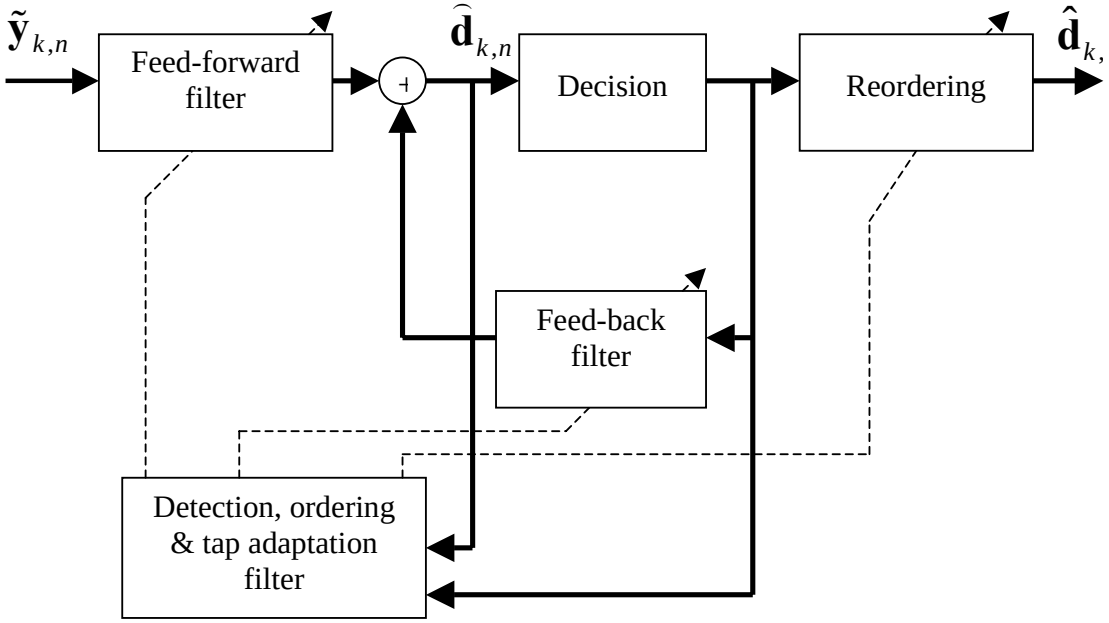

Figure 3.11 Structure of MIMO-FBMC adaptive DFE.

In order to apply this algorithm in a MIMO-FBMC system, its extension to frequency selective channels is required. This is because, in the absence of a CP and for the relatively low number of subcarriers utilized in time-varying systems, the FBMC subchannels are better modeled as frequency selective. Such a frequency selective version of the algorithm of [33] was presented in [34]. The algorithm retains the nice numerical behavior of its flat counterpart.

We herein present an adaptation of the computationally efficient square-root DFE of [34] to FBMC per subcarrier equalization. Consider a subcarrier k. Each of the N_t stages of the associated equalizer, say stage p, is a DFE consisting of a feed-forward filter of length $L_f N_r$, $\mathbf{f}_{k,n}(p)$, and a feed-back filter of length $L_b N_t + p - 1$, $\mathbf{b}_{k,n}(p)$. The DFE output is given by[5]:

$$\widehat{d}_{k,n}^{o_p} = \mathrm{Re}\left\{ \underbrace{\left[\mathbf{f}_{k,n}^H(p) \quad \mathbf{b}_{k,n}^H(p) \right]}_{\mathbf{w}_{k,n}^H(p)} \mathbf{y}_{k,n}(p) \right\} = \mathrm{Re}\left\{ \mathbf{w}_{k,n}^H(p)\mathbf{y}_{k,n}(p) \right\}, \tag{3.40}$$

where o_p denotes (as before) the stream detected at this stage, and

$$\mathbf{y}_{k,n}(p) = \left[\overline{\mathbf{y}}_{k,n}^T \quad \hat{\mathbf{d}}_{k,n}^T(p) \right]^T, \tag{3.41}$$

with

$$\overline{\mathbf{y}}_{k,n} = \left[\tilde{\mathbf{y}}_{k,n-L_f+1}^T \quad \tilde{\mathbf{y}}_{k,n-L_f}^T \quad \cdots \quad \tilde{\mathbf{y}}_{k,n}^T \right]^T \tag{3.42}$$

and

[5] This form of OQAM DFE, adapted via LMS, was also studied, for single-antenna (SISO) single-carrier systems, in [35] and later in [36][37] for SISO FBMC/OQAM. See also [38][39][40][41] for FBMC/OQAM SISO equalization structures.

$$\hat{\mathbf{d}}_{k,n}(p)=\left[\hat{\mathbf{d}}_{k,n-L_b}^T \quad \hat{\mathbf{d}}_{k,n-L_b+1}^T \quad \cdots \quad \hat{\mathbf{d}}_{k,n-1}^T \quad \hat{d}_{k,n}^{o_1} \quad \hat{d}_{k,n}^{o_2} \quad \cdots \quad \hat{d}_{k,n}^{o_{p-1}}\right]^T, \tag{3.43}$$

where $\hat{d}_{k,n}^{o_i}=\mathrm{dec}\left[\widehat{d}_{k,n}^{o_i}\right]$. Note that this decision corresponds to the input symbol at the subcarrier k and time $n-\Delta_k$, with Δ_k being the equalizer's delay.

This equalization scheme achieves two goals simultaneously. Not only it updates the equalizer taps in an RLS manner, but also specifies, for each time instant, the ordering in which the streams must be detected. As already mentioned, in a V-BLAST-type scheme, streams achieving lower mean squared detection error are extracted in earlier stages. Let us assume that the equalizer of the p th stage must be computed given the DFEs of the previous stages and symbol decisions according to the ordering $\left\{o_1,o_2,\ldots,o_{p-1}\right\}$. The remaining stream indices form the set $O_p=O\setminus\left\{o_1,o_2,\ldots,o_{p-1}\right\}$. To find out which of these streams achieves the lowest squared error and hence should be detected at the current stage, all the respective equalizers must be updated first. The equalizer of the p th stage corresponding to the r th stream, $\overline{\mathbf{w}}_{k,n}^{(r)}(p)$, is obtained by minimizing the following LS cost function:

$$E_{k,n}^{(r)}(p)=\sum_{l=1}^{n}\lambda^{n-l}\left|\hat{d}_{k,l}^{r}-\widehat{d}_{k,l}^{r}(p)\right|, \qquad r\in O_p, \tag{3.44}$$

where λ is the forgetting factor and

$$\widehat{d}_{k,l}^{r}(p)=\mathrm{Re}\left[\left(\overline{\mathbf{w}}_{k,n}^{(r)}(p)\right)^H\mathbf{y}_{k,l}(p)\right]=\left(\overline{\overline{\mathbf{w}}}_{k,n}^{(r)}(p)\right)^T\overline{\overline{\mathbf{y}}}_{k,l}(p), \tag{3.45}$$

with

$$\overline{\overline{\mathbf{y}}}_{k,l}(p)=\left[\mathrm{Im}\left(\overline{\mathbf{y}}_{k,l}\right)^T \quad \mathrm{Re}\left(\overline{\mathbf{y}}_{k,l}\right)^T \quad \hat{\mathbf{d}}_{k,l}^T(p)\right]^T, \tag{3.46}$$

and

$$\overline{\overline{\mathbf{w}}}_{k,n}^{(r)}(p)=\left[\mathrm{Im}\left[\mathbf{f}_{k,n}^{(r)}(p)\right]^T \quad \mathrm{Re}\left[\mathbf{f}_{k,n}^{(r)}(p)\right]^T \quad \mathrm{Re}\left[\mathbf{b}_{k,n}^{(r)}(p)\right]^T\right]^T. \tag{3.47}$$

That is:

$$o_p=\arg\min_{r\in O_p}E_{k,n}^{(r)}(p). \tag{3.48}$$

After updating all tentative equalizers at each stage, the one offering the lowest squared error is selected to yield the equalizer $\mathbf{w}_{k,n}(p)$ (or $\overline{\overline{\mathbf{w}}}_{k,n}(p)=\left[\mathrm{Im}\left[\mathbf{f}_{k,n}^{(o_p)}(p)\right]^T \quad \mathrm{Re}\left[\mathbf{f}_{k,n}^{(o_p)}(p)\right]^T \quad \mathrm{Re}\left[\mathbf{b}_{k,n}^{(o_p)}(p)\right]^T\right]^T$).

A numerically stable version of the above algorithm can result by using the LS normal equations to re-parameterize the equalizers $\overline{\overline{\mathbf{w}}}_{k,n}^{(r)}(p)$ as

$$\overline{\overline{\mathbf{w}}}_{k,n}^{(r)}(p)=\mathbf{R}_{k,n}^{-1}(p)\,\mathbf{v}_{k,n}^{(r)}(p), \tag{3.49}$$

where $\mathbf{R}_{k,n}(p)$ is the Cholesky factor of the DFE input autocorrelation matrix, $\mathbf{\Phi}_{k,n}(p)=\sum_{l=0}^{n}\lambda^{n-l}\overline{\overline{\mathbf{y}}}_{k,l}(p)\overline{\overline{\mathbf{y}}}_{k,l}^T(p)$, and

$$\mathbf{v}_{k,n}^{(r)}(p)=\mathbf{R}_{k,n}^{-H}(p)\,\mathbf{z}_{k,n}^{(r)}(p), \tag{3.50}$$

with $\mathbf{z}_{k,n}^{(r)}(p)=\sum_{l=1}^{n}\lambda^{n-l}\overline{\overline{\mathbf{y}}}_{k,l}(p)\hat{d}_{k,l}^{r}$ being the corresponding cross-correlation vector. The computations can be significantly simplified by exploiting the DFE input structure, namely:

$$\overline{\overline{\mathbf{y}}}_{k,l}(p+1)=\left[\overline{\overline{\mathbf{y}}}_{k,l}^{T}(p)\quad \hat{d}_{k,l}^{o_p}\right]^{T}, \tag{3.51}$$

to arrive at order- and time-recursive ways of updating the quantities involved. Details can be found in [32][33]. Note that further computational savings can result, in slowly fading channels, by updating the ordering only once in a block of symbols instead of on a symbol-by-symbol basis [32].

We have tested the above algorithm in the equalization of Veh-A time-varying 2×2 M-block fading channels, with both FBMC/OQAM and CP-OFDM modulations. Figure 3.12 depicts the results. For the FBMC system, we have utilized the PHYDYAS reference filter bank with $M=64$ and $K=4$. For the feed-forward and feed-back filters in the FBMC case, we chose $L_f=L_b=2$, while the delay was the same for all subcarriers and equal to $\Delta=L_f-1$. In the CP-OFDM case, where the subchannels are flat, we set $L_f=1$ and $L_b=0$. The equalizer filters were initialized by applying the algorithm in a training preamble of 20 pseudorandom OFDM (40 FBMC) symbols.[6] λ was set to 0.9. For CP-OFDM, the CP length was set to the channel order. One can see that the FBMC system is outperformed by the CP-OFDM one, especially for high SNR values. Moreover, as expected, the OFDM equalizer converges faster in the preamble section.

Let us now consider a severely frequency selective channel, of the Veh-B type, and set the CP length to its maximum value allowed in e.g. WiMAX, namely $M/4$. In that case, with $M=64$ subcarriers, the OFDM subchannels are no longer frequency flat and the above equalization scheme, when adapted to flat fading channels, is no longer able to equalize them correctly. This can be seen in Figure 3.13, where the CP-free FBMC system is seen to perform better at medium to high SNR levels.

[6] Alternatively, the initial values of the equalizers could be computed from preamble-based channel estimates (as in, e.g., [37].

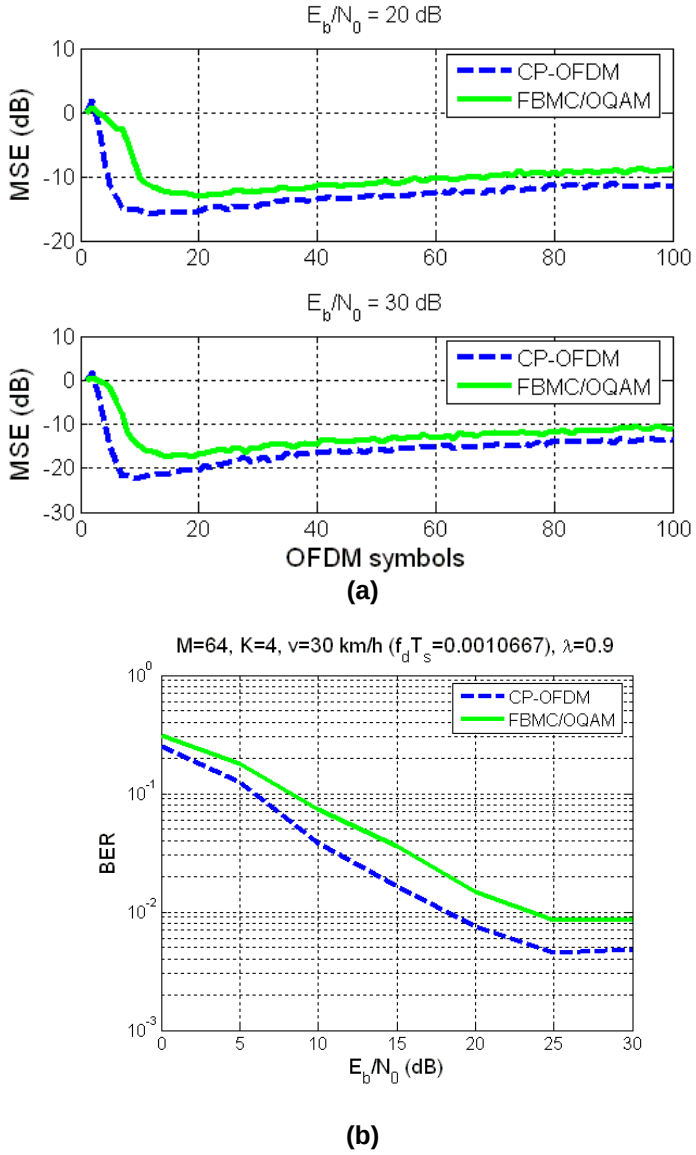

Figure 3.12. Adaptive DFE performance for Veh-A channels with QPSK input, at a speed of 30 km/h. $M = 64, K = 4$; $\lambda = 0.9$; for FBMC: $L_f = L_b = 2, \Delta = 1$. (a) Symbol squared error for SNR per bit equal to 25 and 30 dB. (b) BER vs. SNR.

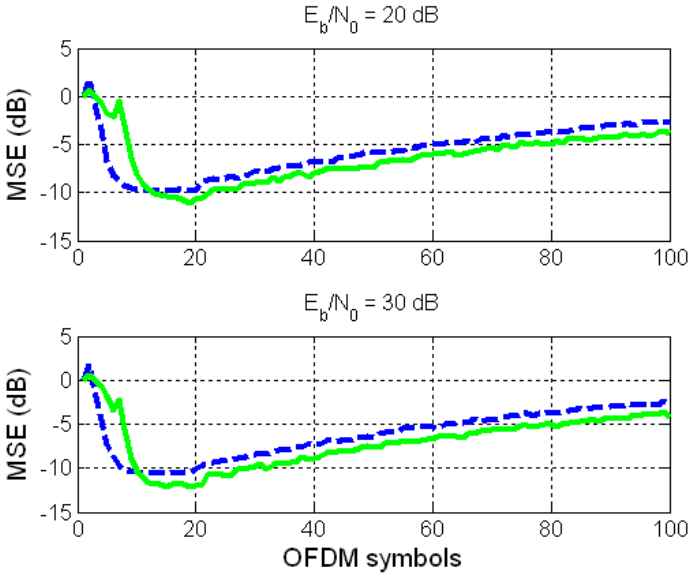

(a)

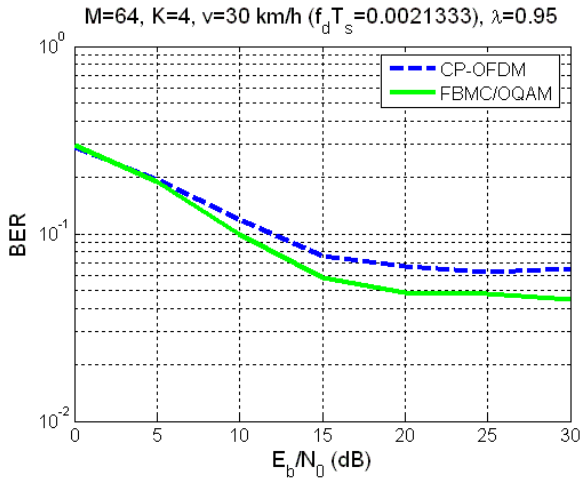

(b)

Figure 3.13. Adaptive DFE performance for Veh-B channels with QPSK input, at a speed of 30 km/h. $M = 64, K = 4$; $\lambda = 0.95$; for FBMC: $L_f = L_b = 3, \Delta = 2$. (a) Symbol squared error for SNR = 25 and 30 dB. (b) BER vs. SNR.

3.3 Single delay STTC and decoding schemes

FBMC systems employing OQAM modulation cannot use the symbol-wise space time block codes (STBC) or space time trellis codes (STTC) developed for transmit diversity in OFDM systems, because of the interference terms which accompany the data. Instead, they resort on delay or time diversity.

3.3.1 Transmit time diversity

Transmit diversity in the time domain implies that the same symbols are transmitted by the 2 antennas, but with a delay. With QAM modulation, a block code has been developed, in which the symbols are taken in pairs and applied in reverse order to the antennas. Such a scheme is not possible with OQAM because the interference terms cannot be completely eliminated at the receive side. Therefore, with FBMC the order of the symbols has to be kept for the different antennas. In this case, for a sub-channel in the FBMC system, the MIMO 2x1 channel is modelled by a 2-coefficient FIR filter, as shown in figure 3.14.

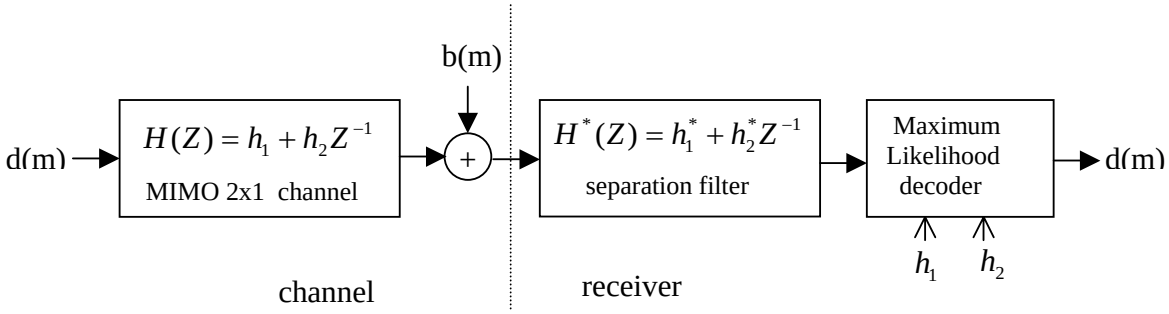

Figure 3.14. Model of transmit time diversity MIMO 2x1

In the sub-channel under consideration, the sequence of data $d(m)$ is assumed real and, taking into account the interference sequence $u(m)$, the received signal is expressed by

$$x(m) = h_1(d(m) + ju(m)) + h_2(d(m-1) + ju(m-1)) \tag{3.52}$$

Since the filter coefficients h_1 and h_2 are assumed to be complex scalars, the real data and the interference samples are mixed up and they must be separated, which is achieved by the conjugate of the channel filter.Then, the received signal is

$$y(m+1) = h_1^* x(m+1) + h_2^* x(m) \tag{3.53}$$

or

$$y(m+1) = |h_1|^2 (d(m+1) + ju(m+1)) + [h_1^* h_2 + h_2^* h_1](d(m) + ju(m)) + |h_2|^2 (d(m-1) + ju(m-1)) \tag{3.54}$$

Then, a sequence free of interference is obtained by

$$\mathrm{Re}(y(m+1)) = |h_1|^2 d(m+1) + 2\,\mathrm{Re}(h_1 h_2^*) d(m) + |h_2|^2 d(m-1) \tag{3.55}$$

In practice, a noise sequence $b(m)$ is added to the received signal, as shown in Figure 3.14, and the data are retrieved through a maximum likelihood decoder. However, the received noise sequence is filtered to produce the noise component accompanying $y(m)$. Therefore, this noise component is correlated and the maximum likelihood technique yields sub-optimal results. In fact, the noise filter has to be included in the calculation of the equivalent signal-to-noise ratio (SNR) of the maximum likelihood decoder. For binary data and channel noise power σ^2, the following value is obtained

$$SNR = \frac{1}{\sigma^2} \frac{|h_1|^4 + 4\left[\mathrm{Re}(h_1 h_2^*)\right]^2 + |h_2|^4}{(|h_1|^2 + |h_2|^2)(1 + \frac{4\left[\mathrm{Re}(h_1 h_2^*)\right]^2}{|h_1|^4 + 4\left[\mathrm{Re}(h_1 h_2^*)\right]^2 + |h_2|^4})} \quad (3.56)$$

An illustration of the impact of the noise filter is given in figure 3.15, where $h_1 = 1$.

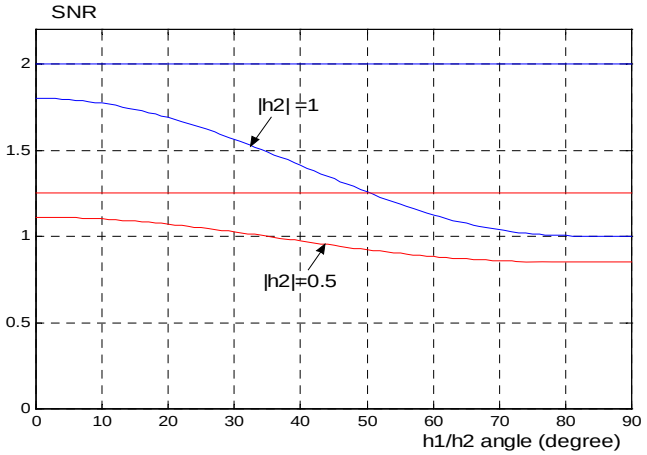

Figure 3.15 Degradation of the SNR due the the noise filter

The average loss of performance with respect to theoretical diversity ($1+|h_2|^2$) is the following

$\|h_2\|$	1	0.5	0.25
Average SNR	1.36	0.93	0.96
Loss (dB)	1.67	1.13	0.44

Clearly, the performance and the complexity of the decoding process are highly dependent on the relative values of the channel coefficients. Then, a decoding strategy can be as follows.

1) a theshold T is defined (example: T=0.1),
2) if $\left|\frac{h_1}{h_2}\right| < T$ or $\left|\frac{h_2}{h_1}\right| < T$, then direct decoding is implemented,
3) if $\mathrm{Im}(h_1 h_2^*) < T$, the separation filter is not needed, a ML decoder with 2 coefficients is implemented and theoretical diversity is achieved,
4) if $\mathrm{Re}(h_1 h_2^*) < T$, a separation filter is needed, a ML decoder with 2 coefficients is employed, but the theoretical diversity is not achieved, due to the noise filter,
5) in the other cases the separation filter needed, a ML decoder with 3 coefficients is implemented and theoretical diversity is not achieved.

Now, the above scheme is generalized to N_t transmit antennas and an iterative technique is proposed to reach the theoretical diversity.

3.3.2 Interference cancellation method

Let us first assume that only the i^{th} antenna is transmitting. At the receiver side, the demodulated signal $y_{k,n}$ at the frequency k and time instant n $(n\tau_0)$ can be written as:

$$y_{k,n} = H_{k,n,i}d_{k,n,i} + I_{k,n,i} + \upsilon_{k,n}, \tag{3.57}$$

where, $H_{k,n,i}$ is the channel coefficient between transmit antenna i and the receiver, at subcarrier k and time instant n. $\upsilon_{k,n}$ is the noise component at subcarrier k and time instant n.

- $$I_{k,n,i} = \sum_{(k',n')\neq(k,n)} H_{k',n',i}d_{k',n',i} \sum_{m=-\infty}^{\infty} g_{k,n}[m]g^*_{k',n'}[m]. \tag{3.58}$$

We assume that we have a prototype filter well localized in time and frequency. This implies that, in the previous equation the main contribution comes from the closest neighborhood i.e. $g_{k,n}[m]g^*_{k',n'}[m]$ takes a significant value only for $|k-k'|\leq 1$ and $|n-n'|\leq 1$. Moreover, if we assume that the channel is constant over a set of at least three consecutive sub-carriers and a set of at least three consecutive time indeces, then we can rewrite the previous expression as in [23]:

$$I_{k,n,i} \approx jH_{k,n,i}\underbrace{(-j)\sum_{(k',n')\neq(k,n)} d_{k',n',i} \sum_{m=-\infty}^{\infty} g_{k,n}[m]g^*_{k',n'}[m]}_{u_{k,n,i}}. \tag{3.59}$$

Thus, the demodulated signal can be approximated by:

$$y_{k,n} \approx H_{k,n,i}(d_{k,n,i} + ju_{k,n,i}) + \upsilon_{k,n}. \tag{3.60}$$

Throughout the remainder of the section, we will consider (3.60) as the expression of the signal at the output of the demodulator.

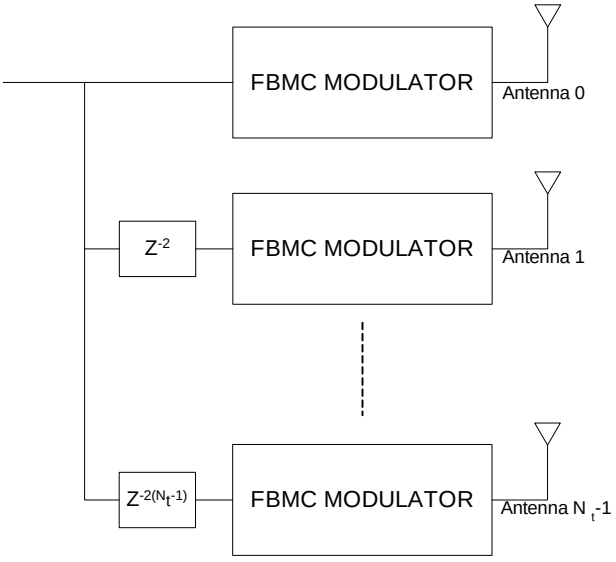

Figure 3.16 FBMC Single delay STTC transmitter

Let us consider the single delay STTC scheme with N_t antennas as shown in Figure 3.16. The real data to be transmitted are modulated by an FBMC modulator and transmitted by the first antenna. The same stream of data is delayed by $2n_i$ real data before being modulated by FBMC modulator and transmitted by the n_i^{th} antenna. The delay $2n_i$ is chosen to have the same delay as with a CP-OFDM system although a delay of n_i could also be chosen. We denote by $a_{k,n}$ the real data from the main stream of data at frequency k and time index n. Thus, at a given sub-carrier k the transmission is given at antenna i by: $d_{k,n,i} = a_{k,n-2i}$. At the receiver side, the demodulated signal can be written as:

$$y_{k,n} = \sum_{i=0}^{N_t-1} H_{k,n,i}(d_{k,n,i} + ju_{k,n,i}) + \upsilon_{k,n}$$

where $\upsilon_{k,n}$ is the noise component at the sub-carrier k and time instant n. As the same stream of data is transmitted over the N_t antennas, we have: $u_{k,n,i} = u_{k,n-2i,0} = b_{k,n-2i}$. In the remainder of the section, we will assume a channel constant over time i.e. ($H_{k,n,i} = H_{k,i}$), we get:

$$y_{k,n} = \sum_{i=0}^{N_t-1} H_{k,i} \underbrace{(a_{k,n-2i} + jb_{k,n-2i})}_{x_{k,n-2i}} + \upsilon_{k,n}. \tag{3.61}$$

The problem is to recover from $y_{k,n}$ the data $a_{k,n}$. The presence of the term $b_{k,n-2i}$ makes the decoding process from $y_{k,n}$ difficult. Some processing should be carried out in order to recover the real data.

For the case $N_t = 2$, it has been shown in [42] that, if we define $z_{k,n+2}$ as:

$$z_{k,n+2} = H_{k,1}^* y_{k,n} + H_{k,0}^* y_{k,n+2}. \tag{3.62}$$

Then we have:

$$\Re\{z_{k,n+2}\} = \Re\{H_{k,1}^* y_{k,n} + H_{k,0}^* y_{k,n+2}\} = |H_{k,1}|^2 a_{k,n-2} + 2\Re\{H_{k,1}^* H_{k,0}\} a_{k,n} + |H_{k,0}|^2 a_{k,n+2} + w_{k,n+2}, \tag{3.63}$$

with $w_{k,n+2} = \Re\{H_{k,1}^* \upsilon_{k,n} + H_{k,0}^* \upsilon_{k,n+2}\}$. Let $2L_f$ denote the frame length, for $e \in \{0,1\}$, if we denote by:

$$\underline{t}_e = \begin{bmatrix} \Re\{z_{k,e}\} & \Re\{z_{k,e+2}\} & .... & \Re\{z_{k,e+2(L_f-1)}\} \end{bmatrix}^T \tag{3.64}$$

$$\underline{a}_e = \begin{bmatrix} a_{k,e} & a_{k,e+2} & \ldots\ldots & a_{k,e+2(L_f-1)} \end{bmatrix}^T, \ \underline{w}_e = \begin{bmatrix} w_{k,e} & w_{k,e+2} & ... & w_{k,e+2(L_f-1)} \end{bmatrix}^T$$

and

$$\underbrace{\begin{bmatrix} |H_{k,0}|^2 & 0 & \ldots & \ldots & 0 \\ 2\Re\{H_{k,0}H_{k,1}^*\} & |H_{k,0}|^2 & \ddots & \ldots & \vdots \\ |H_{k,1}|^2 & 2\Re\{H_{k,0}H_{k,1}^*\} & |H_{k,0}|^2 & 0 & \vdots \\ 0 & \ddots & \ddots & \ddots & \vdots \\ \vdots & \ddots & \ddots & \ddots & 0 \\ 0 & \ldots & |H_{k,1}|^2 & 2\Re\{H_{k,0}H_{k,1}^*\} & |H_{k,0}|^2 \end{bmatrix}}_{\underline{G}_2}, \tag{3.65}$$

we have:

$$\underline{t}_e = \underline{\underline{G}}_2 \underline{a}_e + \underline{w}_e. \tag{3.66}$$

In this last equation, the imaginary interference term is cancelled. Thus the decoding process can be easily carried out either by using Maximum Likelihood (ML) decoding, Viterbi decoding, or linear equalization such as Zero Forcing (ZF) or Minimum Mean Square Error (MMSE) decoding. More generally with $N_t \geq 2$, let us note and compute:

$$\begin{aligned} z_{k,n+2N_t-2} &= \sum_{p=0}^{N_t-1} H^*_{k,N_t-1-p} y_{k,n+2p} \\ &= \sum_{p=0}^{N_t-1}\sum_{i=0}^{N_t-1} H^*_{k,N_t-1-p} H_{k,i} x_{k,n+2p-2i} + \underbrace{\sum_{p=0}^{N_t-1} H^*_{k,N_t-1-p} \upsilon_{k,n+2p}}_{n_{k,n+2N_t-2}} \\ &= \underbrace{\sum_{i=1}^{N_t-1}\sum_{p=0}^{i-1} H^*_{k,N_t-1-p} H_{k,i} x_{k,n+2p-2i}}_{B_{k,n}} + \underbrace{\sum_{i=0}^{N_t-1}\sum_{p=i} H^*_{k,N_t-1-p} H_{k,i} x_{k,n+2p-2i}}_{A_{k,n}} \\ &+ \underbrace{\sum_{i=0}^{N_t-1}\sum_{p=i+1}^{N_t-1} H^*_{k,N_t-1-p} H_{k,i} x_{k,n+2p-2i}}_{C_{k,n}} + \sum_{p=0}^{N_t-1} H^*_{k,N_t-1-p} \upsilon_{k,n+2p}. \end{aligned} \tag{3.67}$$

$A_{k,n}$ is given by:

$$A_{k,n} = x_{k,n}\mu_k \tag{3.68}$$

Let us compute $A_{k,n}$ for case N_t even and odd :

- Case N_t even i.e. $N_t = 2U_t$

$$A_{k,n} = x_{k,n}\left(\sum_{i=0}^{U_t-1} H^*_{k,2U_t-1-i} H_{k,i} + \sum_{i=U_t}^{2U_t-1} H^*_{k,2U_t-1-i} H_{k,i}\right). \tag{3.69}$$

Using the relation $q = 2U_t - 1 - i$, we have:

$$\begin{aligned} A_{k,n} &= x_{k,n}\left(\sum_{i=0}^{U_t-1} H^*_{k,2U_t-1-i} H_{k,i} + \sum_{q=0}^{U_t-1} H^*_{k,q} H_{k,2U_t-1-q}\right) = x_{k,n}\left(\sum_{i=0}^{U_t-1}\left(H^*_{k,2U_t-1-i} H_{k,i} + H^*_{k,i} H_{k,2U_t-1-i}\right)\right) \\ &= x_{k,n}\underbrace{\left(2\sum_{i=0}^{U_t-1} \Re\{(H^*_{k,2U_t-1-i} H_{k,i})\}\right)}_{\mu_k}. \end{aligned} \tag{3.70}$$

- Case N_t odd i.e. $N_t = 2U_t + 1$

$$\mu_k = (\sum_{i=0}^{U_t-1} H^*_{k,2U_t-i} H_{k,i} + H^*_{k,U_t} H_{k,U_t} + \sum_{i=U_t+1}^{2U_t} H^*_{k,2U_t-i} H_{k,i}). \quad (3.71)$$

Again using $q = 2U_t - i$, we have:

$$\mu_k = (2\sum_{i=0}^{U_t-1} \Re\{(H^*_{k,2U_t-i} H_{k,i})\} + |H_{k,U_t}|^2). \quad (3.72)$$

The expression of $B_{k,n}$ is given by:

$$B_{k,n} = \sum_{q=1}^{N_t-1} x_{k,n-2q} \gamma_q, \quad (3.73)$$

where γ_q are real valued quantities which depend only on the channel coefficients as shown below.
Setting $q = p - i$, we get:

$$B_{k,n} = \sum_{i=1}^{N_t-1} \sum_{p=0}^{i-1} H^*_{k,N_t-1-p} H_{k,i} x_{k,n+2p-2i} = \sum_{i=1}^{N_t-1} \sum_{q=1}^{i} x_{k,n-2q} H^*_{k,N_t-1+q-i} H_{k,i}. \quad (3.74)$$

This last equation is the sum over a triangular set of index therefore the sum can be taken either from lines or from columns where the total is the same. Therefore,

$$B_{k,n} = \sum_{q=1}^{N_t-1} x_{k,n-2q} \sum_{i=q}^{N_t-1} H^*_{k,N_t-1+q-i} H_{k,i}, \quad (3.75)$$

taking $m = i - q$, we get:

$$B_{k,n} = \sum_{q=1}^{N_t-1} x_{k,n-2q} \underbrace{\sum_{m=0}^{N_t-1-q} H^*_{k,N_t-1-m} H_{k,m+q}}_{\gamma_q}, \quad (3.76)$$

- Case $N_t - q$ even i.e. $N_t - q = 2U_q$, then,

$$\begin{aligned} \gamma_q &= \sum_{m=0}^{N_t-1-q} H^*_{k,N_t-1-m} H_{k,m+q} = \sum_{m=0}^{U_q-1} H^*_{k,2U_q+q-1-m} H_{k,m+q} + \sum_{m=U_q}^{2U_q-1} H^*_{k,2U_q+q-1-m} H_{k,m+q} \\ &= 2\sum_{m=0}^{U_q-1} \Re\{H^*_{k,2U_q+q-1-m} H_{k,m+q}\}. \end{aligned} \quad (3.77)$$

- Case $N_t - q$ odd i.e. $N_t - q = 2U_q + 1$, then,

$$\begin{aligned}\gamma_q &= \sum_{m=0}^{N_t-1-q} H^*_{k,N_t-1-m} H_{k,m+q} = \sum_{m=0}^{U_q-1} H^*_{k,2U_q+q-m} H_{k,m+q} + H^*_{k,U_q+q} H_{k,U_q+q} + \sum_{m=U_q+1}^{2U_q} H^*_{k,2U_q+q-m} H_{k,m+q} \\ &= 2\sum_{m=0}^{U_q-1} \Re\{H^*_{k,2U_q+q-m} H_{k,m+q}\} + |H^*_{k,U_q+q}|^2 .\end{aligned} \tag{3.78}$$

The expression of $C_{k,n}$ is given by:

$$C_{k,n} = \sum_{q=1}^{N_t-1} x_{k,n+2q} \beta_q, \tag{3.79}$$

where β_q are real valued quantities which depend only on the channel coefficients as shown below. Setting $q = p - i$, we get:

$$C_{k,n} = \sum_{i=1}^{N_t-2} \sum_{q=1}^{N_t-1-i} H^*_{k,N_t-1-q-i} H_{k,i} x_{k,n+2q}. \tag{3.80}$$

This last equation is the sum over a triangular set of index therefore the sum can be taken either from lines or from columns the total is the same. Therefore,

$$C_{k,n} = \sum_{q=1}^{N_t-1} x_{k,n+2q} \underbrace{\sum_{i=0}^{N_t-1-q} H^*_{k,N_t-1-q-i} H_{k,i}}_{\beta_q}, \tag{3.81}$$

- Case $N_t - q$ even i.e. $N_t - q = 2U_q$, then,

$$\begin{aligned}\beta_q &= \sum_{i=0}^{N_t-1-q} H^*_{k,N_t-1-q-i} H_{k,i} = \sum_{i=0}^{U_q-1} H^*_{k,2U_q-1-i} H_{k,i} + \sum_{m=U_q}^{2U_q-1} H^*_{k,2U_q-1-i} H_{k,i} \\ &= 2\sum_{i=0}^{U_q-1} \Re\{H^*_{k,2U_q-1-i} H_{k,i}\}.\end{aligned} \tag{3.82}$$

- Case $N_t - q$ odd i.e. $N_t - q = 2U_q + 1$, then,

$$\begin{aligned}\beta_q &= \sum_{i=0}^{N_t-1-q} H^*_{k,N_t-1-q-i} H_{k,i} = \sum_{i=0}^{U_q-1} H^*_{k,2U_q-i} H_{k,i} + H^*_{k,U_q} H_{k,U_q} + \sum_{m=U_q+1}^{2U_q} H^*_{k,2U_q-i} H_{k,i} \\ &= 2\sum_{m=0}^{U_q-1} \Re\{H^*_{k,2U_q-i} H_{k,i}\} + |H^*_{k,U_q}|^2 .\end{aligned} \tag{3.83}$$

Therefore,

$$z_{k,n+2N_t-2} = \sum_{q=1}^{N_t-1} \gamma_q x_{k,n-2q} + \mu_k x_{k,n} + \sum_{q=1}^{N_t-1} \beta_q x_{k,n+2q} + \sum_{p=0}^{N_t-1} H^*_{k,N_t-1-p} \upsilon_{k,n+2p}.$$

Thus, by noting: $t^{(1)}_{k,n+2N_t-2} = \Re\{z_{k,n+2N_t-2}\}$, we have:

$$t^{(1)}_{k,n+2N_t-2} = \sum_{q=1}^{N_t-1}\gamma_q a_{k,n-2q} + \mu_k a_{k,n} + \sum_{q=1}^{N_t-1}\beta_q a_{k,n+2q} + \underbrace{\Re\{\sum_{p=0}^{N_t-1} H^*_{k,N_t-1-p}\upsilon_{k,n+2p}\}}_{w_{k,n+2N_t-2}}. \quad (3.84)$$

For $e \in \{0,1\}$, we note: $\underline{t}_e = \left[t_{k,e} \quad t_{k,e+2} \quad ... \quad t_{k,e+2(L_f-1)} \right]^T$,

$\underline{w}_e = \left[\Re\{w_{k,e}\} \quad \Re\{w_{k,e+2}\} \quad .... \quad \Re\{w_{k,e+2(L_f-1)}\} \right]^T$, and

$$G_{N_t} = \begin{pmatrix} \beta_{N_t-1} & 0 & \dots & \dots & \dots & \dots & \dots & \dots & \dots & \dots & 0 \\ \beta_{N_t-2} & \beta_{N_t-1} & 0 & \dots & \dots & \dots & \dots & \dots & \dots & \dots & \vdots \\ \vdots & \ddots & \ddots & \ddots & \dots & \dots & \dots & \dots & \dots & \dots & \vdots \\ \beta_1 & \ddots & \ddots & \ddots & \ddots & \dots & \dots & \dots & \dots & \dots & \vdots \\ \mu_k & \ddots & \ddots & \ddots & \ddots & \ddots & \dots & \dots & \dots & \dots & \vdots \\ \gamma_{N_t-1} & \ddots & \ddots & \ddots & \ddots & \ddots & \ddots & \dots & \dots & \dots & \vdots \\ \vdots & \ddots & \ddots & \ddots & \ddots & \ddots & \ddots & \ddots & \dots & \dots & \vdots \\ \gamma_1 & \ddots & \ddots & \ddots & \ddots & \ddots & \ddots & \ddots & \ddots & \dots & \vdots \\ 0 & \ddots & \ddots & \ddots & \ddots & \ddots & \ddots & \ddots & \ddots & \ddots & \vdots \\ \vdots & \ddots & \ddots & \ddots & \ddots & \ddots & \ddots & \ddots & \ddots & \ddots & 0 \\ 0 & \dots & 0 & \gamma_1 & \dots & \gamma_{N_t-1} & \mu_k & \beta_1 & \dots & \beta_{N_t-2} & \beta_{N_t-1} \end{pmatrix}.$$

We have:

$$\underline{t}_e = \underline{G_{N_t}}\,\underline{a}_e + \underline{w}_e. \quad (3.85)$$

There is no imaginary interference in equation (3.85) and consequently Maximum Likelihood (ML) [45] or linear equalizers can be used to estimate $a_{k,n}$.

The computation of $z_{k,n}$ from $y_{k,n}$ according to equation (3.67) is referred to Preprocessing1 as shown in Figure 3.17. We will now perform a theoretical performance analysis of this scheme in the case of $N_t = 2$.

Let us consider that the noise $\upsilon_{k,n}$ is an AWGN noise with $E\{|\upsilon_{k,n}|^2\} = N_0$. It is worth noticing that $\Re\{w_{k,n}\}$ is Gaussian noise as it is the result of the real part of a linear transformation of Gaussian noise. But the noise is colored since:

- $E\{w_{k,n}w^*_{k,n+2}\} = E\{w_{k,n+2}w^*_{k,n}\} = \dfrac{N_0(|H_{k,0}|^2 + |H_{k,1}|^2)\Re\{(H_{k,0})^* H_{k,1}\}}{2}$
- $E\{w_{k,n}w^*_{k,n}\} = \dfrac{N_0(|H_{k,0}|^2 + |H_{k,1}|^2)}{2} = U_0/2$ (3.86)
- for $q \neq \{0,1\}$ $E\{w_{k,n}w^*_{k,n+2q}\} = 0$.

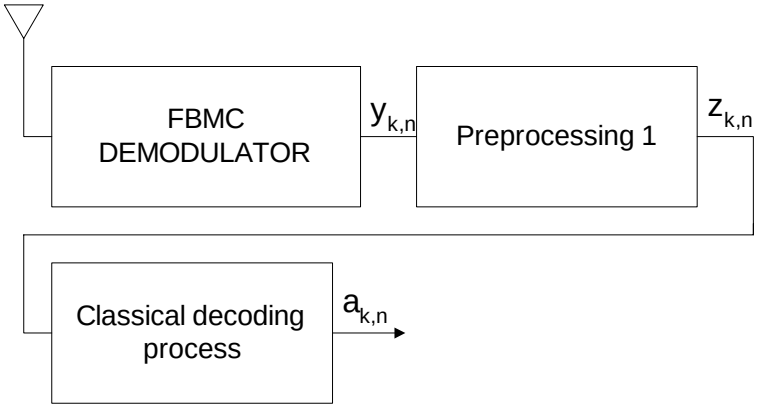

Figure 3.17 FBMC Single delay STTC receiver

Let us recall that if the noise was white the ML performance would have been obtained by the Viterbi decoder. Therefore, the performance of Viterbi decoding in this present case is sub-optimal. In [46] the authors evaluate the loss of performance of Viterbi decoding in presence of correlated noise. The optimal performance using a ML decoding is very complex to implement since it requires an exhaustive search over all the possible transmitted sequences. Another alternative could be to perform a whitening followed by a Viterbi decoding. However, such Viterbi decoding will be more complex since the whitening will increase the number of states. Indeed, the noise $\underline{w}_e$ is colored with a correlation matrix $\underline{R}$. Since $\underline{R}$ is a positive Hermitian matrix, its eigenvalues are real and positive. We have:

$$\underline{R} = \underline{Q} \underbrace{\begin{bmatrix} \lambda_0 & 0 & \dots & 0 \\ 0 & \ddots & \ddots & \vdots \\ \vdots & \ddots & \ddots & 0 \\ 0 & \dots & 0 & \lambda_{L_f-1} \end{bmatrix}}_{\underline{\Lambda}} \underline{Q}^H. \tag{3.87}$$

with $\underline{Q}$ an unitary matrix i.e. $\underline{Q}\underline{Q}^H = \underline{I}_{L_f}$. We denote by

$$\underline{\Lambda}^{1/2} = \begin{bmatrix} \lambda_0^{1/2} & 0 & \dots & 0 \\ 0 & \ddots & \ddots & \vdots \\ \vdots & \ddots & \ddots & 0 \\ 0 & \dots & 0 & \lambda_{L_f-1}^{1/2} \end{bmatrix}. \tag{3.88}$$

Therefore, the whitening process can be done by computing:

$$\underline{y}_e = \underline{\Lambda}^{-1/2}\underline{Q}^H \underline{z}_e = \underbrace{\underline{\Lambda}^{-1/2}\underline{Q}^H \underline{G}_2}_{\underline{H}} \underline{a}_e + \underbrace{\underline{\Lambda}^{-1/2}\underline{Q}^H \underline{w}_e}_{\underline{\mu}_e} = \underline{H}\underline{a}_e + \underline{\mu}_e. \tag{3.89}$$

It can easily be proved that $\underline{\mu}_e$ is AWGN. As we will see in the simulation results section, the presence of the colored noise will lead to a degradation of performance. Let us now present an iterative decoding approach which should improve the performance compared to the previous decoding strategy.

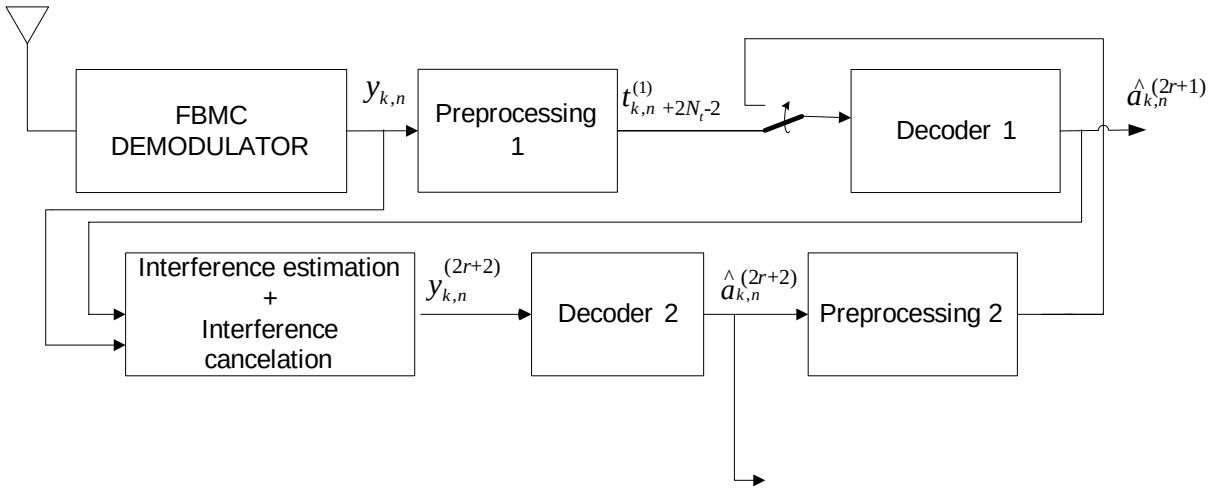

Figure 3.18 Receiver decoding processing for FBMC modulation in the case of single delay STTC transmission.

3.3.3 Iterative method

In this section we propose an iterative decoding procedure for FBMC single STTC decoding. At the output of the Preprocessing1 block (see Figure 3.18), we can perform a decoding procedure (ML, Viterbi, or linear decoding) to derive an estimate value $\hat{a}_{k,n}^{(1)}$ of $a_{k,n}$. From (3.59) and using this estimate $\hat{a}_{k,n}^{(1)}$, we can compute an estimate $\hat{u}_{k,n}^{(1)}$ of $u_{k,n}$ by:

$$\hat{u}_{k,n}^{(1)} = \sum_{(p,q)\neq(0,0)} \hat{a}_{k+p,n+q}^{(1)} \underbrace{\sum_{m=-\infty}^{\infty} g_{k,n}[m] g_{k+p,n+q}[m]}_{\gamma_{p,q}}. \tag{3.90}$$

It is worth noticing that for a well localized prototype filter in time and frequency domain, it is enough to consider the previous sum only for $p,q \in \{1,-1\}$ i.e.

$$\hat{u}_{k,n}^{(1)} \approx \sum_{|p|=1,|q|=1} \hat{a}_{k+p,n+q}^{(1)} \gamma_{p,q}. \tag{3.91}$$

This approximation is justified in [23]. $\gamma_{p,q}$ can be computed off-line since the prototype filter response is known. Then in (3.61) we can remove the contribution of the $u_{k,n}$ components by computing:

$$y_{k,n}^{(2)} = y_{k,n} - \sum_{i=0}^{N_t-1} H_{k,i} \hat{u}_{k,n-2i}^{(1)} = \sum_{i=0}^{N_t-1} H_{k,i} a_{k,n-2i} + \sum_{i=0}^{N_t-1} jH_{k,i}(u_{k,n-2i} - \hat{u}_{k,n-2i}^{(1)}) + \upsilon_{k,n}. \tag{3.92}$$

If we assume a perfect cancellation of the $u_{k,n}$ terms i.e. $u_{k,n} = \hat{u}_{k,n}^{(1)}$, we have:

$$y_{k,n}^{(2)} = \sum_{i=0}^{N_t-1} H_{k,i} a_{k,n-2i} + \upsilon_{k,n}. \tag{3.93}$$

The operation of estimating $u_{k,n}$ and cancelling its contribution to the signal $y_{k,n}$ is referred as "Interference estimation + Interference cancellation" as depicted in Figure 3.18. Thus, we can perform from $y_{k,n}^{(2)}$ a new decoding (Decoder2 block) to obtain a new estimate $\hat{a}_{k,n}^{(2)}$ of $a_{k,n}$. In the same manner,

we can use either a Viterbi/ML decoding or a linear decoder. From $\hat{a}_{k,n}^{(2)}$ and (3.84) we can also compute $t_{k,n+2}^{(2)}$ by:

$$t_{k,n+2N_t-2}^{(2)} = \sum_{q=1}^{N_t-1}\gamma_q \hat{a}_{k,n-2q}^{(2)} + \mu_k \hat{a}_{k,n}^{(2)} + \sum_{q=1}^{N_t-1}\beta_q \hat{a}_{k,n+2q}^{(2)}. \tag{3.94}$$

$t_{k,n+2}^{(2)}$ can also be rewritten as:

$$\begin{aligned} t_{k,n+2N_t-2}^{(2)} &= \sum_{q=1}^{N_t-1}\gamma_q a_{k,n-2q} + \mu_k a_{k,n} + \sum_{q=1}^{N_t-1}\beta_q a_{k,n+2q} + \sum_{q=1}^{N_t-1}\gamma_q(\hat{a}_{k,n-2q}^{(2)} - a_{k,n-2q}) + \mu_k(\hat{a}_{k,n}^{(2)} - a_{k,n}) \\ &+ \sum_{q=1}^{N_t-1}\beta_q(\hat{a}_{k,n+2q}^{(2)} - a_{k,n+2q}) \\ &= \sum_{q=1}^{N_t-1}\gamma_q a_{k,n-2q} + \mu_k a_{k,n} + \sum_{q=1}^{N_t-1}\beta_q a_{k,n+2q} + \textit{noise component}. \end{aligned} \tag{3.95}$$

$t_{k,n+2N_t-2}^{(2)}$ is a new version of the $t_{k,n+2N_t-2}^{(1)}$ signal which is obtained from the estimates of the Decoder2 block output. Thus, this last equation can be used to perform another estimation $\hat{a}_{k,n}^{(3)}$ of $a_{k,n}$ in the same manner as we compute $\hat{a}_{k,n}^{(1)}$. We expect to improve the estimation of $a_{k,n}$ since the noise component in (3.95) should be less correlated than the one in (3.84) . Again from $\hat{a}_{k,n}^{(3)}$ we can derive an estimate $\hat{u}_{k,n}^{(2)}$ of $u_{k,n}$ as in (3.90). Therefore, we can repeat another decoding process as already presented. We can run this decoding process as many times as necessary. The process of computing $t_{k,n+2N_t-2}^{(2)}$ from the $\hat{a}_{k,n}^{(2)}$ is referred as Preprocessing2, see Figure 3.18.

Simulation Results in presence of a Rayleigh channel for $N_t = 2$

In this section, we will evaluate the performance of the two decoding methods that we have presented. We consider a transmission scheme with two transmit antennas $N_t = 2$. For $N_t = 2$ we have:

$$\begin{aligned} y_{k,n} &= \sum_{i=0}^{1} H_{k,n,i}(d_{k,n,i} + ju_{k,n,i}) + \upsilon_{k,n} \\ &= H_{k,0}a_{k,n} + H_{k,1}a_{k,n-2} + \mu_{k,n}, \end{aligned} \tag{3.96}$$

with

$\mu_{k,n} = jH_{k,0}u_{k,n,0} + jH_{k,1}u_{k,n,1} + \upsilon_{k,n}$. We also get:

$$t_{k,n+2N_t-2}^{(1)} = |H_{k,1}|^2 a_{k,n-2} + 2\Re\{H_{k,1}^* H_{k,0}\}a_{k,n} + |H_{k,0}|^2 a_{k,n+2} + w_{k,n+2N_t-2}. \tag{3.97}$$

In this particular case, equation (3.93) becomes:

$$y_{k,n}^{(2)} = H_{k,0}a_{k,n} + H_{k,1}a_{k,n-2} + \upsilon_{k,n}. \tag{3.98}$$

The simulation parameters we consider are given as follows :

- No channel coding;
- QPSK modulation;

• Rayleigh channel per antenna i.e. flat over all the subcarriers. We assume the channel coefficients are perfectly known by the receiver;

• Number of subcarrier $M = 32$;

• We used a truncation of the IOTA (Isotropic Orthogonal Transform Algorithm) prototype function [47]. Its duration is limited to $4T_0$, which leads to a nearly orthogonal prototype filter containing $L = 4M = 128$ taps.

In Figure 3.19 we give the performance of the FBMC decoding structure introduced in Figure 3.17. For FBMC, we consider both ML and Viterbi decoding. ML decoding using an exhaustive search among all possible transmitted sequences of data outperforms Viterbi decoding by 1 dB. This is due to the fact that the noise is colored thus Viterbi decoding is suboptimal. We also give the CP-OFDM performance using a Viterbi decoding. We can see that that CP-OFDM outperforms ML/FBMC by about 1 dB.

In the rest of this section, we will focus on the iterative decoding performance. The simulation results are obtained using Viterbi decoding blocks implemented inside Decoder1 and Decoder2 blocks in Figure 3.18. The Viterbi algorithm implemented in Decoder1 is related to equation (3.38). For QPSK modulation, the trellis is a 4 state trellis with only two possible transitions per state since the detection is performed on real data. Whereas, the Viterbi algorithm implemented in Decoder2 is related to equation (3.39) and is a 2 state trellis with two transitions per state, again since detection is performed on real data. We also consider hard estimation of the data at the output of a given Viterbi decoder. For the CP-OFDM case with QPSK modulation, we have a 4 states trellis with 4 transitions per state as the detection is performed on complex data. Therefore, this Viterbi algorithm is more complex compared with one of the two Viterbi algorithms used in the case of FBMC modulation. The two Viterbi algorithms used in FBMC taken together have a complexity comparable to the one used with CP-OFDM. However, the two Viterbi algorithms used in FBMC operate on a frame sequence which is two times longer than the one for CP-OFDM modulation. Then, in terms of complexity the proposed FBMC structure has a significantly higher complexity than CP-OFDM mainly due to the "Interference estimation + Interference cancellation" block.

In Figure 3.20, we plot the performance of this FBMC receiver structure for different iteration stages as well as the performance of CP-OFDM with ML decoding as a matter of comparison. As the number of iterations increases, the performance of FBMC improves. For $n = 1$ we have a 2 dB degradation compared to CP-OFDM but for $n = 3$ (three Viterbi decoding), we already almost reach the performance of CP-OFDM. For $n = 5$, we have still a slight improvement. In Figure 3.20, we also add the performance assuming a perfect suppression of the interference terms. In that case, there is a possible gain of 0.8 dB since the Viterbi structure with 2 states and two transitions per state (Decoder2) provides better performance than the 4 state Viterbi decoder with 4 transitions per state implemented for CP-OFDM. Indeed, it is possible to show that the structures of the code related to these two trellises have the same minimum distance. However, the potential performance gain is due to the distance distribution associated to the two trellis.

We must emphasize that the BER curves do not take into consideration the loss of efficiency due to the cyclic prefix in CP-OFDM. Therefore, the proposed method has an additional gain since FBMC does not use a CP contrary to CP-OFDM.

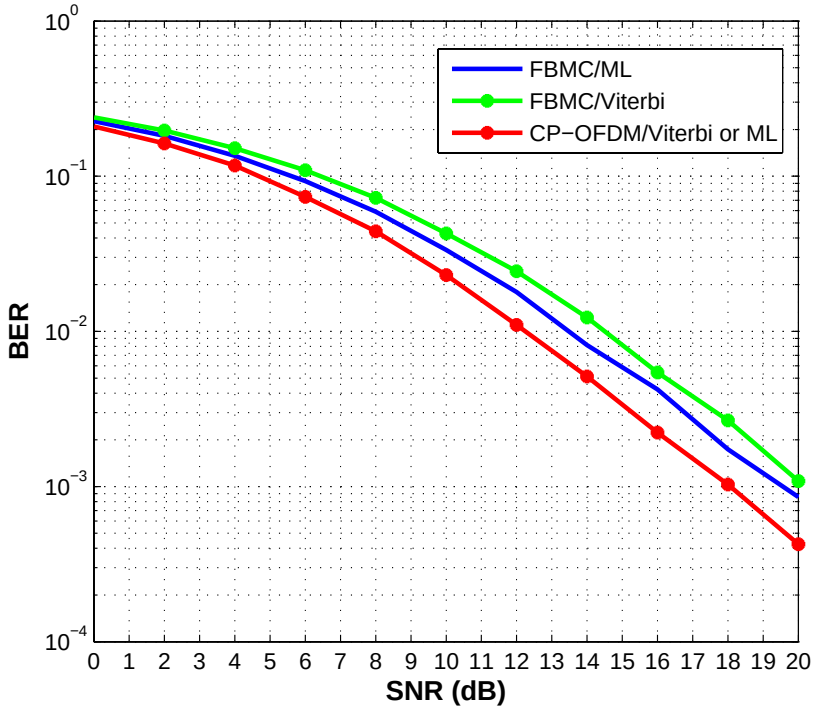

Figure 3.19 Performance of single delay STTC with 2 transmit antennas and one receive antenna (FBMC and CP-OFDM modulation).

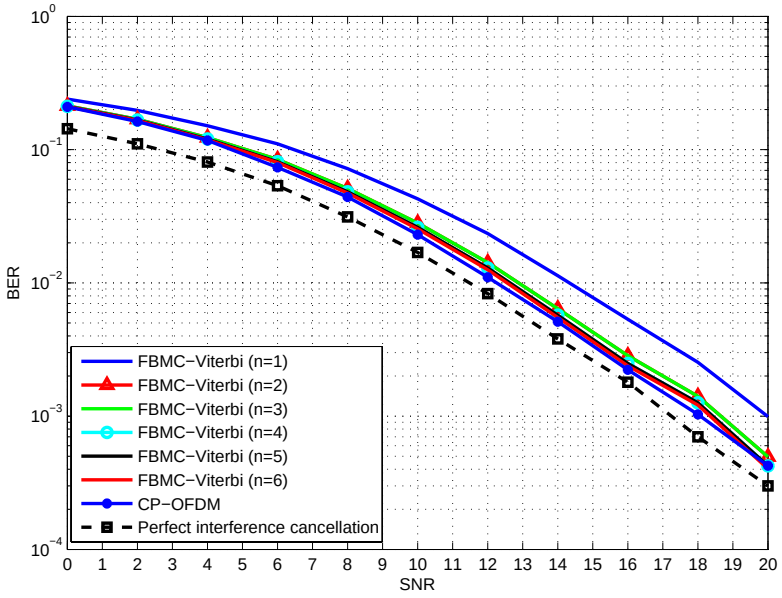

Figure 3.20 Performance of single delay STTC (iterative decoding) with 2 transmit antennas and one receive antenna (FBMC and CP-OFDM modulation).

3.4 Joint beamformer for single user

In addition to MC technologies, many systems have adopted spatial diversity based on the use of multiple antennas at both the transmitter and the receiver as an alternative to boost system capacity [48]. In this sense, multi-input-multi-output (MIMO) channels have become a key research focus in last years. In the following sections we propose a scheme to jointly exploit MC modulations and MIMO systems by means of a per-carrier joint beamforming approach [49]. This joint beamforming solution requires having a channel estimate, also called channel state information (CSI), at both ends of the communication system. In practical systems, this CSI will not be perfect due to several reasons, such as the presence of estimation noise, quantization errors, etc. In the following, we will analyze how the imperfections in the CSI affect the performance of MIMO-FBMC and MIMO-OFDM under joint beamforming. It will be shown that the MIMO-FBMC scheme outperforms its MIMO-OFDM counterpart when the CSI imperfections are kept below a threshold. For high values of the CSI imperfections, additional ISI and ICI components may appear, which degrade the performace of MIMO-FBMC. We have divided the analysis in two main sections: the first one is devoted to the simpler single beamforming case (where only one beamformer per carrier is used) and the second one deals with multiple beamformers, where more than one beamformer per carrier is used.

3.4.1 Single Beamformer

In this section, we take the approach of single joint beamforming per carrier, which requires full knowledge of the MIMO channel estimate at both sides of the communication system and consists in transmitting a single symbol stream per carrier (see Figure 3.21).

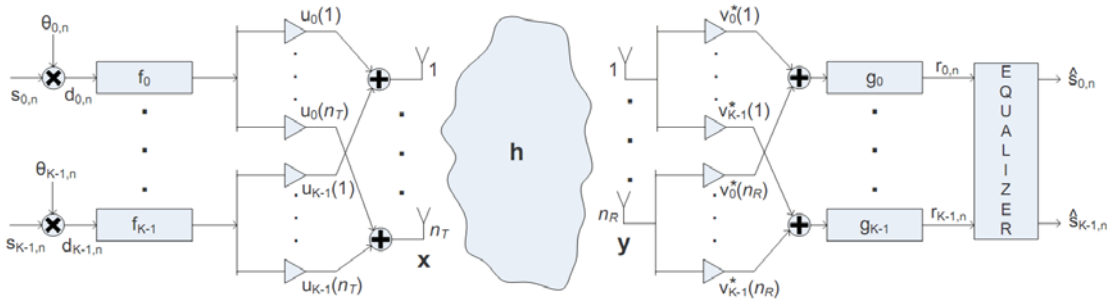

Figure 3.21 Transmitter and receiver architecture for the single joint beamformer in FBMC.

This single stream at each carrier at the output of the bank filter, f_k, is multiplied at the transmitter by a set of weights (one per antenna) collected in the so called transmit beamvector $\mathbf{u}_k \in C^{n_T}$ before sending them through the transmit antennas, obtaining for FBMC:

$$\mathbf{x}(m) = \sum_{k=0}^{K-1} \sum_{n=-\infty}^{\infty} \mathbf{u}_k d_{k,n} f_k(m - \tau n), \tag{3.99}$$

where, in the MIMO case, the j-th entry of vector $\mathbf{x}(m)$ represents the signal transmitted through the j-th antenna.

The MIMO channel is now expressed through a matrix $\mathbf{h}(m) \in C^{n_R \times n_T}$, whose (i, j)-th entry contains the channel impulse response between j-th transmit and i-th receive antennas. The received vector $\mathbf{y}(m) \in C^{n_R}$ is simply the matrix convolution between the channel and the transmitted vector plus the noise vector, $\mathbf{y}(m) = \mathbf{h}(m) * \mathbf{x}(m) + \mathbf{w}(m)$.

At the receiver, the incoming vector $\mathbf{y}(m)$ is multiplied by the K receive beamvectors $\mathbf{v}_k^H$, where $(\cdot)^H$ denotes the Hermitian operator, and each one of the obtained products $\mathbf{v}_k^H \mathbf{y}(m)$ is fed into its corresponding filter g_k. In general, and since the MIMO channel is expected to be frequency selective, the transmit and receive beamvectors, $\mathbf{u}_k$ and $\mathbf{v}_k^H$, can be different for each frequency as it has been indicated by the index k.

The signal at the output of the receiver filterbank $r_{k,n}$ is defined as:

$$r_{k,n} = g_k(m) * \mathbf{v}_k^H \mathbf{y}(m)\Big|_{m=m_0(n)}. \tag{3.100}$$

which is next equalized to obtain the estimation of $s_{k,n}$ (the equalization details are given later).

We derive the effective MIMO channel of the signals transmitted from filter $f_{k'}(t)$ and received at $g_k(t)$ through the MIMO channel, $g_k(t) * \mathbf{h}(t) * f_{k'}(t)$, where filters $g_k(t)$ are the matched filters of $f_k(t)$. They can be expressed as frequency shifted versions, $g_k(t) = f_{k'}^*(-t)e^{-j2\pi\Delta k \Delta f t}$ where $\Delta k = k' - k$ is separation between carriers.

Then,

$$\begin{aligned}
\tilde{h}_{k,k'}(t) &= \int_{-\infty}^{\infty} g_k(\tau) \int_{-\infty}^{\infty} \mathbf{h}(\gamma) f_{k'}(t-\tau-\gamma) d\tau d\gamma \\
&= \int\int_{-\infty}^{\infty} f_{k'}^*(-\tau) e^{-j2\pi\Delta k \Delta f \tau} \mathbf{h}(\gamma) f_{k'}(t-\tau-\gamma) d\tau d\gamma \\
&= \iint\int_{-\infty}^{\infty} f_{k'}^*(-\tau) \mathbf{h}(\gamma) F_{k'}(f) e^{j2\pi f(t-\tau-\gamma)} e^{-j2\pi\Delta k \Delta f \tau} df d\tau d\gamma \\
&= \int_{-\infty}^{\infty} F_{k'}^*(f - \Delta k \Delta f) \mathbf{H}(f) F_{k'}(f) e^{j2\pi f t} df
\end{aligned} \tag{3.101}$$

Where $\mathrm{F}_k(f)$ and $\mathbf{H}(f)$ are the Fourier transform of $f_k(t)$ and $\mathbf{h}(t)$, respectively.

When Δk is large, Fourier response of the filters will not overlap in frequency, thus the integral will approximately be zero. However, when Δk is small, assuming that the channel is slowly varying in frequency, the channel matrix can be approximated by its value at the intermediate frequency. After sampling, the remaining integral becomes the transmultiplexer coefficients, $t_{k-k',n}$ which characterize the ICI and ISI terms centered at $k - k'$ and n when a single symbol $d_{k,l}[n] = 1$ is transmitted through the filterbank system and an ideal channel.

$$\begin{aligned}\tilde{h}_{k,k'}(t) &\approx \mathbf{H}\left(k\Delta f + \tfrac{\Delta k}{2}\Delta f\right)\int_{-\infty}^{\infty} F_{k'}^{*}(f-\Delta k\Delta f)F_{k'}(f)e^{j2\pi ft}df \\ &= \mathbf{H}\left(\tfrac{(k'+k)}{2}\Delta f\right)t_{k'-k,t} \\ &= \mathbf{H}_{k,k'}t_{k-k',t},\end{aligned} \tag{3.102}$$

where the last equality is for compactness of notation. Similarly, when $\Delta k = 0$, the channel response is approximated by the value at the filter response, $\mathbf{H}_k$.

The design of the beamvectors, $\mathbf{u}_k$ and $\mathbf{v}_k^H$, depends on the channel matrix $\mathbf{h}(m)$. As pointed out earlier, we assume that the ISI and ICI components with perfect CSI are equalized (this is true in OFDM if the cyclic prefix is longer than the channel impulse response and an approximation in FBMC), therefore, the beamvectors for a specific carrier depend only on the channel response at such subband.

In the case of single joint beamforming, it was shown in [49] that the SNR-maximizing transmit beamvector at the k-th carrier is equal to a scaled version of the right singular vector $\mathbf{e}_{1,k}$ associated to the maximum singular value λ_k of the matrix $\mathbf{H}_k$, whose (i, j)-th element is the k-th component of the K-point Fourier transform of the channel between j-th transmit and i-th receive antennas (given by $[\mathbf{h}(m)]_{i,j}$). The scale factor is equal to the square root of the power allocated to such carrier, i.e., $\mathbf{u}_k = \sqrt{p_k}\mathbf{e}_{1,k}$, such that the sum of allocated powers is equal to the total transmitted power $P_T = \sum_k p_k$. At the receiver, the beamvector $\mathbf{v}_k^H$ is equal to the spatial matched filter

$$\mathbf{v}_k^H = \alpha_k(\mathbf{H}_k\mathbf{u}_k)^H, \tag{3.103}$$

where α_k is such that the norm $\left\|\mathbf{v}_k^H\right\|$ is equal to 1. The resulting equivalent SISO channel gain of the joint beamforming scheme is thus given by

$$C_k = \mathbf{v}_k^H\mathbf{H}_k\mathbf{u}_k = \lambda_k\sqrt{p_k}. \tag{3.104}$$

Concerning the power allocation, several approaches are possible depending on the adopted figure of merit for the system or optimization criterion, such as the minimization of the probability of error, the minimization of the mean square error, the maximization of a mean value of the SNRs at the different carriers, etc. In [49], all these possibilities are studied. In this paper we will only consider two of them as meaningful examples: uniform power allocation (UPA), where $p_k = P_T/K$, $\forall k$ and the minimum effective probability of error (MEPE) where

$$p_k = \max\left\{\frac{2\log(\lambda_k)-\mu}{\lambda_k^2}, 0\right\}, \tag{3.105}$$

where we recall that λ_k is the maximum singular value of $\mathbf{H}_k$ and μ is such that the power constraint is fulfilled.

In practice, only a channel estimate $\widetilde{\mathbf{H}}_k$ is available to perform the design of the transmit and receive beamvectors, $\tilde{\mathbf{u}}_k$ and $\tilde{\mathbf{v}}_k^H$. This implies that the actual equivalent channel

$$\bar{C}_k = \tilde{\mathbf{v}}_k^H \mathbf{H}_k \tilde{\mathbf{u}}_k \tag{3.106}$$

has a phase and amplitude mismatch with respect to the estimated equivalent channel given by

$$\tilde{C}_k = \tilde{\mathbf{v}}_k^H \widetilde{\mathbf{H}}_k \tilde{\mathbf{u}}_k = \tilde{\lambda}_k \sqrt{\tilde{p}_k}, \quad (\tilde{C}_k \in R^+ \text{ by construction}).$$

While this is not a critical problem in MIMO-OFDM because the orthogonality between subcarriers is preserved even if the channel is not estimated properly, it can be a problem in the case of MIMO-FBMC as it is shown next.

At the output of the equalizer, the estimate of the data symbol $\hat{s}_{k_0,n_0}$ is obtained as,

$$\hat{s}_{k_0,n_0} = \Re\mathrm{e}\left\{ \frac{\theta_{k_0,n_0}^* r_{k_0,n_0}}{\tilde{C}_{k_0}} \right\}. \tag{3.107}$$

Thus, in this imperfect CSI case, the ISI and ICI components in the FBMC system before taking the real part will be given by

$$\begin{aligned} \frac{\theta_{k_0,n_0}^* r_{k_0,n_0}}{\tilde{C}_{k_0}} &= s_{k_0,n_0} + \sum\nolimits_{(k,n)\in R} \frac{\bar{C}_{k_0-k}}{\tilde{C}_{k_0}} t_{k,n} (\pm s_{k_0-k,n_0-n}) \\ &\quad + \mathrm{j} \sum\nolimits_{(k,n)\in I} \frac{\bar{C}_{k_0-k}}{\tilde{C}_{k_0}} t_{k,n} (\pm s_{k_0-k,n_0-n}). \end{aligned} \tag{3.108}$$

Observe that, due to the phase mismatch between the actual equivalent channel and the estimated one $\bar{C}_{k_0-k} \approx \bar{C}_{k_0}$ part of the interference in the "imaginary" term in (3.108) will leak to the real part, which implies that the ISI/ICI components that were cancelled at the detection when perfect CSI was assumed, now will not disappear, worsening thus the detection quality and increasing the error probability.
The above analytic expression in (3.108) will be evaluated numerically in the simulations section, in which a comparison between the performance of MIMO-FBMC and MIMO-OFDM as a function of the CSI imperfections level will be presented. The purpose of the following section will be, thus, to compute the CSI imperfections margin for which the performance of MIMO-FBMC is above that of MIMO-OFDM.

Simulation results

For the sake of simplicity, in this section we will consider a very basic model for the channel estimation error. Precisely, we will assume that $\tilde{\mathbf{H}}_k = \mathbf{H}_k + \Delta_k$ where the entries of Δ_k are independent zero-mean circularly symmetric complex Gaussian random variables with power equal to P_E. This model would fit, e.g., in a situation where the receiver imperfectly estimates the channel in the frequency domain and then feeds back this estimation to the transmitter through an ideal feedback link. It must be highlighted that the results obtained in this section also hold for other models for the channel estimation error.

However, the simple dependence of our model on exclusively the parameter P_E makes it suitable for the purposes of this section.

For the FBMC system we have taken the design in [50] with filter length $L = 2048$, symbol period $\tau = 256$, and inverse of the frequency separation $M = 512$. For the OFDM system, the CP has been assumed to be one fourth of the total symbol duration. The PAM modulation for FBMC is BPSK and QPSK has been considered in OFDM so that the rate is the same in both systems, the total transmitted power has been normalized to $P_T = K$, and the SNR of the system is given by P_T/σ^2, with σ^2 being the power of the noise vector $\mathbf{w}(m)$.

The channel has been chosen to be a Rayleigh distributed 3×3 MIMO channel, whose length has been fixed to 10 with an exponentially decaying power delay profile (the delay spread is equal to 5 times the sampling period).

In Figure 3.22 we have considered the effects of the power allocation in the BER of the FBMC system (in the figures, the legend "OQAM" is a short form to indicate the FBMC system). It can be readily seen that the MEPE power allocation yields always better BER results than UPA. However, as the estimation error P_E increases the advantage margin becomes narrower.

In Figure 3.23 we have compared the performance of the FBMC and OFDM systems as a function of the SNR for two different values of P_E. As expected, for low values of P_E the FBMC system yields a lower BER because, in OFDM, power is wasted transmitting the CP. For higher values of P_E, OFDM performs better because FBMC is suffering from ISI and ICI due to the estimation errors.

Finally, in Figure 3.24 we have chosen two working SNRs and have plotted the BER as a function of the estimation error power P_E. In this case, for $\text{SNR} = 0$ dB it can be clearly seen that there is a crossing point between the two BER curves, which further corroborates the fact that FBMC performs better than OFDM for low values of the estimation error power. However, as the estimation error increases, the performance of OFDM degrades slower than that of FBMC. The same effect is observed for $\text{SNR} = 10$ dB, even though in this case the crossing point is not depicted.

From the results presented, it is clear that FBMC outperforms OFDM in MIMO channels for the single beamforming structure, provided that the CSI imperfections are kept at a low level. Moreover, we can conclude that further research is needed to obtain robust designs against imperfections in the CSI for FBMC schemes, whose performance degrades faster than that of OFDM as the channel estimation error increases. These new robust designs should explicitly take into account the fact that the channel estimation is imperfect, as opposed to the naive approaches already existing in the literature. This will allow obtaining a design less sensitive to those errors and with improved performance.

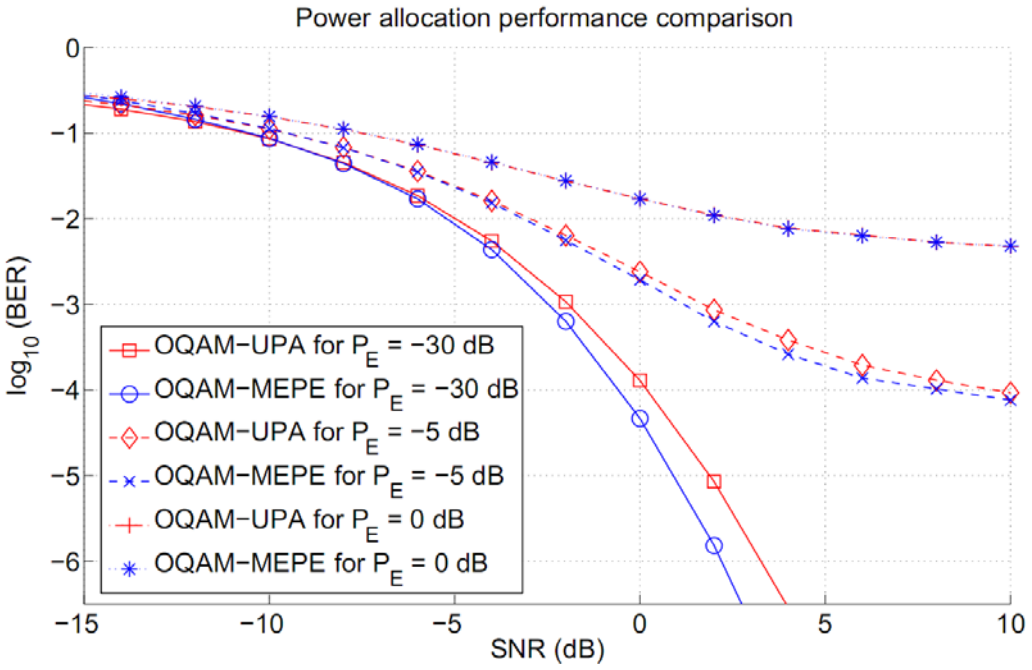

Figure 3.22 Performance comparison for different power allocation strategies

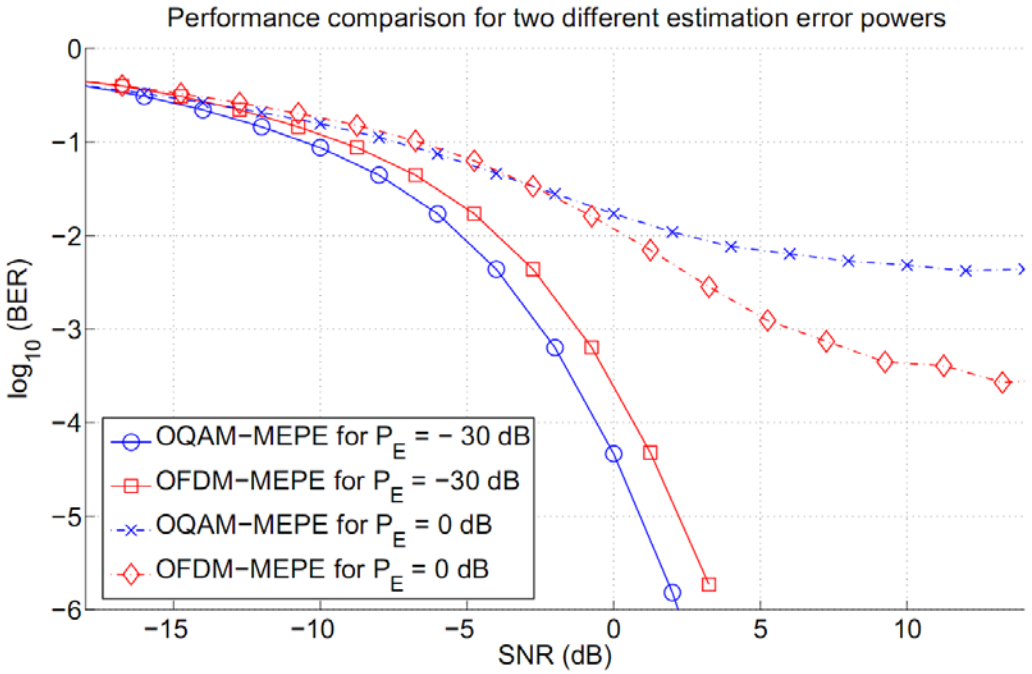

Figure 3.23 Performance comparison for different estimation error powers.

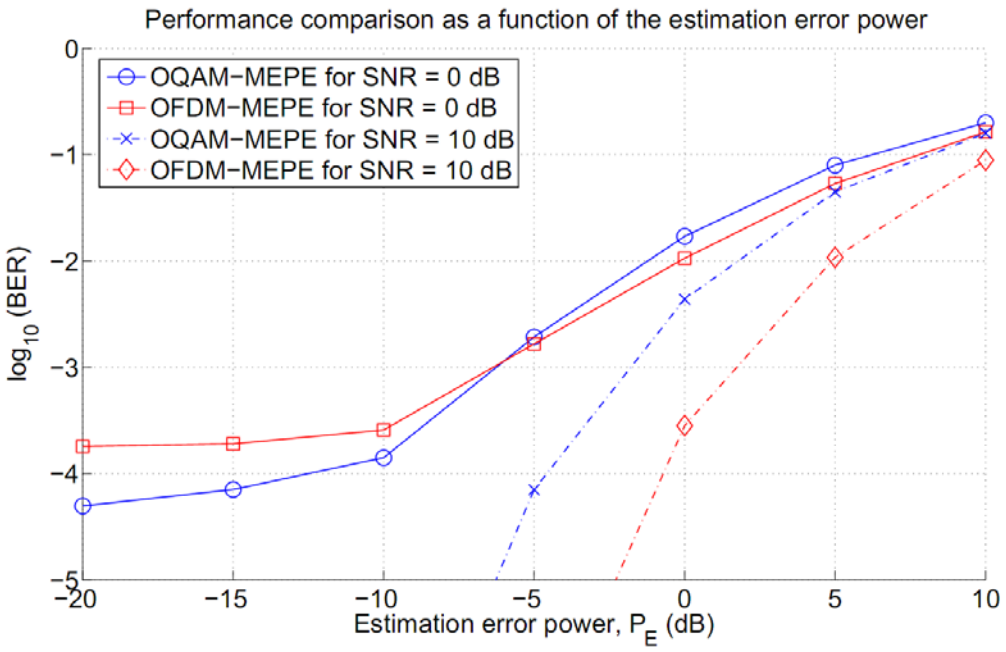

Figure 3.24 Performance comparison as a function of the estimation error power.

3.4.2 Multiple beamforming

In this section, we will consider the more complex case of multiple beamforming and we will analyze how the presence of multiple streams per carrier, together with the effects of imperfect CSI and the channel coherence bandwidth, impact on the performance of MIMO-FBMC and MIMO-OFDM schemes.

Multiple beamforming schemes have proven to be very useful in order to increase throughput in OFDM systems [51]. In this section we extend the multiple beamforming technique for FBMC schemes to improve the performance of such systems.

OFDM is well known in the literature; hence, we focus on the less known modular filterbank schemes (where the FBMC scheme belongs to). Similarly as in the single beamforming case presented above, from the general set of filterbank schemes, we restrict to uniform filterbanks, i.e., those such that the individual finite-length filters $f_k(t)$ can be expressed as shifted versions of the prototype filter $f_0(t)$ [52]:

$$f_k(t) = f_0(t)e^{j2\pi k\Delta ft} \tag{3.109}$$

where Δf is the frequency separation between two consecutive filters. This model suits for OFDM assuming a rectangular prototype filter $f_0(t)$ and the inclusion of the CP.

We consider a MC MIMO system with K subcarriers equipped with n_T antennas at the transmitter and n_R antennas at the receiver. The transmitted signal consists of L parallel streams at each carrier k. Each of the streams is filtered by the corresponding filter f_k and subsequently multiplied by the weighting corresponding to the intended antenna, known as beamformer $\mathbf{u}_{k,l} \in C^{n_T}$ (see Figure 3.25).

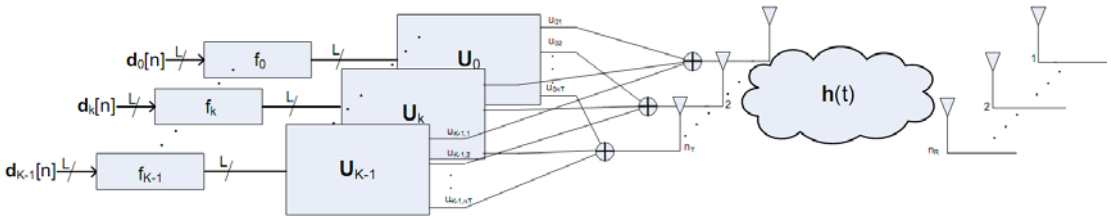

Figure 3.25 Multistream MC transmitter architecture.The receiver is symmetric. In the picture, the beamvectors are noted as $\mathbf{U}_k = \left[\mathbf{u}_{k,1} \quad \ldots \quad \mathbf{u}_{k,L}\right]$ and symbols as $\mathbf{d}_k[n] = \left[d_{k,1}[n] \quad \ldots \quad d_{k,L}[n]\right]^T$

Then, all ouputs for the same antenna are added and connected to the corresponding antenna. Thus, the analogical baseband transmitted signal $\mathbf{x}(t)$ can be expressed as:

$$\mathbf{x}(t) = \sum_{n=-\infty}^{\infty} \sum_{k=0}^{K-1} \sum_{l=0}^{L-1} d_{k,l}[n]\mathbf{u}_{k,l} f_k(t-nT), \tag{3.110}$$

where $d_{k,l}[n]$ denotes the input symbol sequence of the l-th stream in the k-th filter and T is the symbol period. The j-th entry of vector $\mathbf{x}(t)$ represents the signal transmitted through the j-th antenna. Then it is transmitted through the MIMO channel, $\mathbf{h}(t) \in C^{n_R \times n_T}$, whose (i, j)-th entry contains the channel impulse response from the j-th transmitter to the i-th receiver. The received signal is $\mathbf{y}(t) = \mathbf{h}(t) * \mathbf{x}(t) + \mathbf{w}(t)$, where $*$ denotes the convolution operation and $\mathbf{w}(t) \in C^{n_R}$ represents the system noise. The received signal is multiplied by the corresponding receiver beamvector $\mathbf{v}_{k,l} \in C^{n_R}$ and processed through a bank of matched filters, $g_k(t) = f_k^*(-t)$, to obtain the output $r_{k,l}(t) = g_k(t) * (\mathbf{v}_{k,l}^H \mathbf{y}(t))$:

$$r_{k,l}(t) = \sum_{n=-\infty}^{\infty} \sum_{k'=0}^{K-1} \sum_{l'=0}^{L-1} \mathbf{v}_{k,l}^H [g_k(t-nT) * \mathbf{h}(t-nT) * f_{k'}(t-nT)]\mathbf{u}_{k',l'} d_{k',l'}[n] + w'_{k,l}(t), \tag{3.111}$$

where we have defined the equivalent noise, $w'_{k,l}(t) \equiv \mathbf{v}_{k,l}^H [g_k(t) * \mathbf{w}(t)]$.

After analog to digital conversion sampling at $t_n = nT_s + \tau_o$, where τ_o is the delay maximizing the correlation between f_k and g_k. This expression can be approximated at given time n, stream l and frequency k by:

$$r_{k,l}[n] \approx \sum_{n'=-\infty}^{\infty} \sum_{k'=0}^{K-1} \sum_{l'=0}^{L-1} t_{k-k',n-n'} \mathbf{v}_{k,l}^H \mathbf{H}_{k,k'} \mathbf{u}_{k',l'} d_{k',l'}[n'] + w'_{k,l}[n], \tag{3.112}$$

where $\mathbf{H}_{k,k'}$ is the Fourier transform of the MIMO temporal channel $\mathbf{h}(t)$ at frequency $f = \frac{(k'+k)}{2}\Delta f$ (3.102).

From now on, we refer as FBMC for the specific considered scheme, consisting in creating a time-frequency pattern of real and imaginary symbols using an offset *real* PAM modulation and a factor $\theta_{k,n}$ as [53]:

$$d_{k,l}[n] = \theta_{k,n} s_{k,l}[n] = j^{(k+n)} s_{k,l}[n]. \tag{3.113}$$

To recover the transmitted symbols, the received signal $r_{k,l}[n]$ given in (3.112) is multiplied by $\theta_{k,n}^*$ and equalized dividing by the estimated equivalent gain $\hat{H}_{k,l} = \mathbf{v}_{k,l}^H \tilde{\mathbf{H}}_{k,k} \mathbf{u}_{k,l}$.

In practice, the receiver estimates the channel, and the beamformers $\mathbf{v}_{k,l}$ and $\mathbf{u}_{k,l}$, are designed based on the available estimated channel $\tilde{\mathbf{H}}_{k,k}$. The generated pattern causes the interference at large transmultiplexer values $t_{k,n}$ to be pure imaginary and pure real at small $t_{k,n}$ values. Then, at detection,

$$\begin{aligned} \frac{\theta_{k,n}^* r_{k,l}[n]}{\hat{H}_{k,l}} &= \frac{H_{k,l}}{\hat{H}_{k,l}} s_{k,l}[n] + \sum_{\substack{l'=0 \\ l' \neq l}}^{L-1} \frac{\mathbf{v}_{k,l}^H \mathbf{H}_{k,k} \mathbf{u}_{k,l'}}{\hat{H}_{k,l}} s_{k,l'}[n] + \\ &+ \sum_{\substack{(k',n') \in R \\ (k',n') \neq (0,0)}} \sum_{l'=0}^{L-1} t_{k',n'} \frac{\mathbf{v}_{k,l}^H \mathbf{H}_{k,k-k'} \mathbf{u}_{k-k',l'}}{\hat{H}_{k,l}} (\pm s_{k-k',n-n',l'}) + \\ &+ j \sum_{\substack{(k',n') \in I \\ (k',n') \neq (0,0)}} \sum_{l'=0}^{L-1} t_{k',n'} \frac{\mathbf{v}_{k,l}^H \mathbf{H}_{k,k-k'} \mathbf{u}_{k-k',l'}}{\hat{H}_{k,l}} (\pm s_{k-k',n-n',l'}), \end{aligned} \tag{3.114}$$

where R={(0,2),(0,-2),(2,2),(2,-2),(-2,2),(-2, 2)} and the set I contains the remaining elements in the set (k',n') $\in [-2,2]\times[-4,4]$, from the tranmultiplexer response represented in Figure 3.26. The $\pm$ notation has been used to indicate the result of $\theta_{k,n}^* \theta_{k-k',n-n'}$. Taking the real part in (3.114), the ICI and ISI terms in I can be eliminated whenever $\mathbf{v}_{k,l'}^H \mathbf{H}_{k,k-k'} \mathbf{u}_{k-k',l'} / \hat{H}_{k,l}$ is real, while elements in R remain negligible.

time index - n

Frequency index - k	-4	-3	-2	-1	0	1	2	3	4
-2	0	0.0006	-0.0001	0	0	0	-0.0001	0.0006	0
-1	0.0054	0.0429j	-0.1250	-0.2058j	0.2393	0.2058j	-0.1250	-0.0429j	0.0054
0	0	-0.0668	0.0002	0.5644	1	0.5644	0.0002	-0.0668	0
1	0.0054	-0.0429j	-0.1250	0.2058j	0.2393	-0.2058j	-0.1250	0.0429j	0.0054
2	0	0.0006	-0.0001	0	0	0	-0.0001	0.0006	0

Figure 3.26 Graphical representation of the time-frequency response of the FBMC system considered in PHYDYAS project.

Multistream techniques allow us to send up to a maximum of $L \leq \min\{n_T, n_R\}$ streams per carrier with the possibility to distinguish between them at reception. We consider the design of beamformers $\mathbf{u}_{k,l}$ and $\mathbf{v}_{k,l}$ in the high enough coherence bandwidth where ICI and ISI terms are negligible. As pointed out previously, this is possible for OFDM and an approximation for FBMC systems.

Then system (3.112) can then be modeled by

$$\mathrm{r}_{k,l}[n] = \sum_{l'=0}^{L-1} \mathbf{v}_{k,l}^H \mathbf{H}_{k,k} \mathbf{u}_{k,l'} d_{k,l'}[n] + w'_{k,l}[n]. \tag{3.115}$$

Hence, the design of the L beamformers for carrier k only depends on the channel at subband k. A solution for the transmit beamformer design that potentially achieves high throughput for such a channel is derived in [49] and is given by the L right singular vectors associated to the L-th largest singular values $\lambda_{k,l}$ of the Fourier transform MIMO channel matrix, $\mathbf{H}_{k,k}$, $\mathbf{e}_{k,l}^r$, scaled by the square root of the power assigned to stream l in carrier k, $\mathbf{u}_{k,l} = \sqrt{P_{k,l}}\mathbf{e}_{k,l}^r$. The receiver beamformers are the corresponding L orthonormal left singular vectors.

Power can be allocated according to different criteria depending on the performance figure to optimize. We restrict our study to the minimum effective probability of error (MEPE) [49], which, for the single beamforming case above, has been proved to obtain high performance in FBMC schemes.

Sources of error

When a MC system is used in practice, multiple beamformers lead to inherent additional ISI and ICI terms. Next, we detail the sources for such phenomena.

Noise

The ubiquitous thermal noise is usually modeled as zero-mean circular white Gaussian noise with spectral density $N_0/2$ and spatially white at the receiver. After being processed by the receiver bank of filters g_k the power of the effective noise at the l-th stream in the k-th carrier, $w_{k,l}(t)$, can be expressed as

$$P_{w'_{k,l}} = \int_{-\infty}^{\infty} \tfrac{N_0}{2} |G_k(f)|^2 ||\mathbf{v}_{k,l}||^2 \, df = \int_{-\infty}^{\infty} \tfrac{N_0}{2} |G_0(f)|^2 \, df \, . \tag{3.116}$$

Note that it is independent of the beamformer design for orthonormal beamformers and white noise.

Non-orthogonality in $f_k(t)$ and $g_{k'}(t)$

OFDM systems, use the CP to obtain a Toeplitz channel matrix, that is diagonalized by complex exponential filters $exp(j2\pi kn/K)$, which are orthogonal, i.e. lead to orthogonal subchannels. However, using the CP reduces the efficiency of the modulation.

On the contrary, FBMC schemes use non orthogonal $f_k(t)$ and $g_{k'}(t)$ filters and the used of the CP is avoided, which translates into higher efficiency. In non orthogonal MC systems, the transmission of a

symbol over the k-th carrier causes the symbol to interfere the adjacent carriers k' at reception through the channel approximated by $\mathbf{H}_{k,k'}$ (3.102).

The particular pattern $\theta_{k',n'}\theta^*_{k,n}$ cause large ICI and ISI interfering terms to belong to the set I and be completely removed taking the real part, see (3.114), reducing dramatically interference. At expenses of no perfect orthogonality, FBMC schemes do not require CP, increasing the efficiency of the transmission.

Channel coherence bandwidth

The correctness of the approximation described in the section above depends on how flat the channel is around the frequencies of interest, measured by the channel coherence bandwidth. The MIMO channel $\mathbf{h}(t)$ can be coherent or non coherent depending on its power delay profile (PDP). A short effective PDP implies an approximately flat channel, coherent, and then, $\mathbf{H}_{k,k'} \approx \mathbf{H}_{k,k}$, in a small neighborhood of k'.

In the case of perfectly flat channels, $\mathbf{H}_{k,k'} = \mathbf{H}_{k,k}$, all channels share the same singular value decomposition, $\mathbf{u}_{k',l} = \mathbf{u}_{k,l}$, and $\mathbf{v}_{k',l} = \mathbf{v}_{k,l}$. Stream l in k causes no interference in carrier k' whenever $l \neq l'$, due to the orthogonality of beamvectors, $\mathbf{v}^H_{k',l}\mathbf{H}_{k,k}\mathbf{u}_{k,l'} = 0$, $\forall k' \quad \forall l' \neq l$. However, when $l' = l$, equivalent channel takes the value $\mathbf{v}^H_{k',l}\mathbf{H}_{k,k}\mathbf{u}_{k,l} = \lambda_{k,l}\sqrt{P_{k,l}}$. Thus, terms with $l' = l$ in set R and I contribute to the interference. As, by construction, $\lambda_{k,l} \in R^+$, there is no change in the real or pure imaginary nature of the interference and all elements in I can be eliminated with the FBMC scheme, assuming $\hat{H}_{k,l}$ is the actual value of the channel.

However, when $\mathbf{H}_{k,k'} \approx \mathbf{H}_{k,k}$ is only an approximation, the beamformer design differs from carrier to carrier. Consequently, streams $l' \neq l$ are not orthogonal any more at carrier k', $\mathbf{v}^H_{k,l}\mathbf{H}_{k,k'}\mathbf{u}_{k',l'} \neq \mathbf{v}^H_{k,l}\mathbf{H}_{k,k}\mathbf{u}_{k,l}$, causing a rise in contribution from set R and I. Additionally, imaginary terms can leak to the real terms as the quotient $\mathbf{v}^H_{k,l}\mathbf{H}_{k,k'}\mathbf{u}_{k',l'}/\hat{H}_{k,l}$ may be a complex number, modifying the nature of the elements in those sets.

In a non selective channel scenario this quotient has an amplitude close to one and a phase close to 0. Recall that the singular values and vectors of a matrix are continuous functions in small increments of the channel [54], which implies a low leakage in general. When the PDP is longer, the channel is more selective in frequency domain and channels in consecutive carriers cannot be assumed to be similar. Thus, there can be large leakages from I to R. These leakages will produce ICI and ISI terms that can be cancelled with time and frequency post equalizations.

In the OFDM case, thanks to the use of the CP, the interferences described above are not present due to the orthogonality between neighbouring carriers.

Imperfect channel estimation

In practical systems, the MIMO channel is only available through a channel estimate $\tilde{\mathbf{H}}_{k,k}$ to design the transmit and receive beamformers, $\mathbf{u}_{k,l}$ and $\mathbf{v}^H_{k,l}$. Consequently, there is a mismatch between the actual

and the estimated channel, and the actual equivalent channel, $H_{k,l} = \mathbf{v}_{k,l}^H \mathbf{H}_{k,k} \mathbf{u}_{k,l}$, differs from the estimated one, $\hat{H}_{k,l} = \mathbf{v}_{k,l}^H \tilde{\mathbf{H}}_{k,k} \mathbf{u}_{k,l} = \lambda_{k,l} \sqrt{P_{k,l}}$.

Effects induced by the estimation mismatch are twofold. On the one hand, in general $\mathbf{v}_{k,l}^H \mathbf{H}_k \mathbf{u}_{k,l'} \neq 0$, as $\mathbf{u}_{k,l'}$ and $\mathbf{v}_{k,l}^H$ are no longer the actual singular values of the channel and cross-interference between streams at the same carrier k appears. However, this is not a critical problem while the estimated channel $\tilde{\mathbf{H}}_k$ is close to the real one $\mathbf{H}_k$.

As $\mathbf{u}_{k,l}$ and $\mathbf{v}_{k,l}^H$ are not the actual singular vectors, $H_{k,l}$ is no longer ensured to belong to real positive numbers. While in general this is not significant for OFDM schemes because $H_{k,l}$ is a small rotation of $\lambda_{k,l}$ in the complex plane, it can become critical for the FBMC scheme as pointed out previously, which motivates further research involving the robust design of pulse shapes and beamforming weights. Note that the noise power at stream l in carrier k does not increase although the channel $\tilde{\mathbf{H}}_k$ is used in the design as long as $\mathbf{v}_{k,l}$ are still orthogonal.

Simulation results

We have simulated both MIMO-FBMC and MIMO-OFDM schemes in different scenarios to quantify the effects of interferences described.

For OFDM the CP has been assumed to be the 20% of the total symbol ($CP = 1/4$). For the FBMC filter design, we selected a modular filter scheme truncated at 2048 samples, symbol period $T/T_s = 256$, with T_s the sampling period, and $K = 512$ carriers, proposed by Bellanger in [50] due to its excellent trade-off between time and frequency location with an OQAM modulation based on 2 delayed PAM modulations. A QPSK modulation is used in OFDM and so that rate is the same.

We use two streams per carrier, $L = 2$, in a Rayleigh channel MIMO scenario with $n_T = 3$ and $n_R = 3$. The imperfect channel estimation model considered is $\tilde{\mathbf{H}}_k = \mathbf{H}_k + \Delta_k$, where Δ_k is a zero-mean circularly symmetric complex Gaussian random variable with power equal to P_E. However, results presented in this paper also hold for other channel modeling.

The channel coherence bandwidth is modeled by an exponential decaying power delay profile with delay spread 2 times the sampling period and another with 50 times.

Figure 3.27 shows the performance for a high coherent bandwith channel at different P_E values.

For perfect CSI, FBMC performs better than OFDM due to the lack of CP. However, FBMC degradates to a minimum error floor even in the perfect CSI case, due to the ICI terms. The same occurs at low P_E power in low SNR. For high P_E values, the degradation in FBMC is faster than in OFDM due to higher ICI and ISI terms.

In Figure 3.28 a longer PDP is considered. In this case, the performance of FBMC is better than OFDM scheme at low SNR levels, but not in the high SNR regime due to the degradation suffered and the ICI terms from carrier to carrier. It must be highlighted that both BER figures cannot be compared as temporal channel has not been normalized to equivalent gains.

Figure 3.29 depicts the increase in BER as the power of estimation error increases at different *snr* values. Observe that, for SNR = 10 dB and low channel estimation error power values, the performance of MIMO-FBMC is neatly better than that of MIMO-OFDM. Additionally, for a lower SNR of 0 dB the performance of FBMC is slightly better than OFDM for all ranges of estimation error power.

In Figure 3.30, the BER for OFDM and FBMC is depicted for different number of streams assuming that the CSI is perfect. It can be seen that MIMO-FBMC performs better than MIMO-OFDM before it reaches its error floor due to the interference among the different spatial-streams present at each subcarrier.

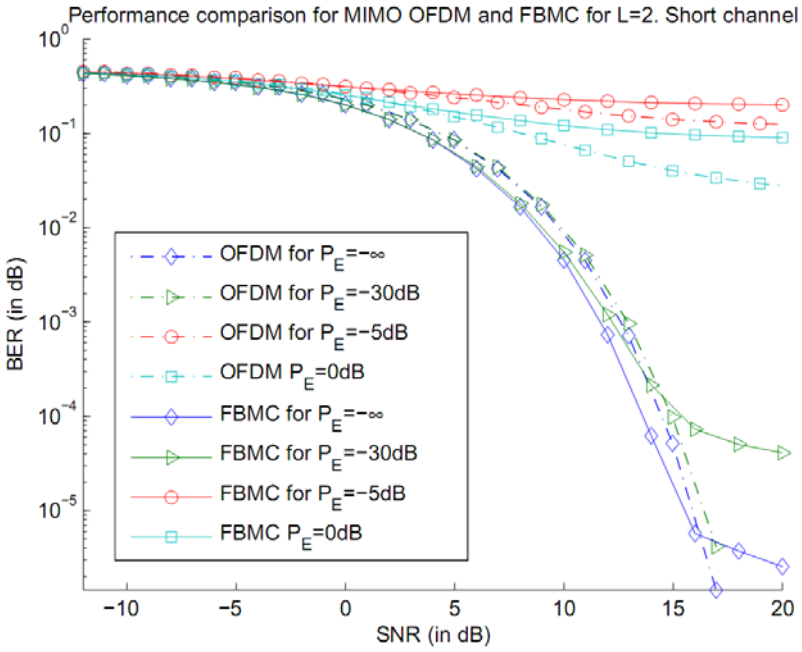

Figure 3.27 Performance comparison for high channel coherence bandwidth and different CSI estimation quality.

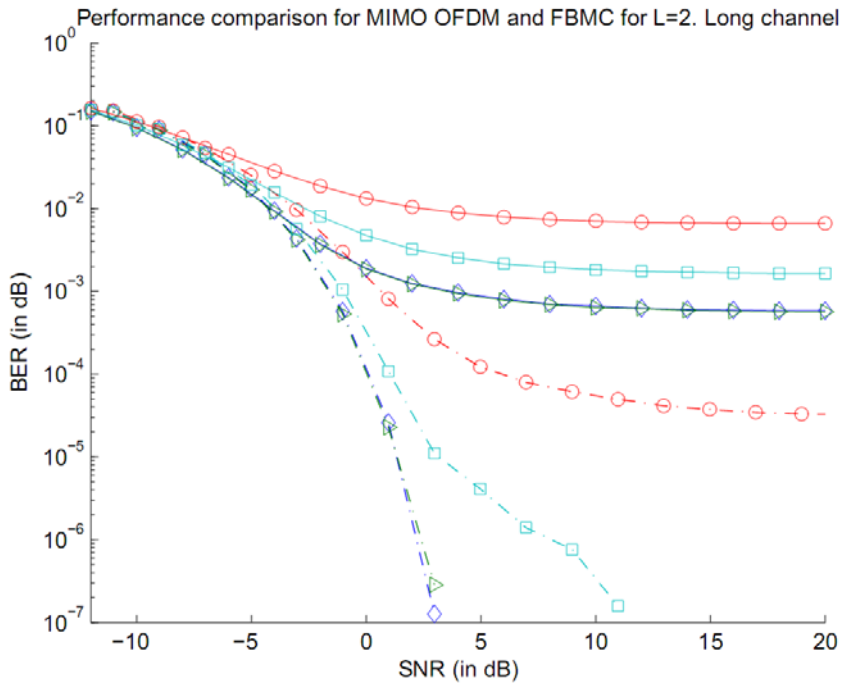

Figure 3.28 Performance comparison for high channel coherence bandwidth and different CSI estimation quality. The legend is the same as in Fig. 3.26.

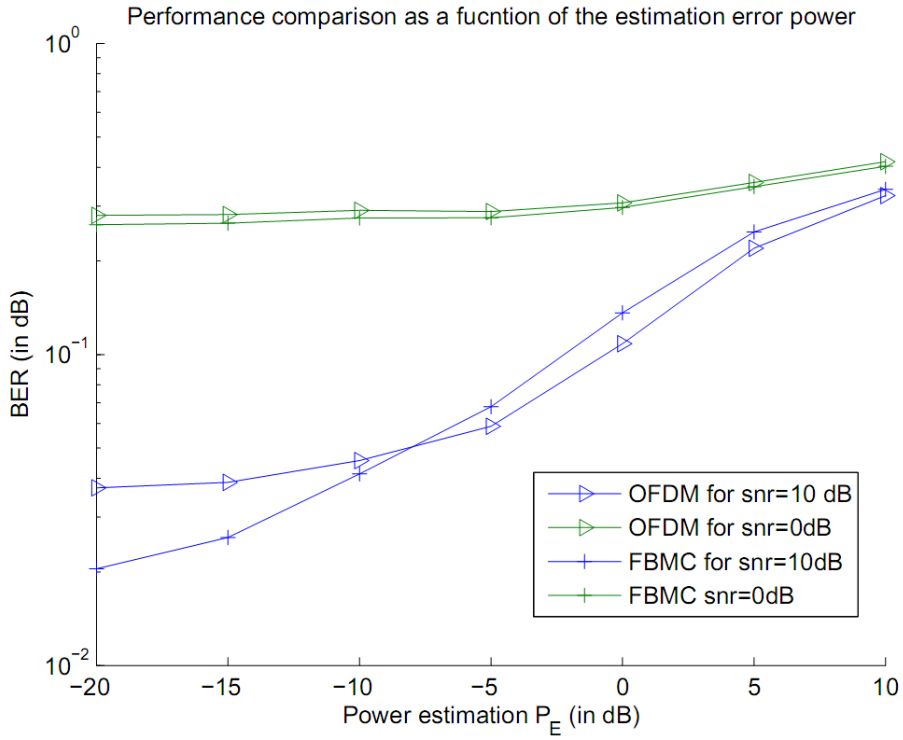

Figure 3.29 BER Performance in function of estimation error power P_E .

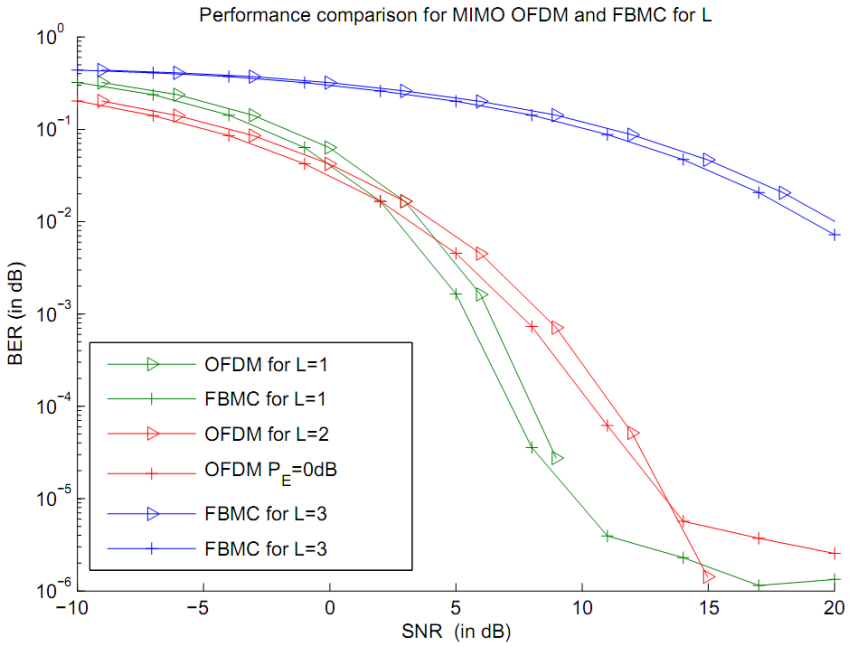

Figure 3.30 BER performance for different number of streams L with perfect CSI.

3.5 Joint beamforming for multiuser

As it has been described in Section 3.4, whenever the quality of the channel state information is high enough, the performance of FBMC in a single user scenario where both the transmitter and receiver are equipped with multiple antennas is superior to that of traditional OFDM thanks to the boost in spectral efficiency due to the lack of a power consuming CP in the former system.

Another advantage of FBMC over OFDM is that the transmission pulses are better localized in the frequency domain, meaning that the frequency span of the FMBC pulses is shorter than that of OFDM pulses. A possible situation where this superiority of FBMC can be exploited is in the Multiple Access Channel (MAC) scenario.

In the MAC, multiple users transmit information to a base station, which decodes the corresponding messages. A possible transmission scheme for the MAC in multicarrier systems is to allocate non-overlapping groups of carriers to the different users so that the transmission of the active users is simultaneous in time, reducing thus the average delay.

Since synchronization among all the users is practically infeasible, a guard frequency band has to be placed between the frequency groups corresponding to different users so that interference among users is avoided. The better frequency localization of the FBMC pulses allows the system designer to reduce the guard frequency band between users with respect to the frequency band needed in OFDM.

Consequently, from all that has been said above, the total bandwidth to be shared by the users can be used more efficiently in FBMC than in OFDM because the guard frequency band is narrower and because there is no need of a CP.

In the following, we compare the performance of FBMC and OFDM in the MAC scenario for the case where the users and the base station are equipped with multiple antennas, which, as it has been pointed out previously, enhances the performance of the system with respect to the single antenna case. Specifically, we consider that, similarly as in the single user case, single joint beamforming is performed at each subcarrier between the corresponding user (i.e., the one assigned to this specific subcarrier) and the base station. Moreover, for the sake of simplicity, we also assume that the users and the base station have perfect CSI.

3.5.1 System model for the MAC

In this section, we describe the mathematical model for the multiuser MAC scenario jointly for FBMC and OFDM. Despite the fact that we will not explicitly take into account the particularities of each system in this unified formulation, it is clear that the CP prefix has to be added in the transmission of OFDM symbols and that additional ISI and ICI terms will appear in the received signal in FBMC.

As it has been pointed out in the introduction, we assume that, if a subcarrier (or group of subcarriers) is assigned to a particular user, indexed by *u*, this user will beamform its information symbols through the eigenmode associated with the highest singular value $\lambda_{u,k}$ of the channel response between the user and the base station, denoted by $\mathbf{H}_{u,k}$. In addition, we consider that this particular user allocates a fraction of her total available power, $P_u^{\max}$, to this carrier and refer this power by $p_{u,k}$. Consequently, the equivalent SISO channel gain between the user and the base station at carrier *k* will be given by

$$C_{u,k} = \mathbf{v}_{u,k}^H \mathbf{H}_{u,k} \mathbf{u}_{u,k} = \lambda_{u,k} \sqrt{p_{u,k}}, \tag{3.117}$$

where $\mathbf{v}_{u,k}^H$ and $\mathbf{u}_{u,k}$ denote the receive and transmit beamformers, respectively, which correspond to the left and right singular vectors associated with the highest singular value of the channel matrix.

Let K_T denote the total number of contiguous subcarriers, which are available for transmission. The division of this available frequency band among the users is done by making *G* groups of *K* adjacent subcarriers and leaving S unused subcarriers between two contiguous groups. It is straightforward to check that, leaving also a guard frequency band of *S* subcarriers at the beginning and at the end of the whole band, the following equation must be fulfilled:

$$GK + (G+1)S = K_T. \tag{3.118}$$

Observe that the parameter *S* will be lower for FBMC than for OFDM, meaning that, since K_T and *K* are constant parameters, the number of available groups *G* will be higher in FBMC than in OFDM.

In the setting defined above, the system parameters to be designed are:

- The assignment of each frequency group to one user (one user may have more than one group assigned).
- The power that each user allocates to the frequency bands she has available.

Typically, the assignment of frequency groups to the users is done based on the perceived link quality that each user has on this specific group, which, in this case is related to the equivalent SISO channel gain, $C_{u,k}^2$. Loosely speaking, a quality label is associated for all the users to each one of the groups. Then, a scheduler decides which user is assigned to each group based on the labelling (and, possibly, some additional criteria such as fairness among users, delay tolerance of each user, …). However, the labelling itself for each user depends on how many groups are assigned to that particular user (i.e., if only one group is assigned to a particular user, her perceived quality will be higher than if ten groups are assigned to this same user as the available power for that user has to be shared among all the groups). Consequently, for a general power allocation criterion, the labelling is a non-trivial function of the power allocation and the number of groups assigned to that user, which further implies that a different labelling is needed depending on how many groups are assigned to each user, which makes the problem intractable in practice.

One possibility to overcome this difficulty is to choose the maxmin power allocation policy for the users. This policy coincides with the MEPE policy (presented in the previous section for single user scenarios) for the case where the available power tends to infinity, which justifies its choice (especially at high SNR) due to the good BER performance of the MEPE power allocation. Essentially, the maxmin power allocation boils down to assigning:

$$p_{u,k} = \frac{1}{\lambda_{u,k}^2} \frac{P_u}{\sum_k \frac{1}{\lambda_{u,k}^2}} \tag{3.119}$$

where the second factor is merely a normalizing factor to make sure that the assigned power does not exceed the available power for each user P_u and the summation spans all the carriers assigned to user *u*. Then, the perceived link quality $C_{u,k}^2$ is such that

$$C_{u,k}^2 = \frac{P_u}{\sum_k \frac{1}{\lambda_{u,k}^2}} = C_u^2 \tag{3.120}$$

where the second equality indicates that the link quality is independent of the subcarrier index.

In the following, we prove that, by using this specific power allocation, the relation between the labelling (perceived quality) and the number of groups assigned to each user has a strikingly simple relationship.

First of all, let's rewrite (3.120) according to

$$C_u^2 = \frac{P_u}{\sum_k \frac{1}{\lambda_{u,k}^2}} = \frac{P_u}{\sum_{g \in G_u} \sum_{k \in g} \frac{1}{\lambda_{u,k}^2}} \tag{3.121}$$

where we have transformed the whole summation among all the carriers assigned to the user in a double summation along the different groups assigned to the user (denoted by G_u). Now, (3.121) can be trivially rewritten as:

$$C_u^2 = \frac{P_u}{\sum_{g \in G_u} \sum_{k \in g} \frac{1}{\lambda_{u,k}^2}} = \frac{P_u}{\sum_{g \in G_u} \frac{1}{\sum_{k \in g} \frac{1}{\lambda_{u,k}^2}}}. \quad (3.122)$$

Realizing now that $C_{u,g}^2 = \frac{1}{\sum_{k \in g} \frac{1}{\lambda_{u,k}^2}}$ corresponds to the perceived link quality for user *u* and group *g* when unit power is assigned to it, the total link perceived quality is, finally,

$$C_u^2 = \frac{P_u}{\sum_{g \in G_u} \frac{1}{C_{u,g}^2}}. \quad (3.123)$$

which implies that the power allocation among the groups fulfils the same strategy as the power allocation among the subcarriers (c.f. (3.120)).

Consequently, if the maxmin power allocation is used, the labelling for each group corresponds to the perceived link quality when unit power is assigned to it. Then, to compute the perceived link quality for one user, given the labelling for each group, we simply need to evaluate (3.123).

Observe that, since the link quality is the same for all subcarriers belonging to the same user, if the user performs some kind of bit loading algorithm, all the subcarriers will be assigned the same constellation.

3.5.2 Performance criterion and problem statement

Once we know how to compute the perceived link quality for one user C_u^2, given the frequency groups assigned to it, it remains to find a criterion to assign the frequency groups to the different users. Consequently, we define the variable $\rho_{u,g}$, which is equal to either 1 or 0 depending on whether group *g* has been assigned to user *u* or not. We will make use of this definition later.

In multiuser scenarios, such as the one considered in this section, it is usually meaningful to maximize the sum-rate achieved by the users while guaranteeing that a certain (and possibly different) minimum rate is achieved by each individual user.

In this case we consider packet transmissions of length *N*. It is easy to see that the rate for each user is then proportional to

$$b_u K_u (1 - BER(C_u^2, b_u))^N, \quad (3.124)$$

where b_u is the number of bits per symbol of the chosen constellation for user *u*, K_u is the total number of carriers assigned to user *u*, and $BER(C_u^2, b_u)$ is the bit error probability (which depends on the perceived link quality and the bits per symbol).

Consequently, the group allocation optimization problem can be formally stated as follows:

$$\begin{aligned} \underset{b_u, P_u, \rho_{u,g}}{\text{maximize}} \quad & \sum_{u=1}^{U} b_u K_u (1 - BER(C_u^2, b_u))^N \\ \text{subject to} \quad & P_u \le P_u^{\max} \\ & \rho_{u,g} = \{0,1\} \\ & C_u^2 = \frac{P_u}{\sum_{g,\rho_{u,g}=1} \frac{1}{C_{u,g}^2}} \\ & b_u K_u (1 - BER(C_u^2, b_u))^N \ge R_u^{\min} \\ & K_u = K \sum_g \rho_{u,g} \end{aligned} \quad , \tag{3.125}$$

where we have added a maximum available power constraint per user $P_u \le P_u^{\max}$.

Observe that the main differences between FBMC and OFDM will lie in the following facts:

- The number of carriers per group *K* will be bigger in FBMC than in OFDM due to the better frequency localization of the filterbank pulses.
- The maximum power constraint for FBMC will be higher for FBMC than for OFDM because no power is wasted transmitting the CP.
- The $BER(C_u^2, b_u)$ function will be different because the transmission system model is different (in OFDM we have perfect orthogonality, whereas in FBMC we have some (very small) ISI and ICI components, which have, nonetheless, to be taken into account in the problem formulation).

3.5.3 Simulations

To compare the performance of FBMC and OFDM in this multiuser case with multiple antennas, we have assumed that the CSI is perfect at all sides of the communications link. For OFDM the length of the CP is taken to be 20 % of the total symbol duration. In addition, we have chosen the following parameters for the simulation of the scenario: the total number of subcarriers K_T is equal to 512, the frequency separation between groups is equal to S_{FBMC} = 2 subcarriers in FBMC and S_{OFMD} = 3 subcarriers in OFDM to guarantee that the interference between the users is kept at a minimum. Finally, the available constellations for data transmission are BPSK, QPSK, 16-QAM, and 64-QAM for OFDM and their offset counterparts for FBMC.

We have simulated the achievable aggregated throughput for a 20 user system with no minimum rate requirements per user (i.e., some users may have zero throughput during parts of the transmission) for a block length of *N* = 1024 channel uses. The maximum transmitted power per user is equal to 40 dB (with unit noise power). The normalized throughput (per subcarrier and channel access) can be found in the following table as a function of the number of subcarrier groups *G*.

Subcarrier Groups	1	10	20	40	60
FBMC	0.9	4.1	5.1	4.7	4.2
OFDM	0.8	3.9	4.6	4.2	3.3

As it can be seen, for a low number of subcarrier groups, only a few users can be served and, due to the individual power constraints, the whole band cannot be efficiently used because a poor constellation has to be chosen (such as BPSK) so that the BER does not degradate the achievable rates. In the other extreme, for large number of subcarriers groups efficiency is also lost due to the fact that the band occupied by all the frequency guards (between each subcarrier group) is also large. This implies that there is an optimal number of groups so that the overall throughput is maximized. In addition, the table also shows the superior rate performance of FBMC when compared to traditional OFDM, thanks to the savings in CP power and the lower separation between frequency groups.

3.6 Optimal precoding at the transmitter

In this work, we are concerned with optimal precoding techniques with FBMC modulation in Multiple Imput Single Output MISO context. The precoding techniques enable to obtain array gain in addition with the spatial diversity gain of the channel. The fact that FBMC is based on the transmission of real data means that the coefficients that we are going to apply to the transmitted data will be real valued ones.

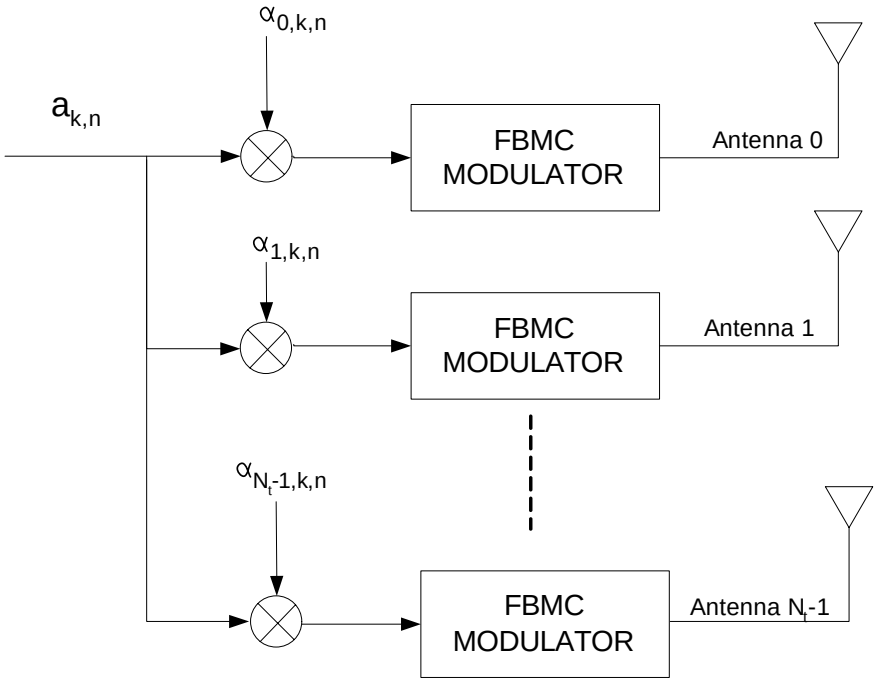

Figure 3.31: FBMC Beamforming transmitter structure

Let us consider a precoding scheme with N_t transmit antennas and a single receive antenna as shown in Figure 3.31. The channel is assumed to be known by the transmitter and the receiver. The real data are multiplied by *real coefficients* $\alpha_{0,k,n}$, then they are modulated by a FBMC modulator and transmitted by the first antenna. The same stream of data is multiplied by a *real coefficient* $\alpha_{i,k,n}$ before being modulated by a FBMC modulator and transmitted by the i^{th} antenna. We denote by $a_{k,n}$ the real data from the main stream of data at frequency k and time index n. Thus, at a given sub-carrier k the transmission is given at antenna i by: $d_{k,n}^{i} = \alpha_{i,k,n} a_{k,n}$. $\alpha_{i,k,n}$ are the real coefficients which are derived in

order to maximize the Signal to Noise Ratio (SNR) at the received side. At the single receive antenna side, the demodulated signal can be written as:

$$\begin{aligned} y_{k,n} &= \sum_{i=0}^{N_t-1} H_{k,n,i}(d_{k,n}^{i} + ju_{k,n,i}) + \upsilon_{k,n} \\ &= \sum_{i=0}^{N_t-1} H_{k,n,i}(\alpha_{i,k,n} a_{k,n} + ju_{k,n,i}) + \upsilon_{k,n}, \end{aligned} \tag{3.126}$$

where $\upsilon_{k,n}$ is the noise component at the sub-carrier k and time instant n. We have:

$$\begin{aligned} u_{k,n,i} &\approx (-j) \sum_{(k',n')\neq(k,n)} d_{k',n'}^{i} \sum_{k=-\infty}^{\infty} g_{k,n}[k] g_{k',n'}^{*}[k] \\ &= (-j) \sum_{(k',n')\neq(k,n)} \alpha_{i,k',n'} a_{k',n'} \sum_{k=-\infty}^{\infty} g_{k,n}[k] g_{k',n'}^{*}[k]. \end{aligned} \tag{3.127}$$

As the channel is considered to be constant over a given set of sub-carrier and a given set of time instant, we will also consider the coefficient $\alpha_{i,k',n'}$ to be constant over the same set of sub-carrier and time instant. Thus we can write,

$$u_{k,n,i} \approx \alpha_{i,k,n} \underbrace{\sum_{(k',n')\neq(k,n)} a_{k',n'} \sum_{k=-\infty}^{\infty} g_{k,n}[k] g_{k',n'}^{*}[k]}_{v_{k,n,i}}. \tag{3.128}$$

Therefore, (3.126) can be rewritten as:

$$y_{k,n} = \sum_{i=0}^{N_t-1} H_{k,n,i} \alpha_{i,k,n} (a_{k,n} + jv_{k,n,i}) + \upsilon_{k,n}, \tag{3.129}$$

As the same stream of data is transmitted over the N_t antennas, we have: $u_{k,n,i} = u_{k,n,0} = u_{k,n}$. Then, we get:

$$\begin{aligned} y_{k,n} &= \sum_{i=0}^{N_t-1} H_{k,n,i} \alpha_{i,k,n} (a_{k,n} + ju_{k,n}) + \upsilon_{k,n} \\ &= (\sum_{i=0}^{N_t-1} H_{k,n,i} \alpha_{i,k,n})(a_{k,n} + ju_{k,n}) + \upsilon_{k,n}. \end{aligned} \tag{3.130}$$

Now, we will search for the values of $\alpha_{i,k,n}$ that maximize the SNR. Let us denote by:

$$\underline{\alpha} = \begin{bmatrix} \alpha_{0,k,n} & \alpha_{1,k,n} & \alpha_{2,k,n} & \dots & \alpha_{N_t-1,k,n} \end{bmatrix}^T$$

$$SNR(\underline{\alpha}) = \frac{|\sum_{i=0}^{N_t-1} H_{k,n,i} \alpha_{i,k,n}|^2}{N_0}. \tag{3.131}$$

subject to the power constraint: $\sum_{i=0}^{N_t-1} |\alpha_{i,k,n}|^2 = 1$. In the case $N_t = 2$, as we will show, the SNR curve is concave. However, for $N_t \geq 3$ the optimization problem will be done on a non-concave curve. Indeed

for $N_t = 3$ and using random Raleigh channels, we replace $\alpha_{2,k,n}$ by: $\alpha_{2,k,n} = \sqrt{1-(\alpha_{0,k,n}^2 + \alpha_{1,k,n}^2)}$ or $\alpha_{2,k,n} = -\sqrt{1-(\alpha_{0,k,n}^2 + \alpha_{1,k,n}^2)}$. As a matter of example, for $\alpha_{2,k,n} = -\sqrt{1-(\alpha_{0,k,n}^2 + \alpha_{1,k,n}^2)}$, we plot the SNR curve as a function of $\alpha_{0,k,n}$ and $\alpha_{1,k,n}$. We consider $\alpha_{0,k,n}$, $\alpha_{1,k,n}$ in $[-1,1]$. The SNR curves are not concave as we can see in Figure 3.32. Thus, techniques like Lagrange optimization can not be carried out. In the case $N_t = 2$ we will derive the optimal solution, whereas for $N_t \geq 3$, we will look at a sub-optimal solutions.

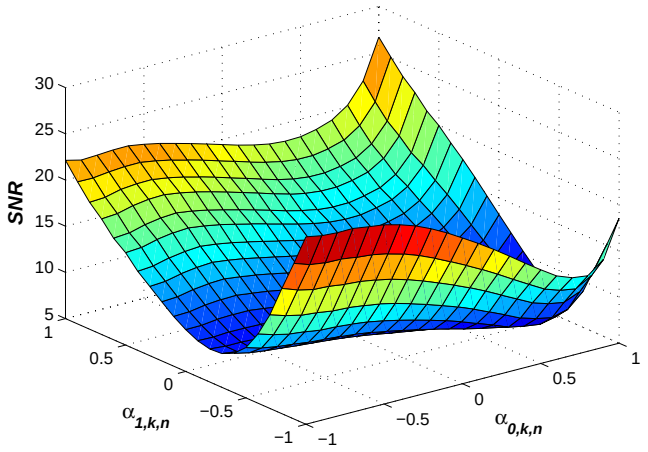

Figure 3.32 SNR curve as a function of $\alpha_{0,k,n}$ and $\alpha_{1,k,n}$ ($\alpha_{2,k,n} = -\sqrt{1-(\alpha_{0,k,n}^2 + \alpha_{1,k,n}^2)}$)

3.6.1 Optimal solution for $N_t = 2$

In the case of $N_t = 2$, the SNR expression is given by:

$$\begin{aligned} SNR(\underline{\alpha}) &= \frac{1}{N_0}(\underbrace{|H_{k,n,0}|^2}_{a_0}\alpha_{0,k,n}^2 + \underbrace{|H_{k,n,1}|^2}_{a_1}\alpha_{1,k,n}^2 \\ &\quad +2\alpha_{1,k,n}\alpha_{0,k,n}\underbrace{\Re\{H_{k,n,0}H_{k,n,1}^*\}}_{b}) \\ &= \frac{1}{N_0}(a_0\alpha_{0,k,n}^2 + a_1\alpha_{1,k,n}^2 + 2b\alpha_{1,k,n}\alpha_{0,k,n}). \end{aligned} \quad (3.132)$$

with, $\alpha_{0,k,n}^2 + \alpha_{1,k,n}^2 = 1$. Let us assume that $a_1 \geq a_0$ if it is the opposite case it is sufficient to inverse a_0 Resp.($\alpha_{0,k,n}$) and a_1 Resp.($\alpha_{1,k,n}$). Then, we can express $\alpha_{0,k,n} = \pm\sqrt{1-\alpha_{1,k,n}^2}$. Let us first consider the case $\alpha_{0,k,n} = \sqrt{1-\alpha_{1,k,n}^2}$, then

$$SNR(\underline{\alpha}) = \frac{1}{N_0}((a_1 - a_0)\alpha_{1,k,n}^2 + a_0 + 2b\alpha_{1,k,n}\sqrt{1-\alpha_{1,k,n}^2}) \quad (3.133)$$

with $\alpha_{1,k,n} \in [-1,1]$. As $(a_1 - a_0)\alpha_{1,k,n}^2 + a_0 > 0$, $SNR(\underline{\alpha})$ is maximized when $2b\alpha_{1,k,n}\sqrt{1-\alpha_{1,k,n}^2}$ is positive i.e. b and $\alpha_{1,k,n}$ have the same sign. So the value of $\alpha_{1,k,n}$ that we are seeking has the same sign as b. Let us derive the $SNR(\underline{\alpha})$ function, and by setting the derivation equal to 0, we obtain:

$$(a_1 - a_0)\alpha_{1,k,n}\sqrt{1-\alpha_{1,k,n}^2} = b(-1+2\alpha_{1,k,n}^2). \tag{3.134}$$

It can be showed that the only solution of interest is given by:

$$\alpha_{1,k,n} = sign(b)\sqrt{\frac{1}{2} + \frac{(a_1 - a_0)}{2\sqrt{(a_1 - a_0)^2 + 4b^2}}}. \tag{3.135}$$

Let us look at the second derivation in order to show that the value obtained when the first derivation is null corresponds to the global maximum. Using (3.134), it is possible to show that the second derivation is equal to:

$$= \frac{-2b}{\alpha_{1,k,n}(1-\alpha_{1,k,n}^2)^{\frac{3}{2}}}. \tag{3.136}$$

As b and $\alpha_{1,k,n}$ have the same sign the second derivation is negative in the area of interest, thus the value of $\alpha_{1,k,n}$ which corresponds to the zero of the first derivation is a global maximum. The second case is similar to the first case when replacing b by $-b$. It can be showed that we obtained the same SNR maximal value in both cases.

3.6.2 Sub-optimal solution for $N_t \geq 3$

As the SNR optimization problem is done on non-concave curve for $N_t \geq 3$, we look at sub-optimal solutions. Let us rewrite the SNR expression,

$$\begin{aligned} SNR(\underline{\alpha}) &= \frac{|\sum_{i=0}^{N_t-1} H_{k,n,i}\alpha_{i,k,n}|^2}{N_0} \\ &= \frac{1}{N_0}(\underbrace{|\sum_{i=0}^{N_t-1} H_{k,n,i}^r \alpha_{i,k,n}|^2}_{realpart} + \underbrace{|\sum_{i=0}^{N_t-1} H_{k,n,i}^i \alpha_{i,k,n}|^2}_{imaginarypart}), \end{aligned} \tag{3.137}$$

where , $H_{k,n,i}^r$ Resp.($H_{k,n,i}^i$) is the real part Resp.(the imaginary part) of $H_{k,n,i}$. In this last equation, we distinguish two parts: *the real part* and *the imaginary part*. Let us present two sub-optimal solutions.

- As $H_{k,n,i}^r$ and $H_{k,n,i}^i$ are real values, we perform the optimization either to *the real part* or *the imaginary part* depending on which part brings the most energy. That is, if: $\sum_{i=0}^{N_t-1} |H_{k,n,i}^r|^2 \geq \sum_{i=0}^{N_t-1} |H_{k,n,i}^i|^2$ the beamforming is done only on the *the real part* and in the opposite case the beamforming is done on the imaginary part. Making the beamforming on

the real part Resp. (*the imaginary part*) consists of seeking the value of $\alpha_{i,k,n}$ which maximizes:

$|\sum_{i=0}^{N_t-1} H^r_{k,n,i}\alpha_{i,k,n}|^2$ resp. $(|\sum_{i=0}^{N_t-1} H^i_{k,n,i}\alpha_{i,k,n}|^2)$ using Cauchy-Schwarz equality condition, it corresponds to:

$$\alpha_{i,k,n} = \frac{H^r_{k,n,i}}{\sqrt{\sum_{i=0}^{N_t-1}(H^r_{k,n,i})^2}}, Resp.(\frac{H^i_{k,n,i}}{\sqrt{\sum_{i=0}^{N_t-1}(H^i_{k,n,i})^2}}). \quad (3.138)$$

We refer to this method as Real or Imaginary Optimization (RIO). Let us look at another sub-optimal solution.

- We still consider the SNR expression given in (5.2.12). We define for every antenna i a set named Ω_i by:

$$\Omega_i = \{\frac{H^r_{k,n,i}}{N_r}, \frac{H^i_{k,n,i}}{N_r}, -\frac{H^r_{k,n,i}}{N_r}, -\frac{H^i_{k,n,i}}{N_r}\}, \quad (3.139)$$

where N_r is a per solution constant factor which guarantees $\sum_{i=0}^{N_t-1}|\alpha_{i,k,n}|^2 = 1$. The sub-optimal solution is given by:

$$\underline{\alpha} = argmax\{SNR(\underline{\alpha})\}, \quad (3.140)$$

subject to the constraints:

- $\alpha_{i,k,n} \in \Omega_i$
- $\sum_{i=0}^{N_t-1}|\alpha_{i,k,n}|^2 = 1.$

This method implies an exhaustive search but compared to the RIO solution it performs better since the RIO solution is a candidate in this exhaustive search. We will refer to this method as Sub-optimal Exhaustive Search (SES) method. Moreover, the set Ω_i could be increased in order to improve the performance using for example different combination values between $\frac{H^r_{k,n,i}}{N_r}$ and $\frac{H^i_{k,n,i}}{N_r}$. Other sub-optimal solutions could be derived. [55] presents some sub-optimal solutions in the case of complex beamfoming. Some of these solutions could be adapted to the real precoding case.

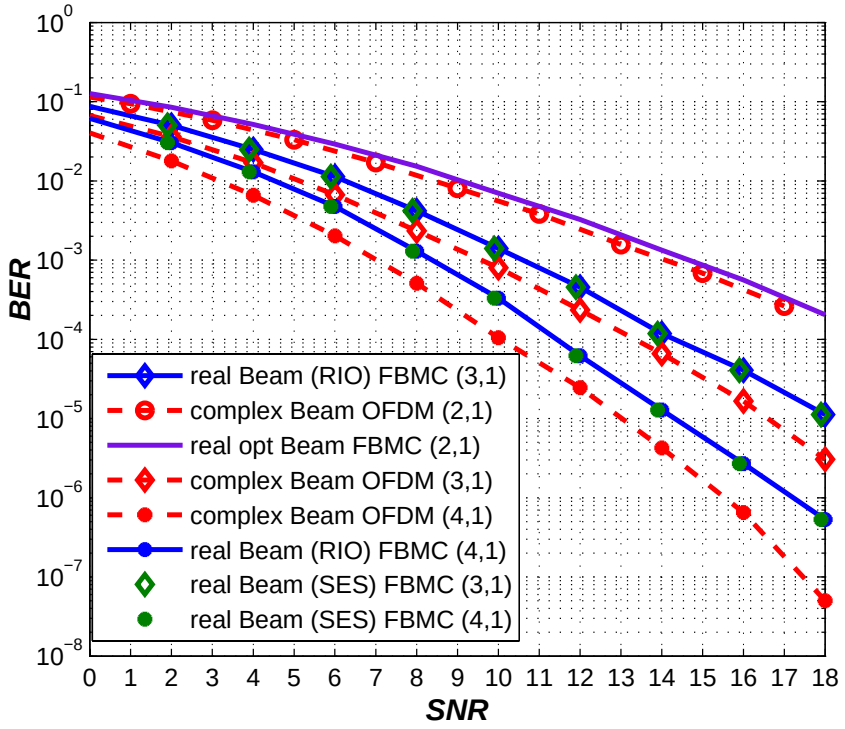

Figure 3.33 Performance of real precoding FBMC compared to complex beamforming CP-OFDM for different values of N_t.

Performance analysis over Raleigh Channel

Let us look at the simulation results of real precoding with FBMC modulation and complex beamforming with OFDM modulation. The simulation parameters are given as follows :

• No channel coding; QPSK modulation; Number of subcarriers $M = 64$;

• Rayleigh channel per antenna i.e. flat over all the subcarriers. We assume the channel coefficients are perfectly known by the receiver and the transmitter;

We use, as indicated earlier and in the continuation of the work [30-45], a truncation of the IOTA (Isotropic Orthogonal Transform Algorithm) prototype function . Its duration is limited to $4T_0$, which leads to a prototype filter containing $L = 4M = 256$ taps, the same length as the Phydyas prototype filter.

As Figure 3.33 shows, the real precoding (SES or RIO methods) with FBMC provides the maximum spatial diversity gain N_t. When comparing the RIO method and the SES method, the SES method performs quite better than the RIO method. The gain is relatively small (about 0.1 dB), therefore the RIO method could be more appropriate since it is very simple to implement compared to the SES method. When we compare the real precoding (SES or RIO methods) with complex beamforming with OFDM modulation, it looses about 0.5 dB for $N_t = 2$, about 1 dB for $N_t = 3$ and about 1.5 dB for $N_t = 4$. We need to investigate other sub-optimal solutions which bring real precoding performances closer to the complex beamforming ones. However, this performance loss has to be mitigated by the amount of information that the receiver should send to the transmitter in order to make the channel known at both sides. In the case of complex beamforming, N_t channel coefficients should be sent, that

is $2N_t$ real data. Whereas in the case of real precoding only N_t real data ($\alpha_{i,k,n}$ coefficients) should be sent. Real precoding will be less affected than complex beamforming by the imperfection (noise + distortion) of the return path (Receiver to transmitter). Indeed, if the total amount of power used for the return path is the same for real and complex beamforming, then, each real data in the real precoding will have a twice bigger power than that used in complex beamforming. Thus, the real precoding coefficients will be better estimated at the transmitted side than those computed in complex beamforming.
Future work involves the integration of the return path to access the global performance. Other sub-optimal methods should also be investigated while considering frequency selective channels.

4 Conclusions

In Section 2.1, preamble based CFO estimation in MIMO FBMC has been proposed based on a training symbol with two identical parts. Only slight performance degradation with respect to MIMO OFDM has been observed at high SNR.
Synchronization and channel estimation based on auxiliary pilots have been evaluated in Section 2.2. Assuming synchronization among antennas, each MIMO link has the same FTD and CFO and can be exploited for enhancing the synchronization parameters estimate. Nevertheless, compared to the SISO case, the performance gain is small.
Frequency sampling based equalizer considered previously for SISO [7] and SIMO [8] has been extended in Section 2.3 to the MIMO case. It is shown that in severely time dispersive channels the multi-tap equalizer structure greatly improves the ability to make use of the increased order of receive diversity in MIMO systems.
In Section 2.4, the Constant Modulus (CM) algorithm has been considered for blind equalization in MIMO FBMC where the number of antennas at the receiver is greater or equal to the number of antennas at the transmitter. The frequency domain equalizer outperforms the proposed blind algorithm. However, the useful rate using this algorithm is higher because no training sequence is required.
Two approaches have been proposed for MIMO channel tracking in Section 2.5: Decision Directed LMS, which is only effective for rather low to medium mobilities, and pilot aided channel tracking with time interpolation. This last scheme will prove to be much more effective in tracking fast varying channels. Its limitation is that one has to experience a delay in providing the channel estimates, equal to at most the period of pilot placement.
In Section 3.1 a practical block-wise Alamouti scheme for FBMC has been developed including a simple channel estimation method based on a specific pilot pattern embedded in the Alamouti-coded symbol block sequence. The performance was found to be quite good in case of stationary channel. With significant mobility, there is a trade-off between detection performance and code block length. With increasing mobility, the data block length has to be reduced, leading to increased overheads due to the pilots/guard periods. Considering system parameterization and pilot overheads similar to those of WiMAX downlink PUSC mode, acceptable performance is achieved with mobilities of some tens of km/h.
Spatial multiplexing with FBMC has been analyzed in section 3.2 for the MIMO 2x2 case. For the general case, different aproaches have been investigated. First, a modified ML decoder adapted to FBMC, taking into account the interference probability distribution, has been proposed. This method shows a slight gain compared to MMSE. Next, an iterative ML decoder based on interference cancellation has been presented obtaining significant gain compared to MMSE algorithm. More work is needed to come up with efficient algorithms for MIMO 2x2 and MIMO 3x3.
The V-BLAST iteration per subcarrier has been applied to MIMO FBMC making use of the decisions made for previous symbols. The results show that FBMC performs slightly better for low and moderate

SNR. An adaptive decision directed feedback equalization implementing the V-BLAST idea has been proposed. OFDM equalizer converges faster in the preamble section and outperforms the FBMC equalizer, especially for high SNR values. In severely frequency selective channel, the OFDM subchannels are no longer frequency flat and the above equalization scheme is no longer able to equalize them correctly.

For MIMO 2x1, transmit time diversity with single delay has been investigated in Section 3.3 and a general strategy for decoding has been described. For the general case, ML and Viterbi decoding have been considered. ML decoding using an exhaustive search among all possible transmitted sequences of data outperforms Viterbi decoding by 1 dB. This is due to the fact that the noise is colored thus Viterbi decoding is suboptimal. Iterative decoding based on the interference estimation has been evaluated offering better performance at expenses of higher complexity.

In Section 3.4 we have studied the single and multiple beamforming structures. We have compared the performance of OFDM and FBMC schemes under imperfect CSI and different channel coherence bandwidths. Thanks to the save in the CP, FBMC achieves better performances for a range of SNR. However, performance degrades faster in FBMC than in OFDM as the channel estimation error increases. There is degradation even in the perfect CSI case due to the interference between streams. Consequently, equalization and robust design techniques are a must to exploit the superior performance of FBMC. These new robust designs should explicitly take into account the fact that the channel estimation is imperfect. This will allow obtaining a design less sensitive to those errors and with improved performance. Joint beamformer for multiuser has been presented in Section 3.5 showing superior rate performance of FBMC when compared to OFDM.

In multiantenna OFDM systems, beamforming can be implemented at the sub-carrier level, with the help of complex coefficients. Since FBMC uses real inputs, a simple scheme to reach similar results consists of applying real coefficients, which optimize the signal-to-noise ratio at the receiver. The scheme is called real precoding, it is described in section 3.6 and simulation results are provided.

5 References

[1] Deliverable 2.2, “Synchronization and initialization with single antenna. Blind techniques,’’ ICT-211887 PHYDYAS, January 2009.

[2] Y. Jiang, H. Minn, X. Gao, X. You, and Y. Li, “Frequency offset estimation and training sequence design for MIMO OFDM, ’’ IEEE Transactions on Wireless Communications, vol. 7, no. 4, pp. 1244-1254, 2008.

[3] M. Morelli, and G. Imbarlina, “A practical scheme for frequency offset estimation in MIMO-OFDM systems,” EURASIP Journal on Wireless Communications and Networking, vol. 2009, article ID 821819.

[4] M. Bellanger, “Analytical expressions for the reference prototype filter,’’ PHYDYAS internal report, February 2009.

[5] Deliverable 3.2, “Optimization of transmitter and receiver”, ICT- 211887 PHYDYAS, July 2009.

[6] Part 16: Air Interface for Fixed and Mobile Broadband Wireless Access Systems Amendment 2: Physical and Medium Access Control Layers for Combined Fixed and Mobile Operation in Licensed Bands and Corrigendum 1, IEEE Std. 802.16e, 2006.

[7] Deliverable 3.1, “Equalization and demodulation in the receiver (single antenna)”, ICT- 211887 PHYDYAS, July 2008.

[8] Deliverable 4.1, “MIMO transmit and receive processing”, ICT- 211887 PHYDYAS, Jan. 2009.

[9] T. Ihalainen, T. Hidalgo Stitz, M. Rinne, and M. Renfors, ”Channel equalization in filter bank based multicarrier modulation for wireless communications,” EURASIP J. Advances in Signal Processing, vol. 2007, Article ID 49389, 18 pages, 2007.

[10] A. J. van der Veen and A. Paulraj, ”An analytical constant modulus algorithm,” *IEEE Trans. Signal Processing*, vol.44 no. 5, pp. 1136-1155, May 1996.

[11] A. J. van der Veen and A. Leshem, ”Constant modulus beamforming,” Chapter 6 in Robust Adaptive Beamforming, (J. Li and P. Stoica, eds.), Wiley Interscience, pp. 299-351, 2005.

[12] J. Yang, J. J. Werner, and G. Dumont, "The multimodulus blind equalization and its generalized algorithms," IEEE J. Select. Areas Commun., vol. 20, no. 5, pp. 997-1015, June 2002.

[13] B. Widrow and S. D. Stearns, *Adaptive Signal Processing*, Prentice-Hall, 1985.

[14] Z. Wu, J. He, and G. Gu, “Design of optimal pilot-tones for channel estimation in MIMO-OFDM systems,” in *Proc. WCNC-2005*, pp. 12-17, New Orleans, LA, March 13-17, 2005.

[15] Q. Sun, D. C. Cox, A. Lozano, and H. C. Huang, “Training-based channel estimation for continuous flat fading BLAST,” in *Proc. ICC-2002*, New York, April 28 – May 2, 2002.

[16] M. Krondorf and G. Fettweis, “Carrier frequency dependent throughput analysis for impaired OFDM links under user mobility,” in *Proc. PIMRC-2008*, Cannes, France, Sept. 15-18, 2008.

[17] S.M. Alamouti, "A simple transmit diversity technique for wireless communications," Selected Areas in Communications, IEEE Journal on , vol. 16, no. 8, pp. 1451-1458, Oct. 1998.

[18] E. Lindskog, A. Paulraj, “A transmit diversity scheme for channels with intersymbol interference,” in *Proc IEEE Int. Conf. on Communications, ICC 2000*, pp. 307-311, June 2000.

[19] Deliverable 2.1, “Data-aided synchronization and initialization (single antenna)”, ICT- 211887 PHYDYAS, Jul. 2008.

[20] R.V. Nee, A.V. Zelst, and G. Awater, "Maximum Likelihood Decoding in a Space Division Multiplexing System", *Vehicular Technology Conference Proceedings, 2000. VTC 2000-Spring Tokyo. 2000 IEEE 51st*, vol. 1, pp. 6-10, May 2000

[21] A. Goldsmith, "Wireless Communications", Cambridge University Press, 2005

[22] A. Papoulis, "Probability, Random variables And Stochastic Processes", fourth edition, McGrawHill, 2002.

[23] Lélé, J.-P. Javaudin, R. Legouable, A. Skrzypczak, and P. Siohan, "Estimation Methods for Preamble-Based OFDM/OQAM Modulations", *European Wireless '07*, April 2007.

[24] J.B. Anderson and S. Mohan, "Sequential Coding Algorithms: A Survey and Cost Analysis", *IEEE Transactions on Communications*, vol. 32, no. 2, pp. 169- 176, Feb. 1984.

[25] S.A.G. Zadeh and M.R. Soleymani, "An iterative M-algorithm based decoder for convolutional codes", *Canadian Conference on Electrical and Computer Engineering*, pp. 1618-1621, May 2005.

[26] G. J. Foschini, G. D. Golden, R. A. Valenzuela, and P. W. Wolniansky, “Simplified processing for high spectral efficiency wireless communication employing multi-element arrays,” *IEEE Journal on Selected Areas in Communications*, vol. 17, no. 11, pp. 1841-1852, Nov. 1999.

[27] A. van Zelst and T. C. W. Schenk, “Implementation of a MIMO-OFDM-based wireless LAN system,” *IEEE Trans. Signal Processing*, vol. 52, no. 2, pp. 483-494, Feb. 2004.

[28] J. Benesty, Y. Huang, and J. Chen, “A fast recursive algorithm for optimum sequential signal detection in a BLAST system,” *IEEE Trans. Signal Processing*, vol. 51, no. 7, pp. 1722-1730, July 2003.

[29] A. Ikhlef and J. Louveaux, “An enhanced MMSE per subchannel equalizer for highly frequency selective channels for FBMC/OQAM systems,” in *Proc. SPAWC-2009*, Perugia, Italy, June 21-24, 2009.

[30] C. Lélé, R. Legouable, and P. Siohan, “Iterative scattered pilot channel estimation in OFDM/OQAM,” in *Proc. SPAWC-2009*, Perugia, Italy, June 21-24, 2009.

[31] G. Ginis and J. M. Cioffi, “On the relation between V-BLAST and the GDFE,” *IEEE Communications Letters*, vol. 5, no. 9, pp. 364-366, Sept. 2001

[32] J. Choi, H. Yu, and Y. H. Lee, “Adaptive MIMO decision feedback equalization for receivers with time-varying channels,” *IEEE Trans. Signal Processing*, vol. 53, no. 11, pp. 4295-4303, Nov. 2005.

[33] A. A. Rontogiannis, V. Kekatos, and K. Berberidis, “A square-root adaptive V-BLAST algorithm for fast time-varying MIMO channels,” *IEEE Signal Processing Letters*, vol. 13, no. 5, pp. 265-268, May 2006.

[34] V. Kekatos, A. A. Rontogiannis, and K. Berberidis, “Cholesky factorization-based adaptive BLAST DFE for wideband MIMO channels,” *EURASIP Journal on Advances in Signal Processing*, vol. 2007, Article ID 45789.

[35] J. C. Tu, “Optimum MMSE equalization for staggered modulation,” in *Proc. 27th Asilomar Conf. Signals, Systems, and Computers*, pp. 1401-1406, Nov. 1-3, 1993.

[36] L. G. Baltar, D. S. Waldhauser, and J. A. Nossek, “MMSE subchannel decision feedback equalization for filter bank based multicarrier systems,” in *Proc. ISCAS-2009*, Taipei, Taiwan, May 24-27, 2009

[37] D. S. Waldhauser, L. G. Baltar, and J. A. Nossek, “Adaptive decision feedback equalization for filter bank based multicarrier systems,” in *Proc. ISCAS-2009*, Taipei, Taiwan, May 24-27, 2009.

[38] G. Lin, L. Lundheim, and N. Holte, “On efficient equalization for OFDM/OQAM systems,” Technical Report, NTNU, July 7, 2005.

[39] T. Wiegand and N. J. Fliege, “Equalizers for transmultiplexers in orthogonal multiple carrier data transmission,” in *Proc. EUSIPCO-96*, Trieste, Italy, Sept. 10-13, 1996

[40] D. S. Waldhauser, L. G. Baltar, and J. A. Nossek, “MMSE subcarrier equalization for filter bank based multicarrier systems,” in *Proc. SPAWC-2008*, Recife, Brazil, July 6-9, 2008.

[41] D. S. Waldhauser, L. G. Baltar, and J. A. Nossek, “Adaptive equalization for filter bank based multicarrier systems,” in *Proc. ISCAS-2008*, Seattle, WA, May 18-21, 2008.

[42] Vahid Tarokh, Nambi Seshadri, and A. R. Calderbank, "Space – Time Codes for High Data Rate Wireless Communication: Performance Criterion and Code Construction", *IEEE Transactions on Information Theory*, Vol. 44 (2), March 1998.

[43] Vahid Tarokh, Hamid Jafarkhani, and A. R. Calderbank, "Space – Time Block Coding for Wireless Communications: Performance Results", *IEEE Transactions on Information Theory*, Vol. 17 (3), March 1999.

[44] M. Bellanger, "Transmit diversity in multicarrier transmission using OQAM modulation", *Wireless Pervasive Computing, 2008. ISWPC 2008. 3rd International Symposium on*, pp. 727-730, May 2008.

[45] G. D. Forney, ``Maximum-likelihood sequence estimation of digital sequences in the presence of intersymbol interference,'' *IEEE Trans. Inform. Theory*, vol. 18, pp. 363–-6378, May 1972

[46] Jin-Der Wang and Hong Y. Chung ``Trellis coded communication systems in the presence of colored noise: performance analysis, simulation, and the swapping technique,'' *Global Telecommunications Conference, 1988, and Exhibition. 'Communications for the Information Age.' Conference Record, GLOBECOM '88*, vol. 2, pp. 1160 - 1165, December 1988.

[47] B. Le Foch, M. Alard and C. Berrou, "Coded Orthogonal Frequency Division Multiplex", *Proceeding of the IEEE*, Vol. 83, No. 6, Jun. 1995.

[48] G. J. Foschini and M. J. Gans, “On limits of wireless communications in a fading environment when using multiple antennas”, *Wireless personal communications*, vol. 6, no. 3, pp. 311–335, 1998.

[49] A. Pascual-Iserte, A. I. Pérez-Neira, and M. A. Lagunas, “On power allocation strategies for maximum signal to noise and interference ratio in an OFDM-MIMO system,” *IEEE Transactions on Wireless Communications*, vol. 3, no. 3, pp. 808–820, May 2004.

[50] M. G. Bellanger, “Specification and design of a prototype filter for filter bank based multicarrier transmission,” in *IEEE International Conference On Acoustics Speech And Signal Processing, (ICASSP’01)*, 2001.

[51] D. Palomar, J. Cioffi, and M. Lagunas, "Joint Tx-Rx beamforming design for multicarrier MIMO channels: A unified framework for convex optimization", *IEEE Transactions on Signal Processing*, vol. 51, no. 9, pp. 2381-2401, 2003.

[52] P. Vaidyanathan, "Multirate digital _lters, _lter banks, polyphase networks, and applications: A tutorial", *Proceedings of the IEEE*, vol. 78, no. 1, pp. 56-93, 1990.

[53] P. Siohan, C. Siclet, and N. Lacaille, "Analysis and design of OFDM/OQAM systems based on filterbank theory", *IEEE Transactions on Signal Processing*, vol. 50, no. 5, pp. 1170-1183, May 2002

[54] J. Magnus and H. Neudecker, "Matrix differential calculus with applications in statistics and econometrics". Wiley, 1999.

[55] J. Lee, R. Nabar, J P. Choi, and H. Lou, "Generalized Co-Phasing for multiple Transmit and receive Antennas, "*IEEE Transactions on Wireless Communications"*, vol. 8, no. 4, pp. 1649-1654, Apr. 2009.

[56] W. Yu and T. Lan, "transmitter optimization for the multi-antenna downlink with per-antenna power constraints," *IEEE Trans. Signal Processing*, vol. 55, no. 6, pp. 2646–2660, June 2007.

[57] D. Gerlach and A. Paulraj, "Adaptive transmitting antenna arrays with feedback", *IEEE Sig. Proc. Lett.*,vol. 1 (10),pp. 150–-152, October 1994.